SEDIMENTOLOGICAL AND MINERALOGICAL CHARACTERISTICS OF LIMPOPO RIVER SANDS AT BEIT BRIDGE BORDER BETWEEN SOUTH AFRICA AND ZIMBABWE

By

Ramavhunga Mukondeleli

Student No: 18022788

A research dissertation submitted to the Faculty of Science, Engineering, and Agriculture, Department of Geography and Environmental Sciences in fulfilment of the requirements for the degree of Master of Environmental Science in Geography at the University of Venda

Supervisor: Prof Beneath Odhiambo

Co-Supervisor: Dr Edmore Kori

February 2025

DECLARATION

I, **Mukondeleli Ramavhunga,** hereby declare that this dissertation, presented for the Master of Environmental Sciences Degree in Geography and Environmental Sciences at the University of Venda, is entirely my creation. It has not been previously presented for a degree at this university or any other educational institution. I assume complete responsibility for its conception and execution, and I have duly acknowledged all sources referenced in this research.

Signature:  **Date: 10/02/2025**

DEDICATION

I dedicate this study to me; this journey has been challenging. It validates my resilience, unwavering determination to become a researcher and my eagerness to achieve my goal. I have come to realise that success is truly attainable only for those who are dedicated and resolute. I further dedicate this research to both my mother, Mrs Ramavhunga N.E., and my father, Mr Ramavhunga M.H. for their never-ending support throughout my studies; your love, sacrifices, and encouragement were never unnoticed.

ABSTRACT

The research aimed to investigate the sedimentological and mineralogical characteristics of Limpopo River sand upstream of Beit Bridge, situated on the South Africa/Zimbabwe border. Due to limited information available about the minerals and sediments associated with Beit Bridge, this study was conducted to fill this knowledge gap and enhance knowledge of the river's history and environmental changes. Samples of sediment representing the river were collected from upstream of Beit Bridge along the Limpopo River. The sieve analysis technique was used to classify the particle size of the samples. The X-ray Diffractometer (XRD) analysis identified mineral composition, detecting quartz, feldspar, and other minerals. The petrographic analysis offered detailed mineral component observations, confirming XRD findings. Subsequently the X-ray fluorescence (XRF) analysis traced sediment provenance by identifying specific elements and compounds, illuminating geological history.

The results showed that sand was the most dominant component across all stations, with varying proportions of fine silt and gravel. XRD and microscopic analysis revealed minerals such as quartz, plagioclase, microcline, muscovite, and actinolite to be dominant. The prevalence of quartz suggests a quartz-rich source, while plagioclase indicates a predominance of igneous and metamorphic rocks in the local geological formations. The geochemical analysis indicated intense weathering, as evidenced by the high concentration of SiO_2 in the sediments. The SiO_2/Al_2O_3 ratio suggests significant leaching processes. Enrichment of Large Ion Lithophile Elements (LILE) in the sediments indicates a provenance from the subduction zone's geochemical region. The Al_2O_3/TiO_2 ratio reflects diverse sources, including basic and ultrabasic plutonic protoliths. These geochemical insights contribute to understanding the area's geological history and mineral resource potential, guiding future exploration and exploitation efforts.

The research successfully determined the sedimentological and mineralogical characteristics of the Limpopo River sand upstream of Beit Bridge. The combination of sieve analysis, XRD analysis, petrographic analysis, and XRF analysis yielded valuable insights into the historical transformations in the river's surroundings and the geological mechanisms that influenced the terrain in the examined area.

Keywords: Beit Bridge, Limpopo River, Mineralogical characteristics, and Sediments

ACKNOWLEDGEMENT

“Trust in the Lord with all your heart, and lean not on your understanding, in all your ways acknowledge him, and he shall direct your paths.” Proverbs 3:5-6.

I would like to express my sincere appreciation and gratitude to:

- My supervisor, Professor Beneath Odhiambo, for his supervision, critical comments, valuable advice, and constructive criticism, throughout this entire study.
- My co-supervisor, Dr. Edmore Kori for his proficient guidance, critical comments, suggestions, encouragement, professional advice, and constructive criticism. I will forever appreciate the time I had the honour of working with him as my co-supervisor and will gladly carry the knowledge he gave me of his human virtue and academic expertise.

LIST OF FIGURES

LIST OF TABLES

LIST OF ABBREVIATIONS AND ACRONYMS

Al	Aluminium
Ba	Barium
BIR	Basic Igneous Rocks
Ca	Calcium
CC	Coefficient of Curvature
Ce	Cerium
CG	Gradation Value
CGA	Citrus Growers Association
Cl	Chlorine
CIA	Chemical Index of Alteration
CO_2	Carbon Dioxide
Cr	Chromium
Cu	Copper
CU	Coefficient of Uniformity
DIC	Differential Interference Contrast
DXRD	Differential X-ray Diffraction
DSD	Detrital sediments
EDI	Equal Discharge Increment
EWI	Equal Width Increment
Fe	Iron
H	Hydrogen
Hf	Hafnium
HFSE	High Field Strength Elements
ICV	Index of Compositional Variability
K	Potassium
LILES	Large-Ion Lithophile Elements
Mg	Magnesium
Mn	Manganese
Na	Sodium

Nb	Niobium
Ni	Nickel
O	Oxygen
P	Phosphorus
Pb	Lead
PIA	Plagioclase Index of Alteration
PVC	Polyvinyl Chloride
REE	Rare Earth Elements
Rb	Rubidium
SEM	Scanning Electron Microscopy
Si	Silicon
Sn	Tin
Sr	Strontium
Ta	Tantalum
Th	Thorium
Ti	Titanium
U	Uranium
UCC	Upper Continental Crust
V	Vanadium
XRD	X-ray diffraction
XRF	X-ray fluorescence
Y	Yttrium
Zn	Zinc
Zr	Zirconium

CHAPTER ONE: BACKGROUND TO THE STUDY

1.1 Introduction

Numerous rivers effectively serve as carriers for both water and sediment from their origins to the oceans. For instance, the Amazon River, which presently accounts for 20% of the total freshwater discharge from rivers into the ocean and transports an annual average of 1200 million tonnes of sediment into the Atlantic (Myint et al., 2019). Over the past 30 million years, the Blue Nile and Tekazze Rivers have gradually eroded about 100,000 km of rock from the Ethiopian Highlands (Williams, 2012). In contrast, the Limpopo River, originating in the central region of Southern Africa, meanders eastward towards the Indian Ocean. As it courses through Botswana, South Africa, and Zimbabwe, the Limpopo River carries a substantial sediment load downstream.

The river flows through a diverse range of environments, including rocky outcrops, sandy floodplains, and wetlands, which contribute different types of sediment to the water body. In the higher sections of the Limpopo River, the riverbed is rocky, and erosion of these rocks produces sediment that is mostly made up of sand and gravel (Januário et al., 2022). As the river flows downstream into the middle and lower reaches, it passes through more sandy areas, which contributes finer sediment, such as silt and clay, to the river. Apart from natural sedimentological origins, human actions like agriculture, mining, and urban development can also add to the sediment burden in the Limpopo River. For example, erosion from agricultural fields and mining activities can add large amounts of sediment to the river, leading to increased turbidity and decreased water quality (Botai et al., 2020).

The term Limpopo is a revised form of the Sepedi word diphororo ta meetse, which translates to "gushing strong waterfalls” (Maposa, 2016). The Limpopo River boasts a vast drainage basin spanning 415,000 km2 and stretches approximately 1,750 km in length (Aghaindum, 2017). It maintains an average annual discharge of 170 m3/s. The Limpopo River basin hosts unique alluvial aquifers, which play a crucial role in subsurface water movement. During times of decreased flow, certain tributaries of the river supply groundwater to towns and mines located near the main river (Kahinda et al., 2016).

Sediment accumulations are prevalent within aquatic ecosystems, originating from the interrelationship of transportation, weathering, and biological activities. According to Mooneyham and Strom (2018), sediments are transported in two different forms, both as suspended and bed load. As described by Langland and Cronin (2003), sediment involves a mixture of both organic and inorganic materials. The inorganic sediments consist of mineral particles formed through the processes of physical and chemical weathering of bedrock.

Inorganic particles can often dominate the composition of suspended sediment in rivers, sometimes comprising more than 70% of its weight (wt.). This inorganic particulate matter comprises primary minerals like felspars, quartz, and carbonates, as well as secondary minerals such as illite, smectite, chlorite, and kaolinite, along with amorphous metal oxyhydroxides. However, the organic component of sediment includes organic particles and microbial communities, including extracellular, detritus, and cellular debris (Droppo, 2001).

According to Revuelta (2017), minerals are naturally occurring, homogeneous solids characterised by a precise chemical composition and a well-organized atomic structure. They typically form through inorganic processes and can vary widely, ranging from clay-sized to sand-sized particles. Clay-sized minerals are the result of the chemical alteration of primary minerals and are generally in the size range of 0 to 2 μm (according to the Wentworth Scale). They exhibit electromagnetic properties and contribute to the cohesive and sticky nature of mud (Maine, 2011). The colloidal fraction of clay minerals comprises particles smaller than 0.1 μm. Silt-sized particles, on the other hand, are produced through the physical weathering of primary minerals and are often composed of minerals such as quartz, feldspar, or micas. These particles fall into an intermediate size range, typically ranging from 2 μm to 5 μm. They can be found in association with clay particles, both in suspended form and within bed sediment. In contrast, sand-sized particles are prevalent in high-energy depositional environments like fluvial settings (Gresina et al., 2023). These are the largest components within the sediment and typically range from 5 μm to 2 mm in size, with quartz being a common constituent. It is important to note that the size-based classification of inorganic particles does not necessarily provide information about the specific mineral composition (Allen, 2013).

Minerals can be found in rivers and are a part of river sediment. Rivers can transport and deposit minerals of various types and sizes, which can have important implications for water quality, aquatic life, and human activities such as mining and agriculture. For example, mining activities can introduce harmful minerals into rivers, leading to water pollution and adverse effects on aquatic life. The natural occurrence of minerals in river sediment can provide important nutrients for aquatic ecosystems and support agriculture in riverine areas.

The Limpopo River basin exhibits various noteworthy geological attributes, such as the Archean Craton, Kalahari Craton, Karoo System, Bushveld Igneous Complex, and the Limpopo Belt (Mosase and Ahiablame, 2018). This river shares its boundaries with Zimbabwe, South Africa, Mozambique, and Botswana. Within the Botswana region of the Limpopo River basin, mining activities are primarily concentrated in mineral-rich Greenstone belts. Valuable metals extracted from these belts include copper (Cu), gold, and Nickel (Ni) (Ashton et al., 2001). In contrast, South Africa plays a prominent role as the world's leading producer of

various metals, including antimony, chromite, fluorite, gemstones, industrial diamonds, manganese (Mn), vanadium (V), vermiculite, and platinum. The country is also actively involved in gold production. Consequently, numerous mining operations have been established in South Africa, focusing on the extraction of a wide range of minerals and precious gems, such as Cu, gold, Ni, asbestos, emerald, pyrite, and tungsten (Ashton et al., 2001). In Zimbabwe, which encompasses the Limpopo River basin upstream of Beit Bridge, most mining activities primarily revolve around gold (Ashton et al., 2001). Therefore, it is of utmost importance to conduct a comprehensive examination of sedimentological deposits in the Limpopo River basin, particularly in the Beit Bridge area. This examination aims to assess the mineralogical composition of the sand deposits and determine the presence of potentially valuable minerals that may hold geological and economic significance. The objective is to gain a better understanding of the mineralogy and texture of these sand deposits and the geological processes responsible for their formation.

1.2 Problem statement

According to Cobbing et al. (2008), studies concerning sedimentological and mineralogical analysis of Limpopo River sands have been conducted before. Sitoe et al. (2015) performed a multi-proxy analysis on a radiocarbon-dated core extracted from an ancient oxbow lake within the Limpopo River plain. The findings show that a limited number of studies concerning sedimentological and mineralogical analysis of Limpopo River sand have been conducted, which has led to a limited understanding of minerals and sediments associated with the Limpopo River. Considering the scarcity of data, this study contributes to the limited research that has been done to date on the sedimentological and mineralogical characterization of the sediments in the Limpopo River. Emphasis was placed on the Beit Bridge area due to the limited research efforts undertaken in the vicinity and the potential of the area to comprise a variety of minerals due to the available minerals found across the Limpopo River Basin.

The Limpopo River basin has served as a significant mineral resource centre, enabling the countries within the basin to extract various minerals from the plains of the river basin (Ashton et al., 2001). For example, Botswana mines Cu, gold, and Ni in the Limpopo River basin. Zimbabwe actively focuses on gold mining in the Limpopo River Basin (Figure 1.1). South Africa has also been involved in the mining of several minerals in the basin, such as gem and industrial diamonds (Venetia Diamond Mine and River Ranch Mine), chromite (River Ranch Mine), platinum (Two Rivers Mine), and gold (Pande Mine). Therefore, it is imperative to do a sedimentology and mineralogy study of the Limpopo River basin at Beit Bridge to gain knowledge regarding the potential mineral deposits in the basin.

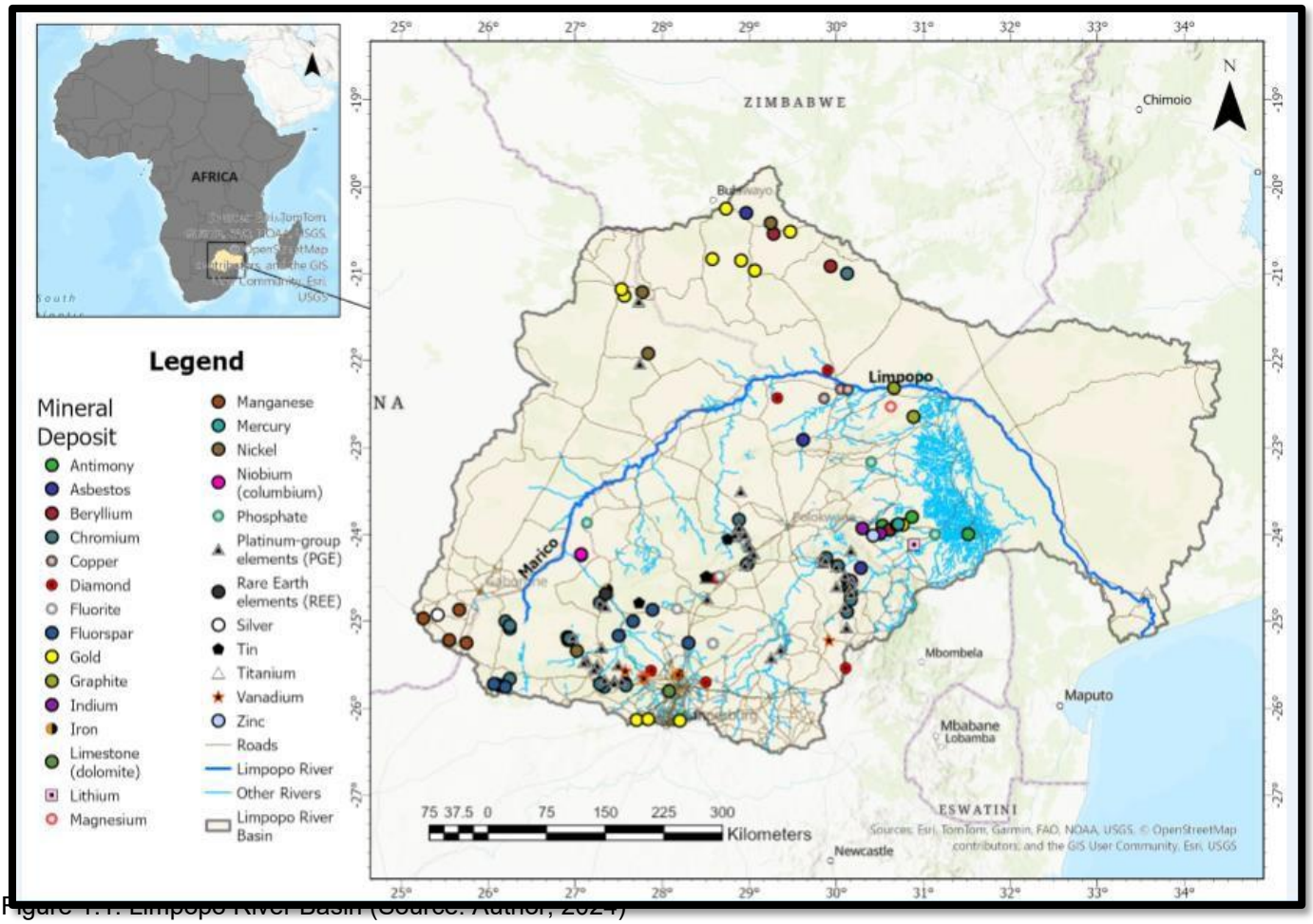

Figure 1.1: Limpopo River Basin (Source: Author, 2024)

1.3 Research Questions

This study seeks to address the following research questions:

- What are the sedimentological characteristics and mineral composition of the study area upstream from Beit Bridge?
- What is the provenance or source material of sedimentological upstream from Beit Bridge?

1.4 Research Aim and Objectives

1.4.1 Research Aim

This study aimed to determine the sedimentological and mineralogical characteristics of Limpopo River sand upstream of Beit Bridge on the South Africa-Zimbabwe border.

1.4.2 Specific Objectives

The specific objectives of the research were to:

- identify the sedimentological properties of the study area upstream from Beit Bridge.
- identify the mineral composition of sedimentological in the study area upstream from Beit Bridge.
- interpret the provenance or source material of sedimentological upstream from Beit Bridge.

1.5 Justification of the Study

The core of sedimentological analysis involves the identification of primary sedimentological elements, such as heavy minerals and clay minerals, as a fundamental aspect of conducting provenance studies (Weltje and Von Eynatten, 2004). Identifying minerals is important because it may help you understand both the landscape and the geologic history of the place. Furthermore, it is necessary for the growth of mineral extraction and processing systems.

1.6 Study Area

The Limpopo River Basin is situated in the eastern regions of Southern Africa, spanning the coordinates of 20 to 26 °S and 25 to 35 °E, encompassing a vast area of 412,938 km2 (Mupangwa et al., 2011). This basin connects four nations: South Africa, Botswana, Zimbabwe, and Mozambique (as illustrated in Figure 1.2). South Africa comprises a significant portion of the basin, accounting for 45% of its total area. The remainder is fairly evenly distributed among Botswana (19%), Mozambique (21%), and Zimbabwe (15%), as reported by Kahinda et al. (2016). Approximately 14 million people inhabit the basin, with a nearly equal division between rural (52%) and urban (48%) areas (Kahinda et al., 2016). The Limpopo River stretches across an approximate length of 1,750 km, originating from the confluence of the Marcio and Crocodile Rivers in South Africa and culminating at its mouth in Xai-Xai, Mozambique, along the Indian Ocean (Kahinda et al., 2016). In its course, the river serves as a natural boundary between South Africa and Zimbabwe until it enters Mozambique at Pafuri. However, for this study, the sediment samples were collected near Beit Bridge, at the border between South Africa and Zimbabwe.

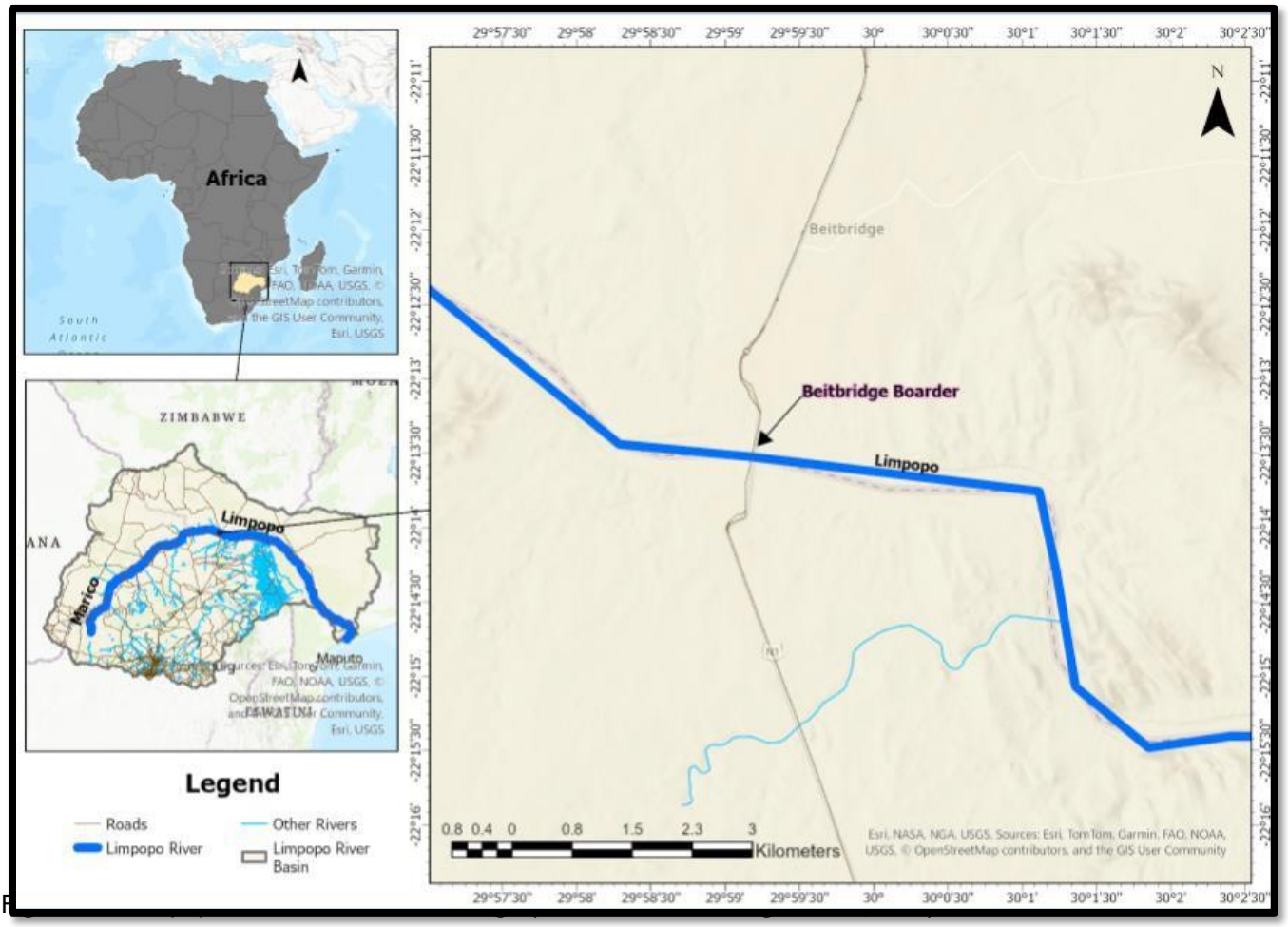

1.6.1 Climate

The climate in southern Africa exhibits significant variability across the region. According to the Köppen Classification Silva (2010) and Shewmake (2008), the Limpopo River Basin is predominantly characterised by a semi-arid climate with hot conditions. Within this basin, there is a range of climatic zones, starting from tropical rainfall near Mozambique's coastal plain, transitioning into tropical dry savannah, and ultimately progressing to a tropical desert as one moves further inland towards the south of Zimbabwe. Climate change within the basin primarily manifests in the form of both floods and droughts, with Mozambique often experiencing recurring flood events, while neighbouring countries primarily contend with droughts. The Limpopo River Basin is well-known for its summer rainfall, with limited precipitation during other seasons (Gbetibouo, 2009). Annual precipitation gradually decreases as one moves westward from the northern Drakensberg Escarpment across the interior plateau. The Drakensberg Escarpment receives the highest rainfall due to the

orographic effect. Precipitation patterns vary widely, ranging from as little as 200 mm in arid regions to as much as 1,500 mm in areas with abundant rainfall. However, the majority of the catchment area typically receives less than 500 mm of annual rainfall (Mzezewa et al., 2010). This region primarily receives approximately 95% of its annual rainfall between October and April, with considerable variability across different areas. Rainfall is characterised by sporadic rainy days, especially in remote regions, and significantly affects agricultural productivity (Botai et al., 2018).

In Botswana, the primary source of rainfall arises from convective thunderstorms, which often occur as localized events with significant spatial and temporal variations. The north-eastern region of Botswana, including a portion of the Limpopo River basin, receives an annual average rainfall of approximately 350 mm, while the south-eastern area experiences about 550 mm of rainfall. Zimbabwe, on the other hand, follows a distinct pattern with a single annual rainy season lasting for five months, spanning from November to March. This rainy season is closely associated with the seasonal movement of the Inter-Tropical Convergence Zone across Southern Africa (Botai et al., 2018). Specifically, in Bulawayo, situated in the southern high veld of Zimbabwe, the average annual rainfall slightly exceeds 600 mm. In contrast, the south-eastern low veld of the country receives less than 400 mm of annual rainfall (Gray, 2008). Summers in the Limpopo River Basin are generally warm, while winters are relatively mild (Kahinda et al., 2016). Temperature patterns are influenced by factors such as altitude and proximity to the ocean. In most parts of the basin, including South Africa, Botswana, and Zimbabwe, the average maximum daily temperatures range from approximately 30-34 °C during the summer months to 22-26 °C in winter. Meanwhile, mean minimum daily temperatures typically vary between 18-22 °C in summer and 5-10 °C in winter (Mosase and Ahiablame, 2018).

1.6.2 Geology

The Limpopo River Basin occupies a significant geological position at the northern boundary of the Kaap-Vaal craton, extending into the southern reaches of the Zimbabwe craton, as reported by Nicoli et al. in 2015. These cratons are separated by the Limpopo mobile belt and the Bushveld Igneous Complex. The cratons themselves form a stable geological shield, mainly comprised of volcanic and metamorphic rocks situated in the Earth's continental crust's lower strata. It's worth noting that the Kaap-Vaal craton is predominantly overlain by sedimentary rocks (Ault et al., 2015). The formation of the Basement Complex, which includes these cratons, spans an impressive duration of one billion years, encompassing the Archaean period. Within this geological context, specific rock types prevail. On the high veldt and escarpment of South Africa, granite and gneiss are predominant, alongside granodiorites,

quartzite, and various moderately metamorphosed sedimentary rocks (Ault et al., 2015). In the southern section of the Limpopo River Basin, particularly in the high veldt region, one can observe the notable occurrence of Karoo sediments, specifically the Vryheid Formation. These sediments encompass a range of types, including sandstones, clay stones, shales, and coal deposits. Furthermore, a strip extending from north-eastern Botswana through southern Zimbabwe features both Karoo sediments and basalt. Similarly, along the borders of Zimbabwe and Mozambique, one encounters Cretaceous sediments composed of sandstones, grits, and conglomerates. As you progress towards the eastern edge of the low veldt and the Lebombo Ridge, the prevalent geological characteristics primarily include Karoo formations, occasionally accompanied by dolerite intrusions.

The topography of the Limpopo River basin exhibits a varied landscape characterised by undulating plains, interspersed with mountain ranges and hills. This basin can be broadly categorised into two distinct plateaus: the northern upland plateau, which includes the Highveld region in Zimbabwe and the Strydpoort, Waterberg, and Drakensberg Mountains in the southern part; and the southern lowland coastal plateau, which extends across north-eastern South Africa, south-eastern Zimbabwe, and southern Mozambique (Manyanga, 2006).

1.7 Organisation of the Dissertation

The dissertation comprises six chapters, each presenting distinct yet interconnected content. In Chapter One, the sedimentology, mineralogy, and provenance of the Limpopo River basin and the Beit bridge area were discussed. This chapter serves as an introduction, outlining the problem statement, research objectives and providing a detailed description of the study area. Chapter Two is dedicated to the literature study, offering insights into the current state of knowledge concerning sedimentology and mineralogy in rivers. The steps, instruments, and equipment necessary to find the sedimentological characteristics, mineral compositions, and provenance are all covered in Chapter Three. Chapter Four of this research delves into the interpretation and discussion of the experimental outcomes, which were acquired through the examination of sieve sample distribution. The results of this investigation have allowed for a meticulous assessment of the sedimentological traits exhibited by the samples, thus fulfilling the first objective of this study. Furthermore, in Chapter Five, we delve deeply into the comprehensive examination of heavy elements, Rare Earth Elements (REE), and High Field Strength Elements (HFSE). These analyses serve as instrumental tools for ascertaining the provenance context of the sediments and, consequently, effectively addressing the second and third objectives of this research. Finally, in Chapter Six, a comprehensive synthesis of the

primary discoveries, deductions, and recommendations derived from this study is provided. This chapter not only encapsulates the essential takeaways but also serves as a valuable reference point for prospective research endeavours in this field.

1.8 Chapter Summary

This chapter offers an initial presentation on the Limpopo River, underscoring its importance as a significant waterway in the region of Southern Africa. This chapter discourses sedimentological deposits originating from a variety of origins such as solid rock formations, floodplains, marshes, and anthropogenic endeavours like farming and mining. Furthermore, the section explores the heterogeneous nature of sediments within the river, encompassing clay, silt, and sand particulates, along with their respective mineral compositions. Moreover, it briefly explains on the climatic attributes of the Limpopo basin, known for being predominantly semi-arid and warm, characterised by distinct climatic regions. Ultimately, the section wraps up with an outline of the geological setting of the Limpopo River Basin, highlighting the existence of enduring geological shields constituted of volcanic and metamorphic rock formations.

CHAPTER TWO: LITERATURE REVIEW

2.1 Introduction

This chapter gives a thorough examination of sedimentology, thoroughly delving into the intricate details regarding the origins, categorisation, and implications of various forms of sediment. The geological mechanisms and phenomena are thoroughly analysed, which are essential in the sediment accumulation, involving a diverse range of natural processes such as fluvial, aeolian, and glacial activities, along with the influence of human interventions. Furthermore, this chapter extensively explores the process of sediment settling in aqueous settings, engaging in an in-depth discussion on the dynamics of particulate matter settling, the intricate cycling of nutrients, and the accumulation of contaminants within these environments. The chapter researches the geological diversity exhibited by the Limpopo River basin situated in the southern region of Africa, which extends across numerous countries. Within this discussion, attention is drawn towards the distinctive characteristics of the basin, such as plateaus, hills, escarpments, and plains, elucidating their profound influence on the climate and topography of the surrounding area. Moreover, an in-depth analysis is conducted on the abundant mineral deposits and geological points of interest within the basin, emphasising their significant roles in the economic sector.

2.2 Defining Sediments

Sediments typically consist of a mixture of various materials, encompassing both organic and inorganic components. This terminology is frequently utilised to characterise sediment particles that are rich in minerals, encompassing elements such as clay, silt, and sand, in addition to the organic matter in various stages of decomposition and inorganic biogenic materials (Jović et al., 2023; Pico et al. 2023). In Koselleck's (2018) terminology, sediments are characterised as the Earth's substances, such as gravel, sand, mud, and lime that undergo transportation and deposition through various natural forces like wind, ice, gravity, and water. Over time, these materials accumulate and solidify to create sedimentary rocks. Depending on the process of accumulation, sediments are further categorised into residual sediments, mechanical, chemical, and organic sediments (Kundu, 2023).

Residual sediments are described as residue material originating directly from rock formations without undergoing any significant transportation. Residual accumulates are typically encountered in tropical regions characterised by elevated temperatures and abundant rainfall (Bogado et al., 2019). Nonetheless, Huat (2012) describes residual residues refers to rock material that has transformed into sediment, leading to the loss of its original rock-like texture

and weight changes in its composition. In a more expansive context, residual residue can be defined as residue material that originates from the weathering and fragmentation of rocks within its original location (Pawlik et al., 2016).

Chemical sediments originate from chemical reactions that occur within water saturated with positively and negatively charged ions. These ions are naturally attracted to each other, leading to the formation of ionic and covalent bonds as they solidify into mineral crystals (Bogado et al., 2019). Various types of chemical sediments exist, including evaporites and chemical limestone. Evaporite chemical sediments are created when water evaporates from lakes or oceans (Huat, 2012). During the evaporation process, water transitions from a liquid to a gaseous state, leaving behind elements like calcium (Ca), sodium (Na), and chlorine (Cl) in the remaining water, leading to their precipitation (Warren, 2016). This phenomenon enriches the water with these elements, contributing to the formation of evaporite minerals and sediments, which are commonly found in arid regions where evaporation rates surpass rainfall significantly (Warren, 2006). Evaporites are prevalent in desert environments, particularly in areas with ephemeral lakes like playa lakes or in the shallow, warm parts of the ocean near desert regions, where the process of evaporation is prominent (Tamagawa, 2022). Mechanically formed sediments, on the other hand, primarily result from physical processes rather than chemical reactions. In essence, these sediments are created when existing rocks break down into smaller particles through physical means (Zhang and Krooss, 2001).

Organic sediment rocks take shape under varying levels of pressure and temperature over extended periods. The specific types of organic sediment formed depend on the extent of pressure and temperature involved in their formation. Frequently, sediments are conveyed not solely by water, using fluvial processes, but also by wind, employing aeolian processes, and glaciers (Ferguson et al., 2022; Belnap et al., 2011). These natural forces carry sediments, contributing to the formation of sediments.

2.2.1 Fluvial Processes

Fluvial transport and deposition are represented by beach sands and river channel deposits, but sediment also frequently settles out of still or slowly flowing water in lakes and seas (Satır and Doğan-Sağlamtimur, 2020) (Figure 2.1).

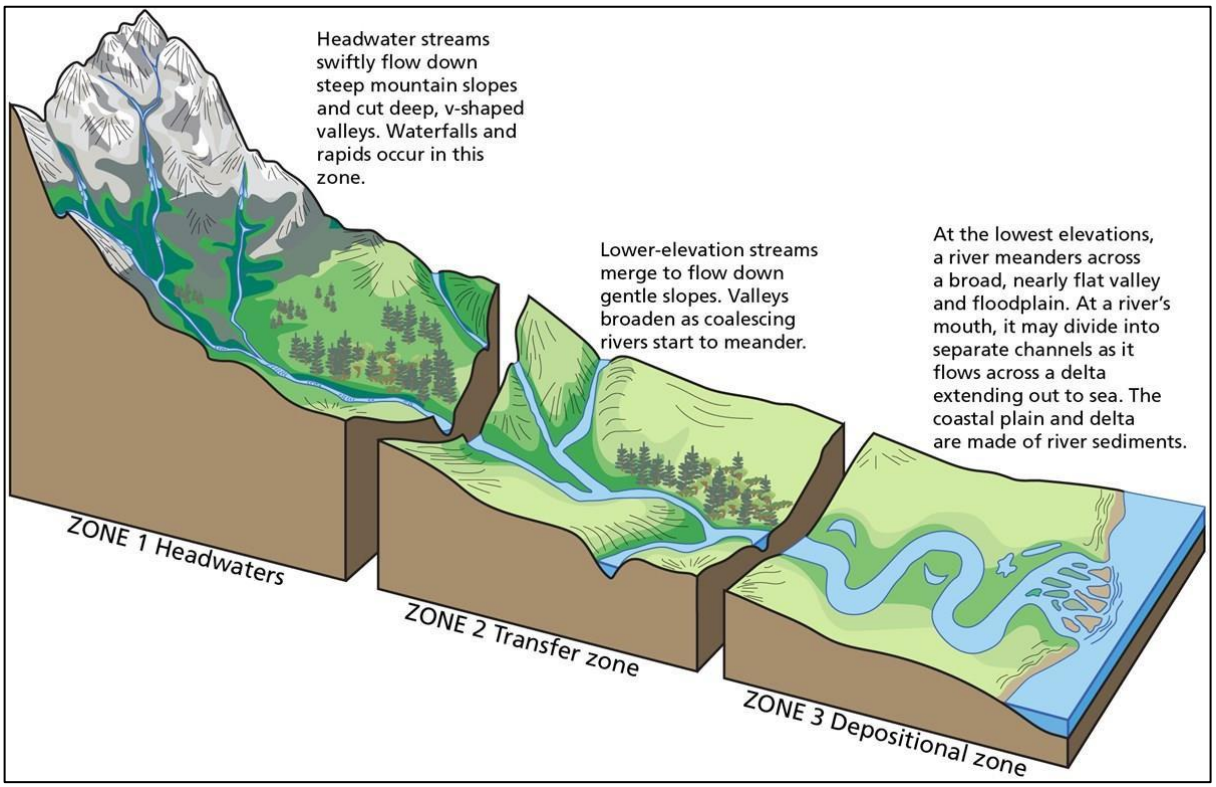

Figure 2.1: Rural Systems and Fluvial Platform (Source: National Park Service, 2022)

A shear stress is immediately applied to the stream bed by the water as it flows across it. If the cohesive strength of the substrate is lower than the applied shear force, or if the bed consists of loose silt that can be moved by such forces, then the bed will only be eroded by clearwater flow (Negara et al., 2023). Additionally, if the river carries a lot of sediment, this material might help the riverbed wear down faster through abrasion. The shards themselves are also crushed, getting smaller and more rounded at the same time in a process known as attrition (Koyuncu and Le, 2024; Ferguson et al., 2022). Sediments within river systems are transported in three distinct modes: bedload, which includes coarser fragments moving near the riverbed; suspended load, encompassing finer particles carried within the water column; and dissolved material, consisting of substances in a dissolved state (Hoitink, 2023). Each type of sediment has a specific threshold velocity, known as the entrainment velocity, at which it begins to move, as described by Ali et al. (2017). Notably, even when the flow velocity drops below the entrainment velocity, the absence of significant friction between the sediment grains

and the riverbed allows them to continue their transportation. Eventually, as the velocity decreases further, a point is reached at which these sediment grains can settle and be deposited. This process is illustrated by the Hjulström-Sundborg curve, as depicted in Figure
2.2 (Worrall et al., 2020).

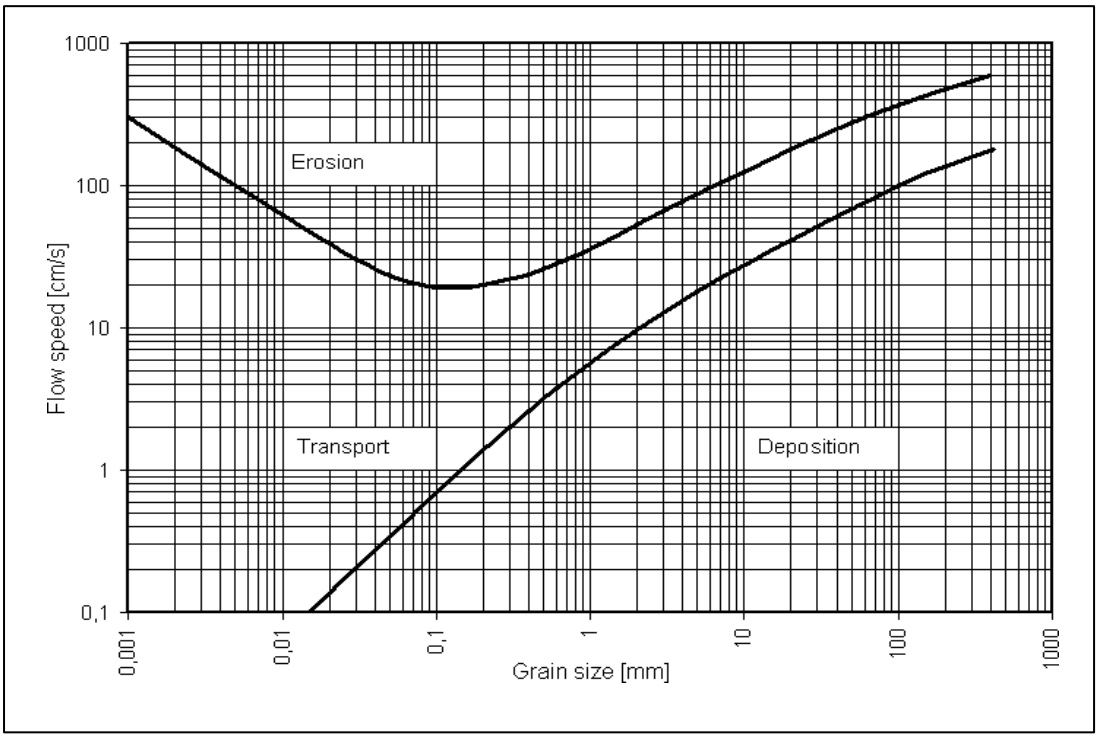

Figure 2.2: The Hjulström-Sundborg diagram showing the relationships between particle size and the tendency to be eroded, transported, or deposited at different current velocities (Source: Naganna et al., 2017)

Rivers undergo a continuous cycle of collecting and depositing solid particles, consisting of rocks and sediments, from their beds along their entire length. In areas where the river's flow is swift, it tends to pick up more particles than it drops. Conversely, in regions with slower flow, more particles are deposited than picked up. The zones where a higher concentration of particles is deposited are known as alluvial or floodplains, and the accumulated material is referred to as alluvium (Kellison et al., 2019). While even small streams contribute to alluvial deposits, it is in the floodplains and deltas of larger rivers that substantial and geologically significant alluvial deposits are typically found. Stream erosion stands out as a notably influential geomorphic force (Leopold et al., 2020). Fluvial processes influence the terrain by wearing down existing land features, moving materials, and depositing them to form fresh land configurations. Fluvial systems play pivotal roles in both human civilization and ecosystems. In addition to sustaining riparian regions, which are crucial for clean water and provide diverse habitats, rivers also serve as sources of water for hydroelectric power generation and as channels for shipping (Robins et al., 2022).

Best and Fielding (2019) reviewed recent progress in four areas of fluvial sedimentology, including the nature of alluvial dunes, the role of fine-grained suspended sediment, the linking of facies models and channel planform, and the reconstruction of drainage networks within ancient sedimentological successions. The study emphasised the need for new research to address various challenges in fluvial sedimentology, such as understanding the stratification produced by dunes, evolving new bedform phase diagrams, developing alluvial facies models beyond channel pattern, and considering process mechanics in fluvial deposit preservation and alluvial architecture. The study highlighted the importance of a process-based approach to sedimentology and the incorporation of modern knowledge and techniques to interpret ancient sediments and reconstruct formative processes. With the aid of significant progress has been made in deciphering the clastic rock record in various sedimentological environments since the 1960s. Advances in methodology and techniques have aided in studying modern and ancient environments, providing new insights into sedimentation across different scales. The review emphasised the importance of a process-based approach to sedimentology and the incorporation of modern knowledge and techniques to interpret ancient sediments and reconstruct formative processes.

Ferguson et al. (2022) also examine the persistent increase in research and publications on fluvial processes and landforms between 1965 and 2000, emphasizing multidisciplinary research contributions. Breakthroughs have been made in understanding the connection of river process and shape at the reach scale, with a particular emphasis on variations between sand- and coarse-bed rivers. Initially, there were more ideas than data to test them, but this changed, and by the early 2000s, getting massive volumes of digital data was easier than knowing how to use it efficiently. GPS, LiDAR, and satellite-derived terrain models have changed landform classification. The use of cosmogenic isotopes to date and estimate denudation rates has also advanced. Continued growth in computer power enabled more detailed numerical modelling, and software packages for satellite image analysis and GIS expanded knowledge of fluvial landscapes. Research expanded to include previously neglected areas like bedrock rivers and headwater streams, with a growing focus on ecological and environmental aspects, such as riparian vegetation interactions, habitat dependencies, and ecological river classification. The field became more multidisciplinary, incorporating ecologists and tectonic geologists, and the literature continued to expand rapidly.

2.2.2 Anthropogenic Factors

Human activities, such as the construction of dams and alterations in land use, have notable impacts on both the quantity of sediment and the rate at which sediment is transported in

waterways. Dams influence the flow of water by either completely detaining it or constricting its passage (Gran and Czuba, 2017). This restricted flow can lead to downstream sections of the river becoming sediment-starved, while sediment accumulates behind the dam. However, when water is released from the dam, it can result in a rapid increase in downstream flow, leading to sediment deposition. On the other hand, human-induced land use changes, including urbanization, agriculture, and construction activities, primarily affect the sediment load rather than the transport rate (Asaeda and Rashid, 2012). These impacts are typically indirect and frequently necessitate substantial rainfall or flooding to facilitate the movement of sediment into water bodies. Bunke et al. (2019) examine the impact of natural and anthropogenic sediment mixing processes on sediment deposition and contaminant accumulation. Sediment accumulation patterns in the Mecklenburg Bight and the Arkona Basin were analysed. Sediment profiles for TOC contents, mercury, and cesium-137 levels in different areas of the Baltic Sea were measured. The findings of this study help identify the influence of natural and anthropogenic mixing on sediment profiles and demonstrates the use of mixed sediment profiles for inferring information about past environmental conditions and anthropogenic impact.

Ai-jun et al. (2020) discuss the response of sedimentation processes in the Minjiang River subaqueous delta to anthropogenic activities in the river basin, highlighting the impact of anthropogenic interventions on the delta ecosystem. The study investigates how changes in the river basin, such as land use changes and dam construction, have influenced sediment transport and deposition in the delta region. It was found that anthropogenic activities in the river basin have led to significant changes in sediment supply to the delta, affecting the distribution and composition of sedimetological deposits. These changes have important implications for the geomorphology and ecological health of the delta ecosystem.

However, anthropogenic land use emerges as a leading factor responsible for elevated sedimentation rates, primarily driven by erosion and runoff (Gran and Czuba, 2017). This surge is attributed to the disturbance of landscapes in activities such as logging, mining, construction, and agriculture. These "disturbed sites" often result in the disruption or loosening of topsoil by removing native vegetation. Consequently, this loosened soil can be readily transported into adjacent rivers or streams through mechanisms such as rainfall, wind, and runoff (Gran and Czuba, 2017).

2.3 Sediment Deposition

Sediment deposition plays a vital role in fostering aquatic ecosystems by replenishing nutrients and forming benthic habitats and spawning grounds (Czuba et al., 2011). This deposition process occurs when suspended particles gradually sink to the bottom of a body of water. Typically, this settling phenomenon occurs as water flow decelerates or comes to a standstill, rendering the heavier particles no longer buoyant due to reduced turbulence. Sediment deposition is observable in a variety of aquatic systems, including high mountain streams, rivers, lakes, deltas, and floodplains. The particles that settle at the bottom of a water body are often termed settleable solids (Shende et al., 2023). When these settleable solids accumulate in riverbeds and streambeds, they are commonly referred to as bedded sediment (Kuforiji and Ayandiran, 2013). The size of settleable solids can vary depending on the specific water system. In regions with high water flow, larger sediment particles such as gravel tend to settle first, particularly in areas with swift currents. In contrast, finer particles like silt and clay may travel longer distances, potentially reaching estuaries or deltas. However, in marine environments, the presence of salt ions in the water causes nearly all suspended sediment particles to settle. (Mehta, 2013). It's important to note that sediment serves as both a source and a sink for pollutants and heavy metals in aquatic ecosystems (Chiaia-Hernández et al., 2022). Any form of sediment can be sampled for sediment analysis using the right sampler. The sampling apparatus and methodologies must be carefully devised to collect a precise volume and surface area of water from a stream, reaching a specified depth, and simultaneously ensuring the sample's protection from external contaminants (Adomat et al., 2022)

2.4 Sediment Analysis

Studies have developed various sampling techniques to collect representative sediment samples for analysis (He et al., 2020; Lis et al., 2021). Awal et al. (2019) discussed several common sediments sampling methods, including the method of point integration, depth integration technique, bed material sampling, and sampling by bed load. Each method has its advantages and is selected based on specific research objectives, site conditions, and the nature of the sediment being studied.

2.4.1 Method of Point Integration

This method entails lowering a sampler into the stream at the exact location where suspended sediments need to be collected. The sampler's nozzle is operated electrically from the surface, and the relative depth of sampling, expressed as a ratio of the sampler's depth to the stream flow depth, can be set at values of 0, 0.2, 0.6, 0.8, and 1. Equation 1 can be used to compute

sampling time, which is the amount of time that passes between a sampler nozzle opening and shutting (Awal et al., 2019).

$$Sampling\ time = \frac{Sample\ volume}{stream\ velocity} \times 0.1841 \quad \text{..... Eq. 1}$$

2.4.2 Depth Integration Technique

This method involves the systematic lowering and raising of a sampler in a river at a consistent speed to collect suspended silt in an isokinetic manner. The utilisation of the depth integration technique is prevalent in the fields of hydrogeology and groundwater studies as a method to ascertain the mean concentration of a particular substance, such as a contaminant, within a specified depth range in an aquifer or soil stratum. For depth integration, two common approaches are employed: the Equal Discharge Increment (EDI) and the Equal Width Increment (EWI) methods (Witt and Ford, 2001). With the EDI approach, the river's cross-section is divided into 3 to 10 identical segments, each with approximately the same discharge. Sediment samples are collected from each segment, and the silt concentration in the river is determined by averaging these samples (Edwards and Glysson, 1988). On the other hand, the EWI method involves dividing the cross-section of the river into 6 to 10 equal segments while ensuring a uniform sampler transit rate in each segment. Much like the EDI method, sediment samples are gathered from each of these segments and then averaged to determine the silt concentration in the river (Baranya and Józsa, 2013).

2.4.3 Sampling by Bed Load

Bed-load sediment consists of sediment particles that move by rolling or sliding along the bottom of a stream. This sampling technique is employed to collect and analyse sediment of this type, which is known as bed-load sediment. It is typically used when sediment movement and water velocity are near the streambed. There are various types of samplers designed for bed-load sampling, including the basket and box sampler, pan-type sampler, and pit-type sampler (Rickenmann et al., 2012).

- Basket and Box Sampler

This sampling apparatus comprises three main components: a container for collecting silt, a supporting frame, and a cable. The sampling process begins by lowering the sampler to the ground, followed by the opening of the gate to allow the passage of water and sediment. After a set duration, the gate is closed, causing the sediment carried by the water to settle inside the container. The observations of sediment movement occur when the gate is both opened and closed (Awal et al., 2019; Edwards and Glysson, 1988).

- Pan-type Sampler

The wedge-shaped sampler gathers the sample in a container after the silt has moved up the inclined surface. This sampler is limited to use in streams with a smooth bed and moderate velocity (Awal et al., 2019; Zobeck, 2006).

- Pit-type Sampler

On the streambed, a concrete structure with various slots is constructed for this kind of sampler. For sediment analysis, a sample of the sediment gathered in the slot is used (Muhammad et al., 2019).

2.4.4 Bed Material Sampling

To examine sediment, samples can also be collected from the material on the riverbed. There are no restrictions on choosing a sampling site. Anomalies, morphologically stable sites, and tributary influxes can be avoided by following the general rules. There are various statistical techniques for choosing the locations to collect bottom-material samples. stratified random method, systematic regular method, and stochastic random method are a few of them (Nittrouer et al., 2012).

The most used methods for collecting bed material samples are grab sampling, dredge sampling, and core sampling. Grab samplers are suitable for low-velocity streams and can collect surface sedimentological effectively. In cases where there are shallow bottoms made of sand or clay, a well-designed grab sampler can generate a pressure wave without any leakage. Some frequently used grab samplers include the Van Veen, Ponar, Orange Peel Bucket, and Shipek samplers. When thick sedimentological deposits are needed for physio-chemical analysis, a vertical tubular sampler similar to a core sampler is employed, following the description by Nittrouer et al. (2012).

2.5 Particle Size Distribution Analysis

The size of the particles in sedimentological shows a lot about the fluid dynamics of the environment, minerals, and geomorphic settings. Particle size is a crucial component of sedimentological analysis in the context of hydropower since different particle sizes have varying possibilities for erosion (Chen et al., 2019). Following are some key particle size analysis techniques: the sedigraph technique, the pipetting technique, and the sieve analysis.

- Sieve Analysis Method

This technique, in which sieves of various sizes are stacked in descending order, is one of the earliest and most straightforward ways to analyse particle size distribution. The top sieve is

filled with the weighted sample, which is then vibrated for around five minutes. To determine the particle size distribution, the weight of the silt overall and in each sieve is recorded. Although it is the simplest and easiest method, it cannot provide a high resolution of the particle size distribution or its form (Chinoda et al., 2009).

According to Li and Li (2018), the causes of dynamic processes and grain-size distributions are understood by analysing grain-size distributions and deciphering sedimentological transport systems. Grain sizes were assessed using surface sediments that were gathered from the Pearl River estuary and its surrounding coastal regions. The analysis of end-member models aims to separate the grain sizes into geologically significant populations. There were found to be six end-members of grain size. Their dominant modes, which correspond to coarse, medium, fine, very coarse, silt, and clay, were 0 Ɵ, 1.5 Ɵ, 2.75 Ɵ, 4.5 Ɵ, 7 Ɵ, and 8 Ɵ, respectively. Sediment transport and deposition processes influence the spatial distribution of six distinct end-members. It's possible that the two coarsest end-members, namely coarse and medium sand, represent remnants of sediments deposited during the last glacial period. The presence of the fine sand end-member, which would be challenging to transport during fair weather, likely signifies deposits resulting from storm events.

Park et al., (2022) used a Microtrac 3500, KIGAM, and performed grain size analysis for samples taken from the same depth as the physical property measurements for the fine fraction (> 4 Ɵ). The sand fraction was examined using a Ro-Tap sieve shaker (< 4 Ɵ). The classification techniques of Folk and Ward (1957) and Folk (1965) were used to determine the relative proportions of sand, silt, and clay (1968). This was to analyse part of the physical property characterization of the Nakdong River valley sediments about depositional units.

Bordy and Catuneanu (2001) conducted a sedimentological investigation focused on the top unit of the Tuli Basin, examining the fluvial terrigenous clastic and chemical deposits. The reconstruction of the paleo-environment in the upper unit relied on a comprehensive dataset, including primary sedimetological structures, paleontological records, borehole data, paleo-flow measurements, and stratigraphic correlations. The dominant facies assemblages in this upper level consist of sandstones and finer-grained sediments, occasionally interbedded with subordinate coarser facies within the formation. These facies assemblages in the top level are believed to have formed in an overbank area of a low-sinuosity, ephemeral stream system inhabited by dinosaurs. The deposition of the higher unit occurred during a period characterised by a semi-arid climate and infrequent precipitation, resulting in occasional but destructive flash floods of significant magnitude and low frequency. Current evidence suggests that in a primarily extensional tectonic setting, the paleo-drainage system indicated a flow direction from northwest to southeast.

2.6 Mineralogy

Aydinalp (2012) defined a mineral as "a naturally occurring solid chemical substance that results from biogeochemical processes, possesses a distinct chemical composition, exhibits a well-organised atomic structure, and displays specific physical properties. This definition laid the groundwork for the mineral classification system in use today (Okrusch and Frimmel, 2020).

The crust of the Earth is made up of a variety of rocks, each of which is a composite of one or more minerals. Any naturally occurring solid substance with a particular composition and crystal structure is referred to as a mineral in geology. The types and ratios of the constituent elements that make up a mineral are referred to as the material's composition (Aydinalp, 2012). The arrangement of these components within the mineral defines its structure. There are more than 3,500 different types of minerals. The only elements that are found in the Earth's crust are oxygen (O), Silicon (Si), Aluminium (Al), Fe, Ca, Na, Potassium (k), Magnesium (Mg), Titanium (Ti), Hydrogen (H), Mn, and phosphorus (P). There are trace amounts or very small levels of all other naturally occurring elements (Aswathanarayana, 2003). The most prevalent crustal elements are Si and O, which combined account for more than 70% of its weight. Therefore, it is not surprising that the silicates, such as olivine, and Mg_2SiO_4, are the most prevalent crustal minerals, followed by the oxides (e.g., hematite, Fe_2O_3). Other significant mineral kinds include carbonates (such as calcite, $CaCO_3$), sulphides (such as galena, PbS), and sulphates (e.g., anhydrite, $CaSO_4$). Most of the earth's crust's plentiful minerals have little use for commerce. Metal and nonmetal minerals that are economically useful and serve as raw materials for industry are typically hard to come by. Finding the locations where they exist and extracting them in adequate amounts requires a lot of skill and work (Aydinalp 2012).

Table 2.1: Elements of the Earth Crust (Oyepata and Simeon, 2022)

Element name	Symbol	Percentage by weight of the earth's crust
Oxygen	O	46.6
Silicon	Si	27.7
Aluminium	Al	8.1
Iron	Fe	5.0
Calcium	Ca	3.6
Sodium	Na	2.8
Potassium	K	2.6
Magnesium	Mg	2.1
All other elements		1.5

2.6.1 Property of Minerals

The first step in mineral identification is the examination of its physical characteristics, many of which can be evaluated using a hand sample. These attributes can be categorized into several groups, encompassing measures of mechanical strength (including hardness, tenacity, cleavage, fracture, and parting), visible macroscopic properties (such as lustre, colour, streak, luminescence, and transparency), magnetic and electrical qualities, radioactivity, and solubility in Hydrogen chloride (Aydinalp, 2012).

2.6.1.1 Hardness and Tenacity

The typical method for determining hardness is to observe which common minerals can scratch which materials. Friedrich Mohs created a standard scale in 1812. The following common minerals make up the Mohs hardness scale from 1 to 10 (Zeng et al., 2021).

1. Talc; 2 Gypsum; 3 – Calcite; 4 – Fluorite; 5 – Apatite; 6 - Orthoclase, 7 – Crystal; 8 – Topaz; 9 – Corundum; 10 – Diamond.

The Mohs scale of hardness shows a generally linear progression up to the corundum. However, it's important to note that a diamond is approximately five times harder than a corundum. Alternatively, hardness can be measured on an absolute scale using a sclerometer, and in comparison, to this absolute scale, the Mohs scale displays nonlinearity (Zeng et al., 2021). Tenacity, on the other hand, characterizes how a mineral responds to forces like crushing, bending, or shattering. Minerals can exhibit various tenacity traits, such as elasticity, brittleness, malleability, sectility, ductility, or malleability. The type of chemical bonding within a mineral, such as ionic or metallic, significantly influences its tenacity properties (Nesse, 2012).

2.6.1.2 Cleavage and Parting

Cleavage refers to a mineral's inclination to break along specific crystallographic planes. In crystallographic terms, this property is described by its quality, which can be perfect or fair, as well as the orientation of the plane (Nesse, 2012). Parting, on the other hand, relates to the tendency of weak points within a mineral to separate along planes due to factors like pressure, twinning, or exsolution. When a mineral exhibits neither cleavage nor parting characteristics, it is said to display fracture, which occurs in a less organized manner. Fractures can manifest in various forms, such as fibrous, splintery, hackly (with jagged and sharp edges), or uneven. Conchoidal fracture, for instance, results in smooth, curved surfaces reminiscent of the interior of a shell when the mineral breaks (Nesse, 2012).

2.6.1.3 Lustre and Transparency

A mineral's ability to reflect or transmit light is one of its diagnostic qualities. Transparency refers to being translucent or opaque. Lustre is the name for this quality of reflection. Native metals and many sulphides have metallic lustres, are opaque, and reflect most of the light that strikes their surfaces. Other nearly opaque or opaque oxides might have a drab or resinous appearance. Minerals that are transparent and possess a lower refractive index, such as quartz or calcite, exhibit a glassy appearance and are described as having a vitreous lustre. On the other hand, transparent minerals with a higher refractive index, like diamonds, display a brilliant appearance and are characterised by an adamantine lustre (Aydinalp 2012).

2.6.1.4 Colour and Streak

Colour serves as a reasonably self-explanatory indicator of reflectance. White, grey, or yellow are the three colours of metallic minerals. The oxide and silicate minerals become opaque or highly coloured when transition metals with unfilled electron shells (such as Chromium (Cr), Mn, Fe, Co, Ni, and Cu) are present, which also causes the streak or mark, they make when scratching a white ceramic tile to be highly coloured (Krivovichev, 2020).

2.6.1.5 Unique Properties

Identifying certain minerals may be made much easier by their readily testable, distinctive features. For instance, while sylvite (KCl) and halite (NaCl) or ordinary table salt share many of the same physical characteristics, they taste quite differently when consumed. Sylvite is more bitter (Smith 2016). Magnetism is another distinct characteristic that can be utilised to distinguish between otherwise comparable and opaque minerals. For instance, a magnet test makes it simple to distinguish between the dense, opaque minerals pyrolusite (MnO_2), ilmenite ($FeTiO_3$), and magnetite (Fe_3O_4). Ilmenite is only slightly magnetic, pyrolusite is completely non-magnetic, and magnetite can be permanently magnetized to create a lodestone (Aydinalp 2012).

2.7 Occurrences and Habitats of Minerals

Minerals originate through inorganic processes. In addition to their physical characteristics, one of the most defining aspects of minerals is the geological context in which they are found. Various minerals are linked to specific locations and are formed through different geological mechanisms (Revuelta, 2017).

2.7.1 Igneous Rock

Igneous rocks require minerals with high melting points that can either coexist with silicate melts or crystallize from them at temperatures exceeding 800°C. Volcanic rocks are often classified based on their silica content, with low-silica igneous rocks (typically around 50% SiO_2) being the most common (Cox, 2013). High-silica igneous rocks are known as silicic or acidic, while basic or mafic rocks are referred to as basic or mafic. Examples of basic igneous rocks (BIR) include basalts, dolerites, gabbros, kimberlites, and peridotites. These rocks often exhibit a dark colour due to the presence of minerals like olivine, pyroxenes, Ca-feldspar (plagioclase), amphiboles, and biotite (Cousin et al., 2017). Silicic igneous rocks, such as granites, granodiorites, and rhyolites, typically contain minerals like quartz, muscovite, and alkali feldspars. These rocks are often light in colour, although colour alone is not always indicative of their classification (Bryan and Ferrari, 2013). In addition to basic and silicic volcanic rocks, there is a third category of igneous rock called pegmatite. Pegmatites are characterised by their very coarse-grained texture and have a composition like silicic igneous rocks. They are often rich in silica content and are considered the end products of igneous fractionation (Cox, 2013).

2.7.2 Metamorphic Minerals

Unlike igneous minerals, which must maintain stability at exceptionally high temperatures, minerals found in metamorphic rocks have formed through the crystallization of pre-existing minerals, rather than originating from molten melts. Low-grade metamorphic environments are those with temperatures between 60°C and 400°C and pressures less than 5 GPa (=15 km depth), whereas high-grade metamorphic environments are those with temperatures above 400°C and/or pressures over 5 GPa (Rubatto, 2017). Zeolites, chlorites, and andalusite are minerals that are common in low-grade metamorphic settings. In high-grade metamorphic settings, you can identify the occurrence of minerals such as sillimanite, kyanite, staurolite, epidote, and amphiboles (Gaidies, 2017).

2.7.3 Sedimentological Minerals

Sedimentary rocks are composed of minerals that either remain stable in low-temperature, water-rich environments, such as clays or are made up of high-temperature minerals that are highly resistant to chemical weathering, like quartz. Minerals with high solubility, such as calcite and halite (rock salt), are chemically precipitated and give rise to evaporite deposits. In contrast, minerals that are less resistant to weathering, like feldspars, break down into clays and accumulate in finer-grained siltstones and mudstones (Lippmann, 2012). Sedimentological minerals can be categorised based on their solubility. Therefore, the least

soluble minerals, such as quartz, gold, and diamond, tend to accumulate in coarse Detrital sediments (DSD). On the other hand, evaporites represent a distinct category of sedimentological minerals and include substances like calcite, gypsum, anhydrite, and halite. DSD minerals encompass quartz, gold, diamond, apatite, various phosphates, as well as calcite and clays, while evaporite sediments are characterised by the presence of minerals like calcite, gypsum, anhydrite, and halite (Dill, 2016).

2.7.4 Hydrothermal Minerals

The deposition of intrusive igneous rocks relates to the fourth main mineral environment, hydrothermal, which is composed of minerals precipitated from hot aqueous solutions. This setting is often classified as metamorphic; however, the minerals present in it are distinct enough that it is beneficial to consider the rocks formed through this process and their elemental composition as a separate group. This distinction arises due to the significant differences compared to contact or regional metamorphic rocks (Pirajno, 2012). These can be divided into three categories: oxidised hydrothermal, low-temperature hydrothermal, and high-temperature hydrothermal (Yang and Park, 2019). Sulphides are primarily hydrothermal. However, they can be found in igneous and metamorphic rocks. High-temperature hydrothermal minerals include gold, silver, tungstate minerals, chalcopyrite, bornite, tellurides, and molybdenite. Conversely, low-temperature hydrothermal minerals consist of barite, gold, cinnabar, pyrite, and cassiterite (Aydinalp, 2012). It's worth noting that sulphide minerals are not stable when exposed to atmospheric conditions. They undergo weathering through oxidation, resulting in the formation of oxides, sulphates, and carbonates of chalcophile metals. These minerals are often found in oxidized hydrothermal deposits. Sulphide minerals are particularly vulnerable to instability in the presence of oxygen. Such deposits are known as gossans, and they are characterised by the iron oxide stains left on the rock's surface. Gossans frequently indicate the presence of deep mineralized zones (Fontboté et al., 2017).

2.8 Elements Mineral and Rocks

The interrelationships between elements (at the bottom), minerals (in the middle), and rocks are illustrated in Figure 2.3. Minerals consist of elements, either individually or in combination. For example, crystals like quartz, alkali-feldspar, and biotite contain some of the most abundant elements found in the Earth's crust (Plummer et al., 2012). Rocks, on the other hand, are composed of minerals, either individually or in various combinations. For instance, granite, a common igneous rock in the Earth's crust, typically consists of approximately equal proportions of quartz and alkali-feldspar, often accompanied by biotite and plagioclase (Fletcher, 2011).

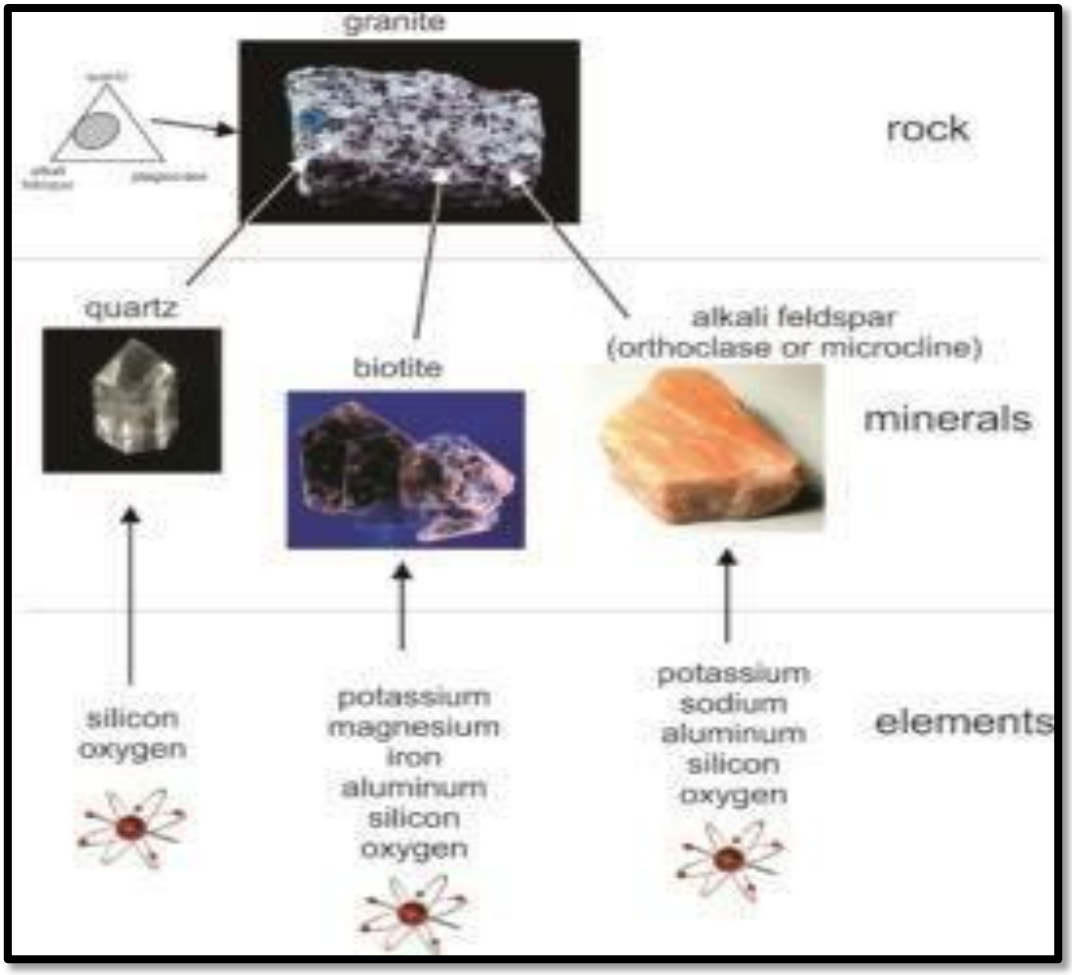

Figure 2.3: Elements, minerals, and rocks (Source: Perkins, 2023)

Every type of rock, including minerals, is composed of one or more elements, which serve as the fundamental building blocks of all matter. While certain minerals, such as diamonds, consist of a single element (carbon), others possess a diverse array of elements. Within the realm of minerals, there are several with inherently consistent compositions. For example, in quartz, the atomic ratio of Si to O is typically nearly 1:2. Other minerals contain elemental substitutions. Therefore, the compositions of different samples may differ greatly. For instance, biotite always contains Si, O, Fe, Mg, and K. Natural biotite compositions are quite variable because they typically also contain smaller amounts of Ma, Na, Ti, and many other elements (Deer, 2011).

The mineralogy at the interface between sediment and water plays a crucial role in controlling the concentrations of trace elements in acid mine drainage. Xie et al. (2018) conducted a comprehensive study combining geochemical and mineralogical investigations in South China's Dabaoshan Mine area. They aimed to establish a quantitative relationship between

iron minerals and heavy metals. This involved sequential extraction experiments and the study of major mineral phases using semi-quantitative XRD, DXRD, and SEM. Their findings revealed that prominent iron-oxyhydroxide minerals, such as schwertmannite, jarosite, goethite, and ferrihydrite, were present in surface sediments along the Hengshi River, and their prevalence increased with rising pH from 2.50 to 6.93. Along this river, there was a decrease in metal concentrations, concurrent with a decline in schwertmannite content, which ranged from 35 weight percent to 6.5 weight percent. The quickly reducible portions of minerals exhibited a greater affinity for metals compared to minerals that are both reducible and generally stable. The retention capacity varied for different heavy elements, with the order being Lead (Pb) > Mn > Zn > Arsenic (As) > Cu > Cr > Cd >Ni, as observed in a qualitative analysis of the heavy metals collected from the sediments.

The Waterberg Group in South Africa comprises four Paleoproterozoic strata, primarily consisting of clastic debris eroded from the Limpopo Belt. Corcoran et al., (2013) conducted a study to investigate the timing of the Limpopo orogeny, which involved the collision of the KaapVaal and Zimbabwe cratons, a geological event that has been a subject of extensive debate among geologists. To uncover the geological history, the researchers utilized various techniques, including point counting, major and trace element geochemistry, and U-Pb detrital zircon geochronology.

Their findings indicated that the sedimentological formations within the study area of the Waterberg Group were primarily sourced from siliceous (rifted margin) sedimentary rocks and minor mafic volcanic rocks of the Archean Beit Bridge Complex in the Limpopo Central Zone. These formations mainly consisted of quartz-rich sandstones, typically beige or brown, with average Quartz-Feldspar-Rock fragments ratios as follows: 80:7:13 (Blouberg), 70:19:11 (Setlaole), 88:5:7 (Makgabeng), and 89:3:8 (Blouberg) in Mogalakwena. Chert and arenite constituted more than 90% of the lithic components across these formations, with occasional small fragments of siliceous gneiss. Remarkably, the Makgabeng dune samples exhibited exceptionally high SiO2 content, ranging from 92% to 99% by weight, despite all formations being enriched in silica. This elevated SiO2 content in the Makgabeng dune samples was attributed to the presence of silica cement and quartz within the rock fragments. In terms of geochemistry, the Mogalakwena Formation, the highest stratigraphically, stood out due to its high levels of Ti and Zr, as well as variations in Rare Earth Elements (REE) patterns within the formation, which were consistent with a mixed provenance. The green and purple sandstones within the Waterberg formations contained the highest abundances of Cr, Ni, Ti, and V despite being minor in volume. This observation supported the idea that these elements were locally sourced from mafic or ultramafic rocks. An analysis of Th/Sc versus Zr/Sc ratios suggested that the sandstones had undergone recycling processes, contributing to

enrichments in Al2O3 compared to Na2O3, CaO, and K2O. The Chemical Index of Alteration (CIA) values, ranging from 57 to 89, indicated extensive chemical weathering of the parent rocks. The presence of both well-rounded and subangular quartz grains further supported their recycled origin. In the lowermost Blouberg Formation, detrital zircons were found with ages ranging from approximately 3379 to 2043 million years ago.

The Orange River, renowned as one of the world's most turbid rivers, annually deposits a staggering 60 million tons of sediment on the western edge of South Africa (Compton and Maake, 2007). This sediment delivery has been ongoing since the fragmentation of the Gondwana supercontinent. Notably, the majority of the Orange River's terrigenous sediment was transported during the warm and humid periods of the middle and late Cretaceous (de Wit, 1999). The upper sections of the Orange River, located above the confluence with the Caledon River, contribute significantly to the river's suspended sediment load. This prompted the need for an investigation into the grain size, mineral composition, and geochemistry of the suspended sediment load. In February 2006, water samples were collected from the Orange River at two locations: upstream of the Aliwal Northbridge and upstream of the Free State Border bridge. These field samples were carefully transported to the sediment laboratory at the University of Stellenbosch for analysis. The analysis involved employing the wet sieving method to determine the sediment grain size, conducting XRD analysis to identify the minerals present in the sediments, and utilising XRF to delve into the geochemical characteristics of the suspended sediment load.

The research conducted by Compton and Maake (2007) produced results indicating that major and trace element ratios strongly suggest that the primary source of the suspended sediment load is the Karoo sedimentary rocks, specifically the upper Beaufort and Stormberg groups, rather than the Drakensberg basalt. Notably, a significant portion of the fine mud suspended load, primarily resulting from the erosion of Karoo sedimentary rock soils, is contributed by the Caledon River. The organic carbon content within the suspended load falls within the range of
1.0 to 1.3 weight %, and the corresponding δ13C values range from -19.7 to -16.90 /00 PDB. These δ13C values indicate a mixture of C3 and C4 vegetation in the catchment area.

In a study conducted by Huang et al. (2020a), the research focused on the highly industrialised river sediments of the Laojie River. The investigation aimed to assess the impact of seasonal fluctuations and spatial distribution on the bioavailability and potential ecological risk of Cu and zinc (Zn) in these sediments. Utilising multivariate statistical analyses and evaluating heavy metal content, pollution indices, and hazard indexes, the study revealed that seasonal fluctuations, especially during the dry season, exerted a significant influence on the levels of heavy metal contamination, pollution indicators, and potential ecological risks. Increased

levels of metal contamination, pollution indices, and ecological risks were observed downstream and midstream of the Laojie River. Cu and Zn were identified as the primary pollutants in the sediments, likely originating from anthropogenic sources. Chemical fraction analysis indicated notable mobility and potential bioavailability concerns for Cu and Zn, particularly in the exchangeable fractions, posing a threat to aquatic life.

Another investigation led by Huang et al. (2020b) focused on the Xiangjiang River, which provides drinking water for the Chinese province of Hunan. This study aimed to assess the pollution levels, contributing factors, ecological concerns, and potential sources of heavy metals in the Xiangjiang River sediments. It was found that all eight heavy metals studied (Zn, Pb, As, Cu, Cr, Ni, Cd, Co) were present in the sediments. Cd pollution was identified as posing significant potential ecological harm. The study indicated that As, Cu, Ni, Pb, and Zn originated from mineral smelting and industrial wastes, while Co, Cr, and Ni were associated with natural sources. The research also highlighted the ecological risks associated with heavy metal pollution in the region.

In a study conducted by Xia et al. (2018), an investigation was carried out on sediments derived from the Wenrui Tang River, situated in an urban watershed located in eastern China. This watershed was characterised by extensive industrialization and unregulated manufacturing activities. The primary objective of this research was to establish a comprehensive understanding of the relationship between land use patterns and the prevalence of heavy metal pollution within the watershed area. The study involved a thorough examination of both the total concentrations and solid-phase fractionation of several heavy metals, including Cu, Zn, Pb, Cr, and Cd, present in the river sediments obtained from the Wenrui Tang River.

To achieve its goals, the research employed advanced analytical techniques, including multivariate statistical analysis and geographically weighted regression methods. The outcomes of this study revealed distinctive spatial patterns of heavy metal contamination across the watershed. Notably, areas in the southwest displayed elevated concentrations of Zn, Pb, and Cd, whereas higher levels of Cu were observed in the eastern region of the watershed. The research identified human activities as the primary contributors to Zn, Pb, and Cd contamination, with Cu originating from both industrial and agricultural sources. Furthermore, the presence of Cr in the sediments was found to be influenced by recent pollution control measures. Overall, this study underscored the significant impact of land use patterns and industrialization on the distribution of heavy metal pollution within the Wenrui Tang River watershed, offering valuable insights for the assessment and remediation of contaminated areas.

Cheng et al. (2021) conducted a mineralogical analysis of sediments sourced from Toson Lake, situated in the north-eastern region of the Qinghai-Tibet Plateau. They employed XRD to investigate the mineral composition of these sediments. The study successfully identified several principal minerals present in the sediments of Toson Lake, which encompassed aragonite, calcite, quartz, halite, albite, muscovite, clinochlore, and dolomite. These minerals were categorized into detrital minerals and carbonate minerals, showing an inverse association between them. The research indicated that Toson Lake was primarily located in a carbonate sedimentological stage, with lacustrine authigenic carbonate contributing to the overall carbonate content.

Cobbing et al. (2008) provide a critical overview of transboundary aquifers (Mozambique/Zululand coastal aquifer, Lesotho/Eastern Free State Karoo aquifer and Limpopo River alluvial aquifer) shared by South Africa, emphasising the need for a modified understanding of transboundary groundwater resources in southern Africa. The study discusses the implications for policy and management of transboundary aquifers, highlighting the importance of technical cooperation, data sharing, and research between riparian states to ensure sustainable utilisation of shared aquifer resources. It aims to address the unique characteristics of transboundary aquifers in South Africa, such as low-yielding aquifers and low population density, which influence the risk of over-pumping or pollution, leading to disputes over shared groundwater resources. An examination of three South African transboundary aquifer systems suggests that each possesses good development potential. However, the development potential of each aquifer needs to be assessed against factors such as surface water/groundwater interactions and groundwater-dependent ecosystems before establishing sustainable utilisation as a transboundary resource. Such assessments will inform the joint development and management of these resources to the mutual benefit of the riparian states. According to reports from the Limpopo River, fortunately, no disputes have yet arisen between the riparian states over the alluvial water resources of the Limpopo River. However, growing pressures for water in this arid region mean that the potential for such dispute cannot be ignored. To avert this situation, water-resource managers in the four countries need to agree on the aquifer characteristics, equitable apportionment of use, and appropriate limits to the use of this shared aquifer resource.

Sitoe et al. (2014) aim to present the results of a multi-proxy analysis on sediment from a relic oxbow lake in the Limpopo River plain, Mozambique, to reconstruct the paleo-environment and past flooding events over the last c. 800 years. It focuses on identifying high-magnitude flooding events through mineral magnetic parameters and grain-size variations in the sediment. The research emphasizes the potential of oxbow lakes and various proxies used in the study for reconstructing past flooding events, which is crucial for flood prediction and

mitigation in Mozambique. The study reconstructed past flooding events in the Limpopo River plain over the last c. 800 years using mineral magnetic parameters and grain-size variations. Four major flooding events were identified during this period, indicating high-intensity river-discharge events in the mid-1200s, late-1300s, mid-1500s, and the last century. The transition of the site from an open oxbow lake to a terrestrial area was reflected in the diatom assemblages, indicating changes in environmental conditions over time. Oxbow lakes and the proxies used in the study show great potential for reconstructing flooding events, which is essential for flood prediction and mitigation in Mozambique.

Kimeli et al. (2021) studied the Umba River basin, a minor hydrological basin in East Africa that spans Tanzania and Kenya. The research aimed to determine the source features, mineralogical and chemical compositions of riverbank as well as bottom sediments in the Umba River. The main minerals identified included quartz, K-feldspars, plagioclase, hornblende, pyroxenes, muscovite, biotite, and clays such as kaolinite. The chemical index of alteration indicated moderate to high levels of weathering of the parent rocks. The geology of the Umba River catchment area featured Palaeozoic Karoo Supergroup rocks dominated by quartz and mafic to intermediate igneous Precambrian basement rocks, overlaid with Mesozoic and Cenozoic sediments. The study suggested that the predominant provenance of sediments in the Umba River catchment area was mafic to intermediate.

2.9 Provenance

In the field of geology, the term "provenance" specifically pertains to the origin of sediments, and this is particularly relevant in sedimentological petrology (Joshi et al., 2021). Sedimentological provenance studies serve the purpose of retracing and comprehensively analysing the journey of sediment particles, beginning from their source rocks in a specific area and culminating in their deposition at a burial site. The central goal of provenance research is to discern the distinctive characteristics of a source area by meticulously examining the composition and texture of sediment. Provenance investigations encompass several critical aspects, including:

- Identifying the sources of the particles constituting the rocks.
- Understanding the mechanisms governing erosion and transportation, responsible for conveying particles from their source areas to depositional sites.
- Evaluating the depositional setting, which entails examining the processes governing sedimentation, also known as the depositional environment.

- Analysing the physical and chemical conditions of the burial environment, as well as the diagenetic alterations that take place within the sediment (Garzanti, 2016; Vermeesch et al., 2016).

Provenance studies are essential for addressing various scientific inquiries, such as unravelling the formation history of continental crust. One common method in provenance research involves employing discrimination diagrams based on the predominant oxide concentrations in sediments and sedimentary rocks to determine the source of sediments from one of four distinct provenance categories:

- Felsic igneous provenance.
- Mafic igneous provenance.
- Intermediate igneous provenance.
- Quartzose sedimentological provenance (Kwankam et al., 2021).

In these studies, key factors such as the nature of source rocks, relief and climate within the source area, tectonic context, the sediment's transport history, and any diagenetic alterations it undergoes all play pivotal roles in determining provenance and are subject to comprehensive examination. These elements could influence how much and how quickly sediment is delivered to the drainage basin and to the systems that convey it. The transformation of source rocks throughout the transportation process has an impact on sediment composition as well (Garzanti, 2016).

2.9.1 Provenance Methods

Provenance analysis methods can generally be categorized into two main groups: petrological methods and geochemical methods. Petrological methods encompass various techniques such as the QFL ternary diagram, heavy mineral assemblages (including indices like the apatite-tourmaline index and garnet zircon index), clay mineral assemblages, illite crystallinity, reworked fossils, palynomorphs, and measurements of stock magnetic properties (Ingersoll, 2012). Please refer to Figure 2.4 for visual representation. On the other hand, geochemical methods include zircon U-Pb dating (along with Hf isotope analysis), zircon fission track analysis, apatite fission track analysis, examination of bulk sediment Nd and Sr isotopes, garnet chemistry, pyroxene chemistry, and amphibole chemistry.

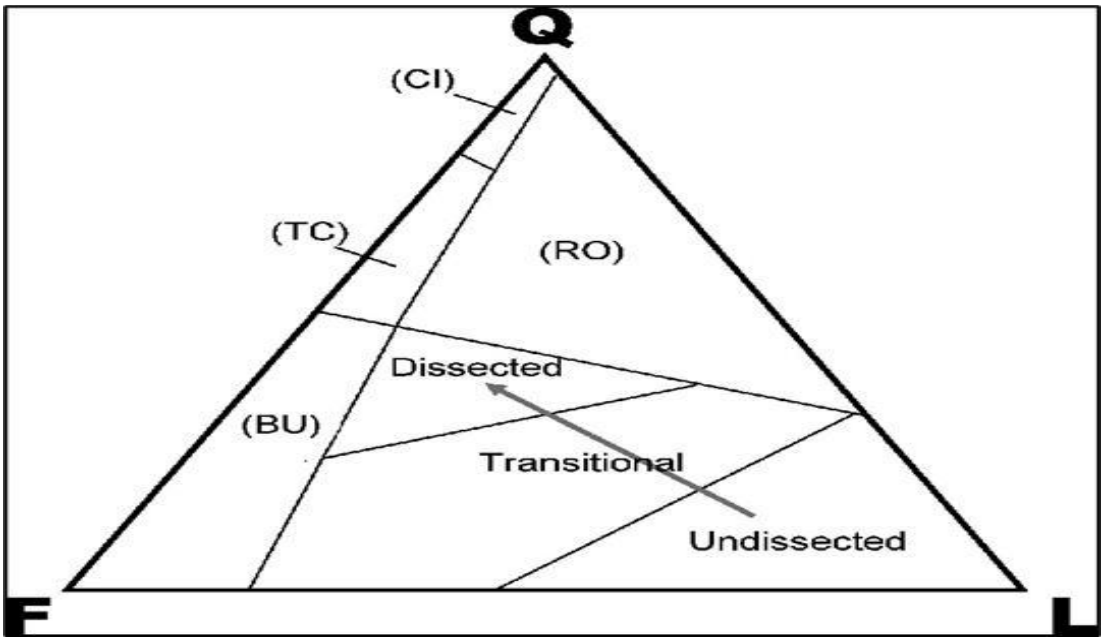

Figure 2.4: QFL Diagram (Source: Kwankam et al., 2021)

2.10 Chapter Summary

This chapter delves into the intricate topic of sediment, encompassing both organic and inorganic materials that are mobilized and deposited by natural geomorphological processes such as aeolian action, glacial movement, gravitational forces, and hydrological systems. The classification of sediments is based on four distinct groups determined by the mechanisms of accumulation they undergo: residual, mechanical, chemical, and organic. Among these groups, water, wind, and glaciers emerge as the primary agents facilitating the transportation of sediment across various landscapes. Fluvial processes, which entail the dynamic interplay of flowing water within riverine and stream environments, play a pivotal role in the sculpting of terrains through the processes of erosion, sediment conveyance, and deposition, thereby giving rise to prominent landforms like canyons and floodplains. Conversely, aeolian processes dictate the movement of sediment under the influence of wind, leading to the configuration of surfaces within arid regions and the formation of distinctive landforms such as dunes. Ice-mediated transport of sediments involves the conveyance of material by glaciers, wherein rocks and minerals are entrained within the ice matrix. Furthermore, the chapter expounds upon particle size distribution analysis as a fundamental methodology employed in the realm of sediment analysis, offering valuable insights into the intricate dynamics of fluid behaviour and the mineralogical composition of sedimentological deposits.

CHAPTER THREE: METHODOLOGY

3.1 Introduction

This chapter outlines the research methodology employed in this study. It encompasses the procedures undertaken to achieve the primary goals and objectives, which encompass both fieldwork activities (such as field description and sample collection) and laboratory work aimed at assessing mineral composition, sediment characteristics, and their origins. The methods employed encompass sieve analysis, XRD analysis, microscopic analysis, and XRF analysis. Figure 3.1 provides a comprehensive overview of the study's conduct and procedures.

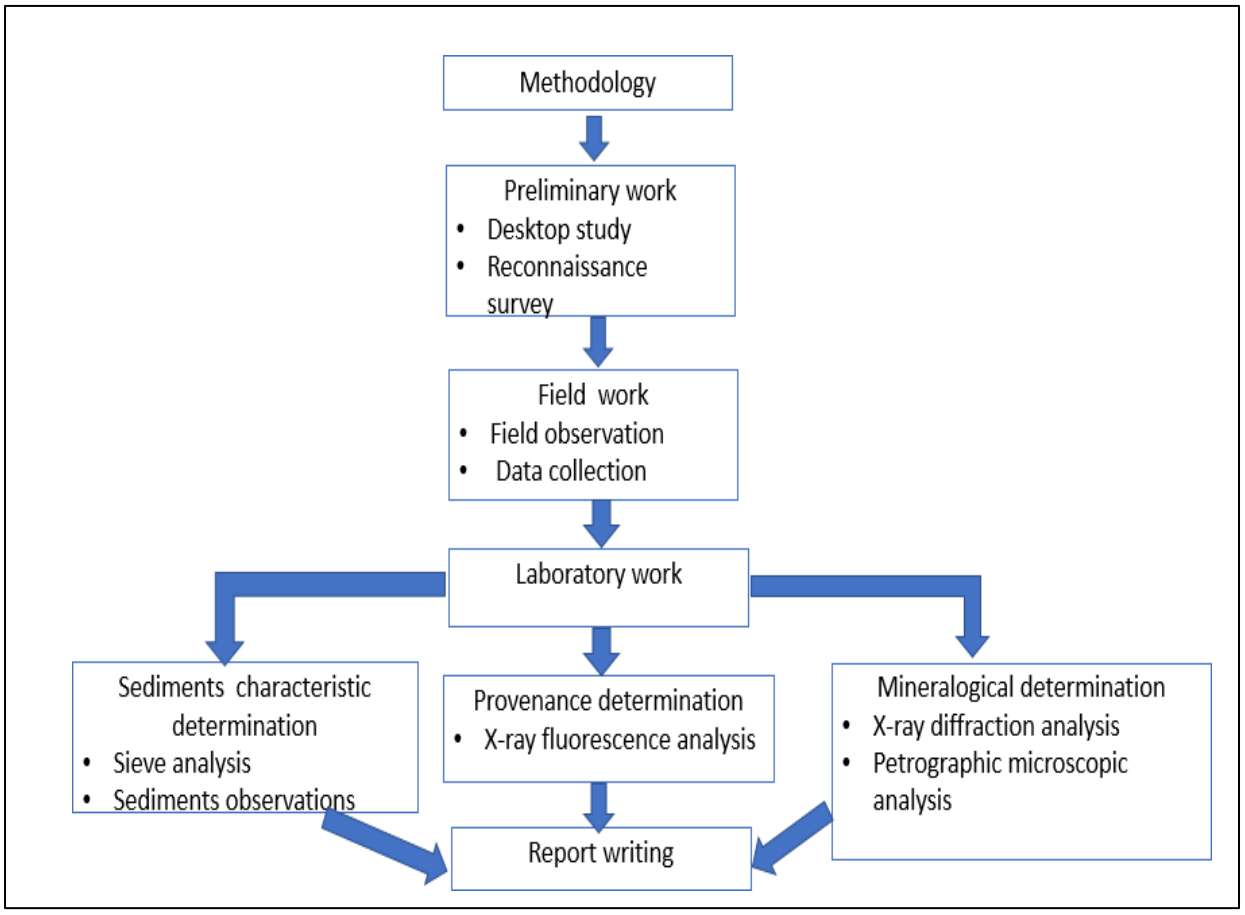

Figure 3.1: Methodology Framework

3.2 Preliminary Work

3.2.1 Desktop Study

The desktop study involved preliminary preparations for fieldwork. This included a thorough examination of satellite imagery and topographical maps to better understand the environmental conditions in the study area and to establish an effective sampling framework.

Additionally, extensive research was conducted by reviewing journal articles and government websites to gather ample information concerning the physical attributes of sands along the Limpopo River at Beit Bridge.

3.2.2 Reconnaissance Survey

During the two-week reconnaissance survey, the study area was thoroughly explored to gain familiarity with the physical environment of the Limpopo River sediments at the Beit Bridge. The water level was closely observed and evaluated to ensure the safety of the researcher during the sampling process. Furthermore, the researcher identified suitable sampling points within the study area.

3.3 Sampling Procedure

According to Baranya and Józsa (2013), sampling is a process in statistical analysis where researchers take a predetermined number of observations from a larger population. Sampling allows researchers to conduct studies about a large group by using a small portion of the population. There are different types of sampling, in this case, purposive sampling was used. Baranya and Józsa(2013) define purposive sampling as a group of non-probability sampling techniques in which units are selected because they have characteristics that you need in your sample. In other words, units are selected “on purpose” in purposive sampling. The Limpopo River basin connects four nations: South Africa, Botswana, Zimbabwe, and Mozambique. The sediment samples were collected between South Africa and Zimbabwe border at Beit Bridge (Figure 3,3). The location was chosen because it is the confluence of all the tributaries upstream into the Limpopo River. This was to ensure the geochemical and mineralogical characteristics of Limpopo River Basin sediments upstream of Beitbridge were covered (Figure 3.4). The study area was divided into five stations and the selected stations were 100 m apart from each other. The 5 sampling Stations represent one large sample that would be collected since all tributaries upstream converge at Beit Bridge. Therefore, these samples give an indication of the composition of the material coming from upstream. (Figure 3.5). The station points were purposively selected, guided by the identification of sandbars for the safety of the researcher and to avoid drowning in high water levels (Figure 3.2). The researcher also avoided areas close to the riverbank this was to avoid sampling sediments deposited by nearby streams and not necessary streams forming the Limpopo River upstream of Beit Bridge which could have affected the geochemical and mineralogical analysis of Limpopo River basin sediments upstream of Beitbridge. Sediment samples were collected in the Beit Bridge area from each of the five stations. A shovel was used to collect the representative samples.

Collected samples were placed in clean plastic bags and then taken to the laboratory for analysis (Figure 3.3). Table 3.1 gives the coordinates of the sampling points.

Figure 3.2: Limpopo River Sediments at Beit Bridge

Figure 3.3: Limpopo River Basin Sediment Sampling

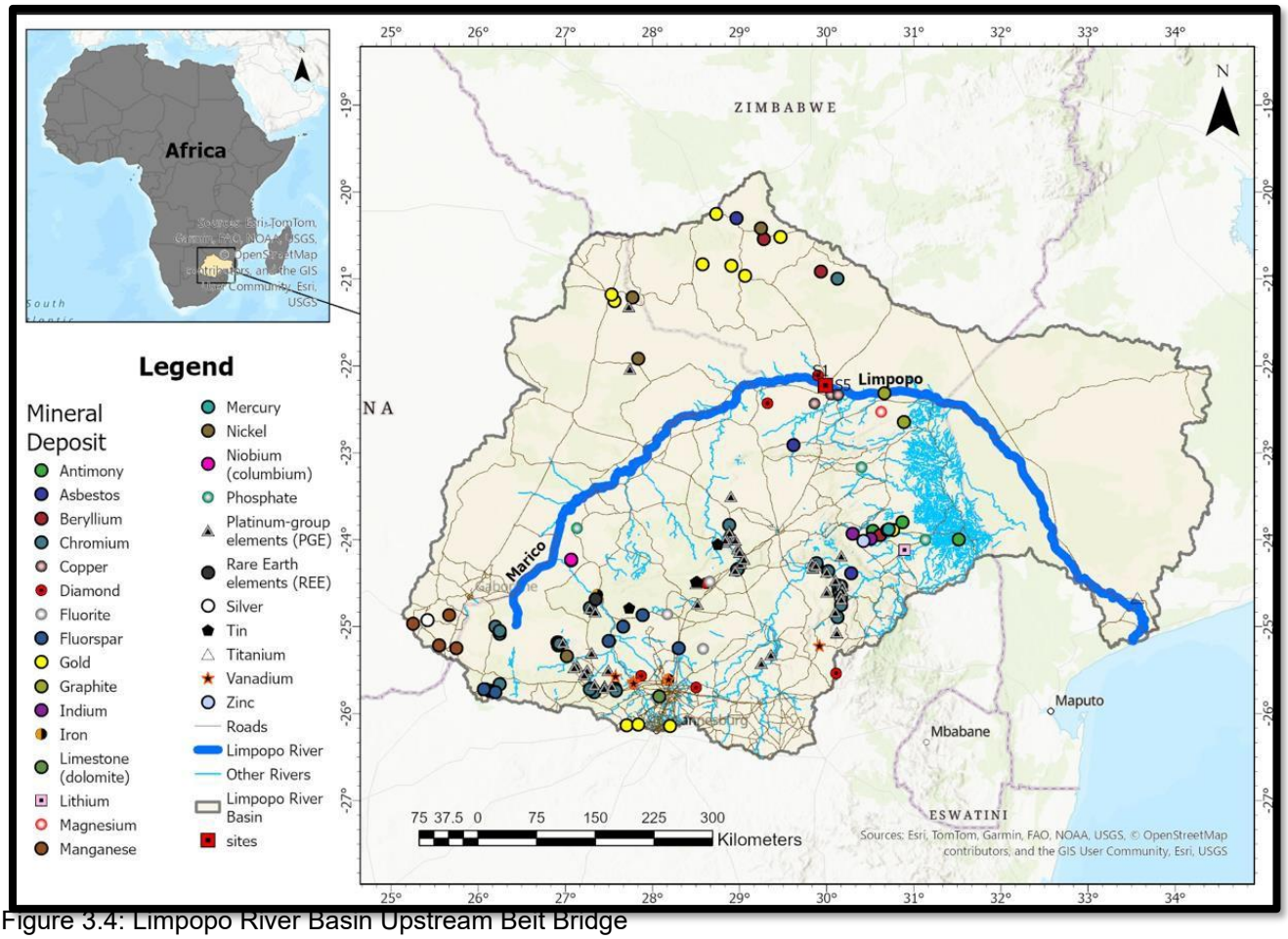

Figure 3.4: Limpopo River Basin Upstream Beit Bridge

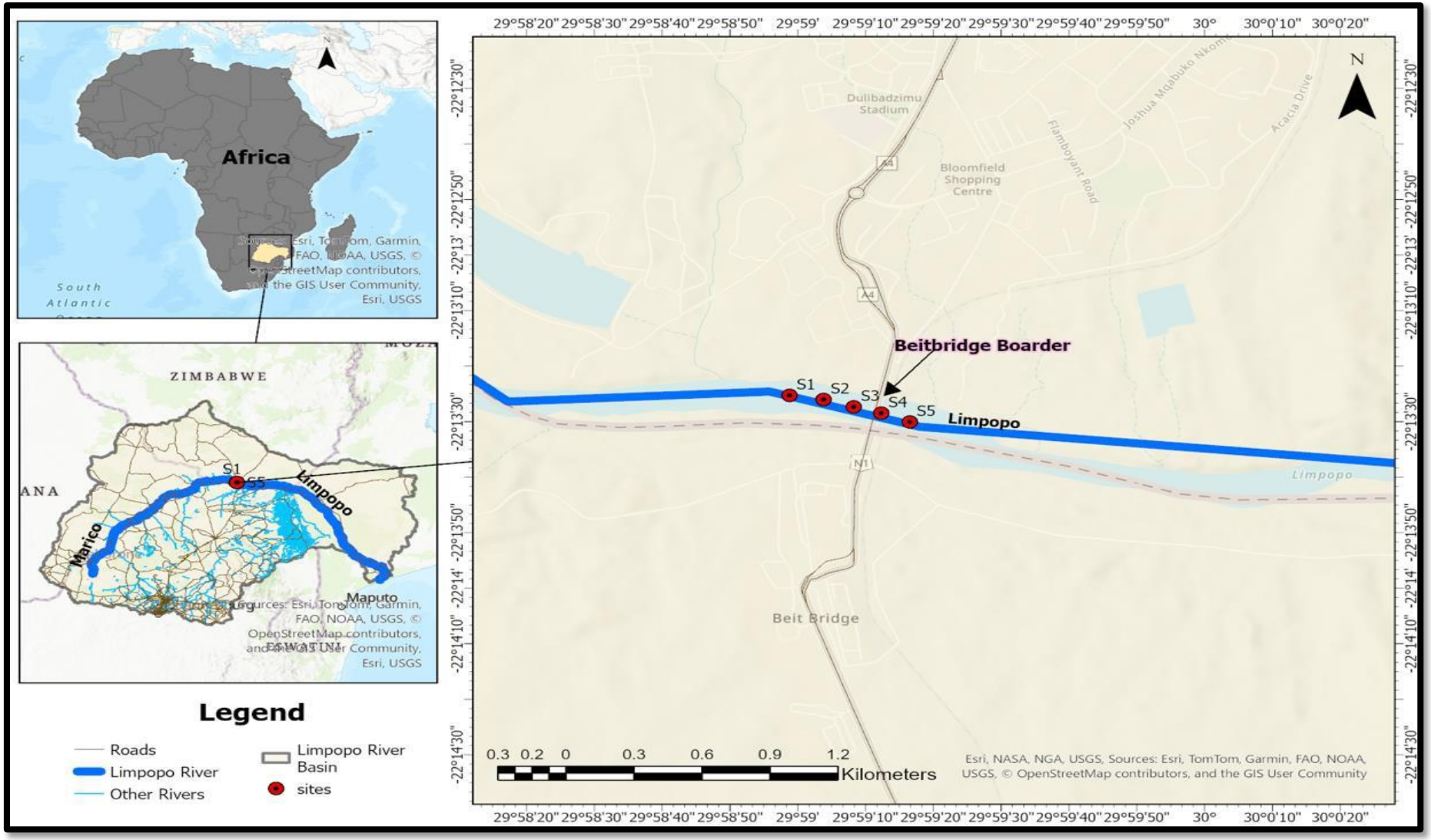
Africa
South Atlantic
ZIMBABWE
ANA
S1
S5
Limpopo
Marico
Maputo
Legend
Roads
Limpopo River
Other Rivers
Limpopo River Basin
sites
Beitbridge Boarder
S1
S2
S3
S4
S5
Limpopo
Dulibadzimu Stadium
Bloomfield Shopping Centre
Flamboyant Road
Joshua Mqabuko Nkomo
Acacia Drive
N1
A4
Beit Bridge
0.3 0.2 0 0.3 0.6 0.9 1.2
Kilometers
Esri, NASA, NGA, USGS, Sources: Esri, TomTom, Garmin, FAO, NOAA, USGS, © OpenStreetMap contributors, and the GIS User Community
29°58'20" 29°58'30" 29°58'40" 29°58'50" 29°59' 29°59'10" 29°59'20" 29°59'30" 29°59'40" 29°59'50" 30° 30°0'10" 30°0'20"
-22°12'30" -22°12'50" -22°13' -22°13'10" -22°13'30" -22°13'50" -22°14' -22°14'10" -22°14'30"

Table 3.1: The coordinates of the Sampling points

Station Points	X -Coordinates	Y-Coordinates
1	29.982999472000074	-22.223690153999939
2	29.984391579000032	-22.223895818999949
3	29.985629181000036	-22.224263332999953
4	29.986757841000042	-22.224578380999958
5	29.987924401000043	-22.225018588999944

3.4 Laboratory Work

Sample preparation took place at the Department of Mining and Environmental Geology at the University of Venda. Additionally, the samples were transported to the XRD Analytical and Consulting cc Lab in Pretoria for XRD analysis. These samples underwent preparation processes for various analyses, including sieve analysis, XRD, petrographic microscopic analysis, and XRF for metal content analysis. The major and trace element values were assessed using Pearson correlation coefficients, and this analysis was conducted using Excel as a tool.

3.4.1 Sedimentological Characteristics Determination (Sieve Analysis)

The Sieve analysis technique was used for this study. Sieves with varying sieve opening sizes ranged from 20mm to 0.063mm in diameter in a stacked configuration. The finest sieve is placed at the bottom of the stack, and each successive sieve is positioned on top in increasing order of sieve size. Sieve analysis is a versatile method that can be used to evaluate the particle size distribution of various types of granular materials, whether they are organic or inorganic (Wawrzeńczyk and Molendowska, 2019; Li and Li, 2018).

The following apparatus and tools were used for the analysis. A mass balance was used to weigh all samples used in this research; the acceptable initial mass ranged from (2000.0 g-2000.1 g). A set of Standard Sieves (20mm, 10mm, 5mm, 2mm,1mm ,0.5mm, 0.25mm, 0.125mm and 0.063mm) in diameter. A sieve brush for cleaning sedimentological stuck on the sieve sets after each sample analysis, a mechanical sieve shaker, a drying oven capable of maintaining a temperature of 110℃, 2 trays (150 X 200 mm) and 45 sample bags to place the different sizes of sedimentological after the sieve analysis.

The samples underwent an initial drying process in an oven at 110°C for 24 hours, as depicted in Figure 3.6. This step was essential to eliminate any moisture content from the samples

before conducting the sieve analysis. Subsequently, the dried samples were allowed to return to room temperature over approximately 2 hours. It was imperative to air dry the sediments to prevent the formation of clumps of fine particles and to avoid clogging the finer sieves. To facilitate the analysis, the mass of the weighing tray was recorded, and then the combined mass of the weighing tray and the sediment samples was also recorded (Figure 3.8). These measurements were crucial for calculating the natural moisture content of the samples using Equation 3.1.

$$W\% = \frac{W2-W3}{W3-W1} \times 100 \quad \text{.....3.1}$$

Where:

W% = the water content of the sample, W1 =

the mass of the weighing can,

W2 = the mass of the moist sediment and W3 =

the mass of the dry sediment.

Figure 3.6 Drying Oven

Furthermore, a gradation test was conducted on a sample of aggregates within the laboratory setting. A representative portion of the aggregates was accurately weighed and then poured

into the uppermost sieve, which featured the largest screen openings (20mm). Each subsequent sieve in the stack had progressively smaller openings than the one above it. At the bottom of this arrangement was a circular pan referred to as the receiver. Particles with a diameter smaller than the mesh opening (0.063mm) would pass through the sieve and collect in the pan.

To facilitate the sieving process, the entire column of sieves was placed onto a mechanical shaker, as depicted in Figure 3.7. The mechanical shaker was programmed to shake the column for 45 minutes per sample. This selected time frame of 45 minutes was deemed adequate to ensure a thorough and complete sieving process (Li and Li, 2018). After the shaking process was finished, the material present in each sieve was weighed. The mass of the sample retained on each sieve was then divided by the total mass to calculate the percentage of material retained on each sieve. Subsequently, an analysis of the average particle size within each sieve was conducted to establish specific size ranges, which were then documented on a screen or graph. Following the shaking of the sediments on a mechanical shaker, the masses of sediments retained on and passing through each sieve were carefully weighed and recorded, as depicted in Figures 3.8 and 3.9. To determine the percent finer for each sieve size, Equation 3.2 was employed in the calculations.

$$F = \sum M - \frac{(M1 + M2 + \cdots Mi)}{\sum M} \quad \text{..... 3.2}$$

Where:

$\sum M$ = the Summation of the cumulative mass retained in each sieve,

$(M1 + M2 + \cdots Mi)$ = the cumulative mass of sediment retained above each sieve and

F = the percent finer on each sieve size.

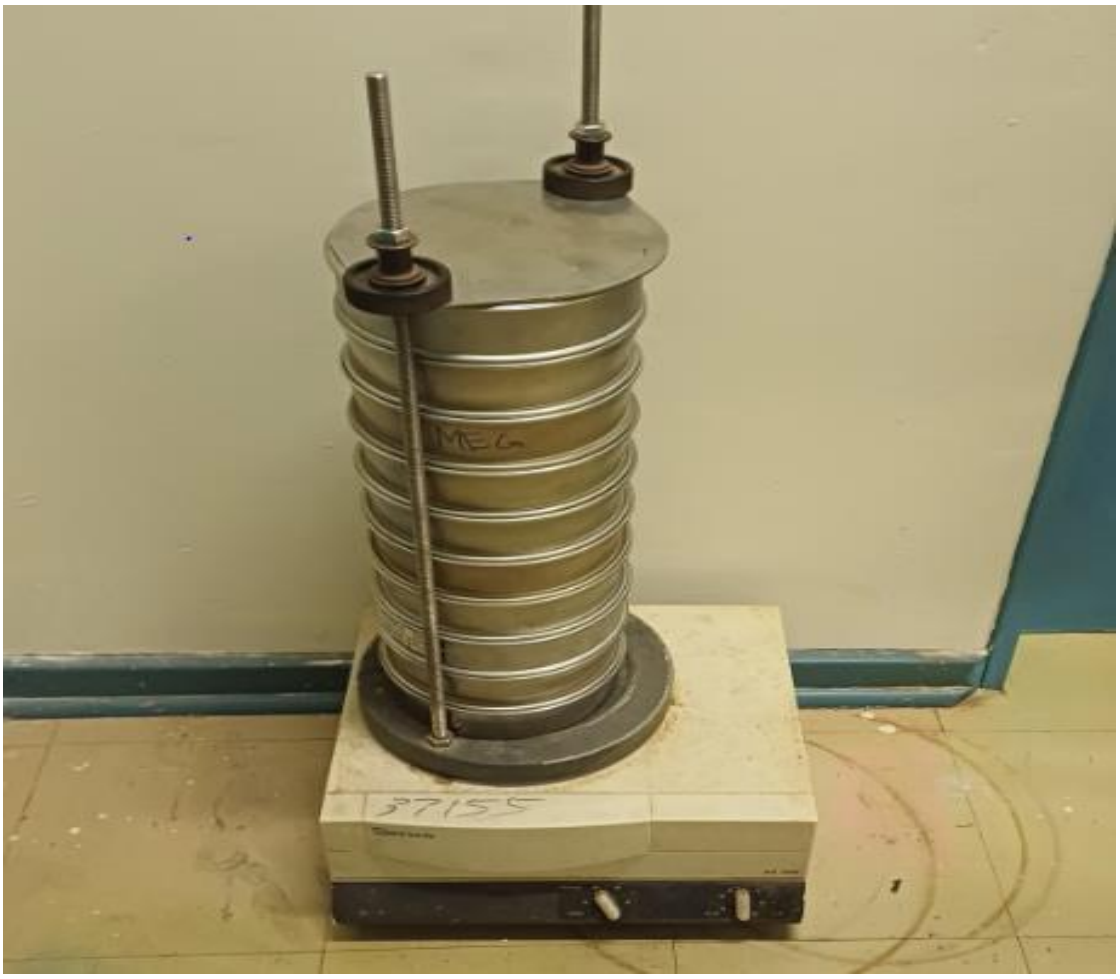

Figure 3.7: Mechanical Sieve with Stack Columns of Different Sizes

Figure 3.8: Mass Balance

Figure 3.9: Different Sedimentological Sizes after Sieving

The sieve data analysis results were further represented through semi-logarithmic plots, commonly known as gradation curves. These curves depicted the relationship between grain size (x-axis) and the percentage of material passing through the sieve (y-axis). To provide a clearer visualisation of the particle size analysis, the x-axis was scaled logarithmically. From these gradation curves, essential engineering parameters such as D10, D30, and D60 were determined. D10 signifies a crucial parameter, indicating that according to the particle distribution curve, 10% of the particles are finer, while 90% are coarser than D10. Similarly, D60 represents the particle size where 60% of the particles are smaller by weight, leaving 40% larger. Likewise, D30 denotes the particle size at which 30% of the particles are smaller by weight, while the remaining 70% are larger. The values obtained from D10, D30, and D60 were then utilised to calculate additional parameters such as the Coefficient of Uniformity (CU), the Coefficient of Curvature (CC), and the Gradation Value (CG).

The CU is calculated as the ratio of D60 to D10, as defined by Equation 3.3. A CU value falling within the range of 4 to 6 Xie et al. (2018), indicates that the sediments are well graded. According to Xie et al. (2018), well-graded sediments encompass a variety of particle sizes,

demonstrating a favourable distribution of particle sizes. In contrast, uniformly graded sediments feature consistent particle sizes. Sediments with a CU value less than 4 are categorized as either poorly graded or uniformly graded. The CC is determined using Equation
3.4. To be considered well-graded, the CC value must fall within the range of 1 to 3. The CG was computed based on Equation 3.5. The grading curve of a specific sediment type is characterised by three geometric properties: CC, CG, and CU. These properties collectively provide insights into the particle size distribution within the sediment.

$$CU = \frac{D60}{D10} \quad \text{.....3.3}$$

$$CC = \frac{D30}{D60 \times D10} \quad \text{.....3.4}$$

$$CG = \frac{D30^2}{D60 \times D10} \quad \text{.....3.5}$$

3.4.2 Determination of Mineralogical Characteristics

Mineral characterization and identification involved the assessment of the samples' physical and chemical properties. X-ray diffraction was used to analyse and gain insights into the mineral composition of the sediments. Furthermore, thin sections were prepared and employed for microscopic analysis. These analytical techniques were employed to ascertain and detail the mineralogical composition of the river sediments.

The experiment involved the use of various apparatus and tools, including 15 parts resin, 2 parts hardener, a micrometre gauge, a Bushler Petro Thin Section System, a Streuers Accutom-50 cutting machine, a Potopol-35 polishing machine, an Olympus BX51 petrographic microscope, an X-ray diffraction machine, a Vacutec drying oven, and grit. These tools and equipment were utilised throughout the experiment to conduct different tasks and measurements.

3.4.2.1 Petrographic Microscopic Analysis

Before the microscopic examination, the samples were prepared for thin sections. A thin-section analysis was conducted on sediment samples to examine their mineral composition, texture, and fabric at a microscopic level. Thin sections are extremely thin slices of sediment samples that are mounted on glass slides and viewed under a petrographic microscope. The thin section analysis provides valuable information about sedimentological processes, depositional environments, diagenetic alterations, and the history of the sediment. It helps in identifying sedimentary rock types, determining grain size distribution, assessing the degree of sorting, and examining features like sedimentological structures, cementation, and porosity.

The detailed examination of thin sections aids in the interpretation of sedimentological processes, geological history, and the formation of sedimentological deposits and bonding samples, cutting of bonded samples, grinding, and polishing (Stoops, 2021).

The first step of preparing a thin section was to analyse for hardening of sediments. Since the researcher was dealing with loose sediments, the loose sediments were grouped according to their sieve sizes. The resin was then used to harden the loose sediments into solid rock. The samples were left to dry for 10 days for effective hardness (MacKenzie, 2017). After the hardening process, the samples underwent cutting using a Bushler petro-thin sectioning system, resulting in smaller sizes. These samples were transformed into rectangular blocks measuring approximately 50 x 80 mm (as depicted in Figure 3.10). Subsequently, these rectangular blocks were further refined to dimensions of 30 x 40 mm using Streuers Accutum-50 equipment. To achieve a smooth surface suitable for the bonding process, the blocks underwent polishing with Si carbide grit in a sequence of 120, 220, 400, and 800 grit sizes. Once polished, the samples were meticulously cleaned with deionised water. Following the cleaning step, they were subjected to a 15-minute drying period at room temperature in a Vacutec drying oven. Afterwards, the samples were allowed to cool down to room temperature before proceeding with the bonding process.

In the sample preparation process, epoxy was employed as a bonding solution. This involved the meticulous mixing of hardener and resin in a specific ratio of 2 parts hardener to 15 parts resin. To securely affix the samples onto frosted glass slides, the epoxy bonding solution was utilised. These bonded samples were then placed on a bonding jig for 24 hours, ensuring a strong and stable connection (MacKenzie, 2017). Following the bonding phase, the samples underwent an initial cutting step to reduce their thickness from 40 mm to 10 mm. This cutting process was carried out using the Streuers Accutum-50 cutting machine and typically lasted approximately 8 to 20 minutes per sample. Subsequently, the samples were subjected to grinding to achieve a fineness of 50 micrometres, a procedure that took around 30 minutes. The instrument's programming allowed for the grinding process to be carried out automatically, stopping when the desired fineness was attained.

Figure 3.10: A Bushler petro-thin sectioning system for cutting during the thin section preparation

Figure 3.11 A Streuers Accutum-50 cutting machine for cutting the samples for thin section preparation

The last phase in the thin section preparation process involved polishing. The ground samples were positioned within a RotoPol-35 polishing machine, utilising the appropriate polishing disk, and underwent polishing for an estimated two hours, following the guidelines provided by Pike and Kemp in 1996 (Figure 3.12).

Subsequently, the thickness of the prepared samples was carefully examined using a micrometre gauge to ensure they met the required thickness criteria, which was approximately 30 µm or less. Once all these steps were completed, the meticulously prepared thin sections were then subjected to petrographic microscopic analyses for mineral identification and characterisation.

Figure 3.12: The RotoPol-35 polishing machine used during the thin section preparation

In this context, an Olympus BX51 petrographic microscope was used. This particular microscope is known for its versatility and is equipped with various features and components. As described by MacKenzie (2017), the Olympus BX51 microscope incorporates multiple light sources, including transmission, reflection, and metal halide, enhancing its adaptability. Furthermore, it is equipped with a Nomarsky filter that enables the application of differential interference contrast (DIC) microscopy. The microscope utilises the Microscope Objective Lenses for Industry, which are specially designed to deliver high-quality imaging across a range of microscopy techniques. These techniques encompass darkfield, brightfield, DIC, polarized light, and fluorescence microscopy, making the Olympus BX51 a versatile instrument for various analytical purposes. (MacKenzie, 2017).

From a technological perspective, microscopes exhibit diverse designs, encompassing variations not only in their physical appearance but also in the arrangement and functioning of crucial components. In this study, an Olympus BX51 petrographic microscope was used. According to MacKenzie (2017), the Olympus BX51 microscope stands out as a versatile instrument, equipped with multiple illumination sources, including transmission, reflection, and metal halide light sources. Notably, it is equipped with a Nomarsky filter, facilitating the application of DIC microscopy. What further distinguishes the Olympus BX51 petrographic microscope is its MPLFLN-BD lenses, which are specially crafted to deliver exceptional imaging quality across a range of microscopy techniques. These lenses are optimized for various applications, including darkfield, brightfield, DIC, polarised light, and fluorescence microscopy, enhancing the microscope's versatility and usability for different research purposes (MacKenzie, 2017).

During the analysis, thin sections of samples were observed using the Olympus BX51 microscope. The thin section was placed under the microscope and minerals were observed on the thin sections through a microscope eyepiece. This enabled the researcher to characterise the mineralogy of Limpopo River sediments (Figure 3.13). XRD was also used to analyse and understand the mineralogy of the sediments. According to Stoops (2021), XRD analysis is one of the vital analyses for determining mineralogical characteristics. The analysis identifies different minerals in any sample. The collected samples were transported to the XRD Analytical and Consulting cc Lab in Pretoria, South Africa, where they underwent preparation and analysis procedures.

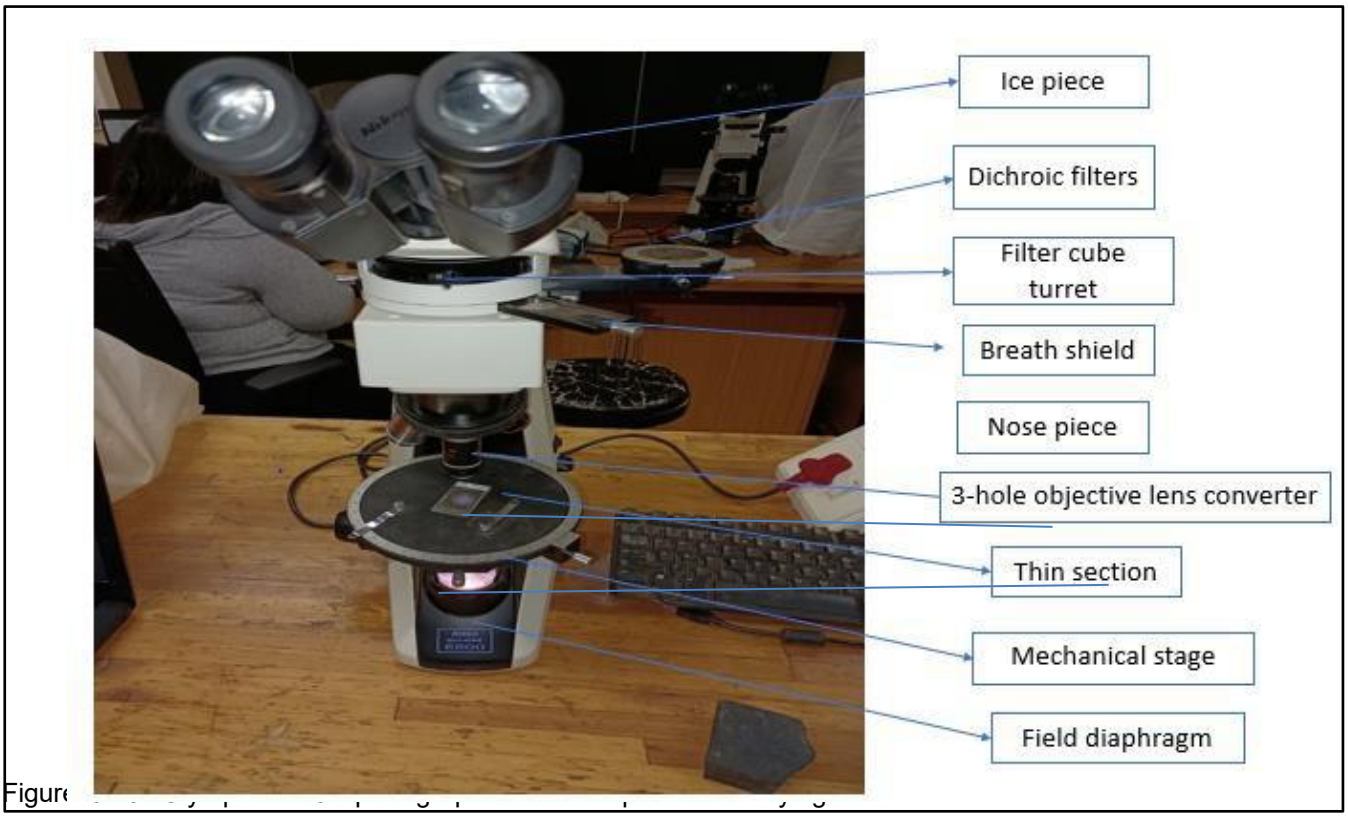

Figure

preparation

3.5 Metal Content Analysis

Metal content analysis involves the identification and quantification of minute quantities of metals, including heavy metals, within a sample. In this specific instance, XRF was employed to determine trace metal levels present in sediments from the Limpopo River near Beit Bridge. XRF, as depicted in (Figure 3.14), is a non-destructive analytical technique utilized to determine the elemental composition of substances. XRF analysers measure the secondary X-ray emissions (fluorescence) emitted by a sample when it is stimulated by a primary X-ray source, enabling the determination of the sample's chemical composition. Using XRF spectroscopy, the composition of materials can be qualitatively and quantitatively examined. This technique relies on the detection of distinct collections of characteristic fluorescent X-rays emitted by the elements present in a sample, which can be seen as individualized "fingerprints." The results from the XRF were analysed using the Pearson correlation coefficients.

The sediment samples were already ground to fine grain sizes from different sediment samples collected. The sediment samples, already ground to fine grain sizes, were collected from various locations. Each sample was analysed in triplicate, with an average analysis time

of approximately 30 minutes per sample. The Polyvinyl chloride (PVC) rings were washed thoroughly with soap and water and rinsed with iodised water (Figure 3.15). Then, the sediment samples were placed in each PVC cup and labelled (Takahashi, 2015). The PVC cups with the samples were then sealed with a transparent film covering and a PVC ring that held the films in place. The prepared PVC-sealed cup with the samples was then placed in the XRF until the readings from the XRF were concluded, refer to (Figure 3.16). For the experiment, several apparatus and tools were utilised, including 5 PVC cups, 5 transparent films, 5 PVC rings, and X-ray fluorescence. These items were employed in the experimental setup to facilitate the research process and data collection.

Figu

Figure 3.15: Pouring of Sediment samples into the PVC cup during the XRF sample preparation

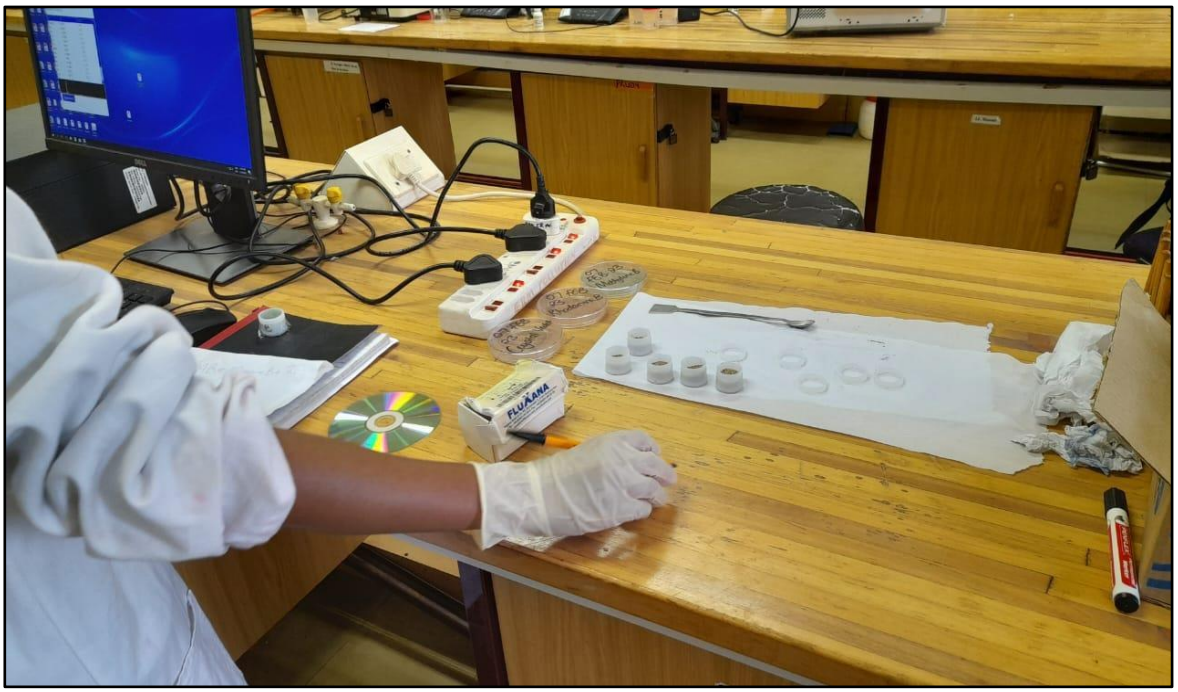

Figure 3.16: During the preparations of the sample for the XRF analysis

To assess the extent of weathering that contributed to the formation of sediments, we can employ geochemical analysis focusing on major element data and several key indices. The Chemical Index of Alteration (CIA), Chemical Index of Weathering (CIW), and Plagioclase Index of Alteration (PIA) are particularly useful in this regard (Corcoran et al., 2013).

The CIA and CIW indices serve as valuable tools in gauging the extent of chemical weathering that has affected the rocks under study. A higher value for either the CIA or CIW indicates a more significant level of weathering that has taken place over time. In contrast, the PIA is specifically designed to evaluate the alteration of plagioclase, a mineral commonly found in various types of rocks. Researchers can obtain a more profound insight into the weathering mechanisms that have influenced the source rocks and the environmental conditions that were predominant during their initial formation through the utilisation of these indices (Atabo and Sunday, 2020; Odigi and Amajor, 2009).

The Chemical Index of Alteration (CIA) was used to evaluate the degree of weathering. The CIA index serves the purpose of quantifying the level of alteration undergone by minerals, with a focus on the transformation of feldspar into aluminous weathering products (Jian et al., 2013). The CIA ratios observed in feldspar and unaltered source rocks tend to hover around the value of approximately 50, indicative of a moderate degree of weathering, whereas, in the case of residual weathering products like kaolinite and gibbsite, these ratios can escalate to as high as 100, signifying a more advanced stage of alteration. The calculation of this index is facilitated through the consideration of molecular proportions, as outlined in Equation 3.6, which provides a systematic and quantitative approach to assessing the chemical changes occurring within a given geological system (Nesbitt and Young, 1982; Chaudhuri and Brookins,1979).

$$CIA = [Al_2O_3/ (Al_2O_3+CaO^* +Na_2O+K_2O)] \times 100 \quad \text{3.6}$$

Where CaO* is the CaO residing only in the silicate fraction. High CIA values reflect the removal of mobile or unstable cations (Ca, Na, K) relative to highly immobile or stable residual constituents (Al, Ti) during weathering. Conversely, low CIA values indicate a near absence of chemical alteration and consequently may reflect cold and/or arid conditions. CIA = 50 - 60 indicates an incipient weathering, CIA = 60 - 80 an intermediate weathering, and CIA > 80 extreme weathering.

Chemical Index of Weathering (CIW) effects can also be evaluated using the CIW in molecular proportions identical to the CIA, from Equation 3.7:

$$CIW = Al_2O_3/ (Al_2O_3+CaO^* +Na_2O)] \times 100 \quad \text{3.7}$$

The CaO* residing exclusively in the silicate fraction is denoted as CaO* in this context. The utilization of this equation proves to be more suitable for grasping the magnitude of plagioclase alteration in isolation, as K2O is deducted from Al2O3 in both the numerator and denominator of the CIA equation. Nevertheless, scholars such as Fedo et al. (1995) have contended that the application of the CIW calculation for quantifying the intensity of chemical weathering may be unsuitable and should be approached with prudence. This caution is warranted due to the equation yielding values of 80 for unweathered potassic granite, and values nearing 100 for clay minerals like kaolinite, illite, and gibbsite. These values are similar to those observed for residual products of CIW for minerals such as smectite (80), kaolinite, illite, and gibbsite (100). Both the CIA and CIW metrics are construed similarly, with an assigned value of 50 denoting unaltered upper continental crust (UCC) and approximately 100 indicating highly weathered substances where alkali and alkaline-earth elements have been entirely leached out (Atabo and Sunday, 2020).

Plagioclase Index of Alteration The degree of the chemical weathering can be estimated using the PIA modified from the CIA equation to monitor plagioclase. The PIA is calculated according to the following equation in molecular proportions (Roy and Roser 2013):

PIA = 100 × (Al2O3 - K2O) / (Al2O3 + CaO* +Na2O - K2O) 3.8

Where CaO* is the CaO residing only in the silicate fraction. A significant point to consider is that the PIA values exceeding 84 are indicative of a high degree of chemical weathering processes having taken place, thereby suggesting a more intense level of alteration. Conversely, PIA values that are closer to around 50 are associated with unaltered or freshly obtained rock samples, indicating a lesser degree of weathering (Jian et al., 2013). This distinction in PIA values serves as a useful metric in assessing the extent of weathering undergone by the samples under investigation. Specifically focusing on the Post-Archean Australian Shales (PAAS) in this context, it is noted that these shales exhibit a PIA value of 79, falling within the range that suggests a moderate level of chemical alteration (Wang et al., 2020).

3.6 Chapter Summary

This chapter delineates the methodological approach employed for the examination of the mineral constitution and sediment attributes prevalent in the vicinity of Beit Bridge along the Limpopo River. The methodologies encompassed various analytical techniques such as sieve analysis, X-ray diffraction (XRD), microscopic scrutiny, and X-ray fluorescence (XRF) analysis. The commencement of the study entailed a comprehensive literature review and preliminary field survey to amass pertinent data and pinpoint suitable sampling locations. The

sediment specimens were procured from five designated stations, meticulously processed, and subjected to thorough scrutiny within the confines of the laboratory setting. The utilization of sieve analysis facilitated the determination of particle size distribution, while XRD analysis was instrumental in discerning the mineral composition, and XRF analysis provided insights into the metal content present. Additionally, a microscopic examination was carried out to delve into the intricate mineralogical properties. The methodological framework seamlessly amalgamated both field-based data collection efforts and sophisticated laboratory methodologies to explore the nuanced sediment characteristics in the proximity of Beit Bridge.

CHAPTER FOUR: SEDIMENTOLOGICAL AND PETROGRAPHIC PROPERTIES OF THE SEDIMENTS

4.1 Introduction

This chapter presents and discusses the results obtained from the mechanical and petrographic analyses of the sediments collected from the Limpopo River at Beit Bridge. This chapter addresses the objectives 1 and 2 of the study. In addition, results from the engineering parameters, including the coefficient of uniformity, gradation, sorting, and particle size distribution were discussed extensively. Moreover, the results of the mineralogical composition of the samples were discussed extensively. Furthermore, Thin sections results of the sediments were discussed. The first section provides an overview of the sediment characteristics, while the later part of the chapter presents a systematic analysis of the mineral compositions of the sediments, in which their mineral constituents are thoroughly elucidated.

4.2 Physical Properties of the Sediments

In this study, the samples collected from the research area have been classified according to their texture characteristics. The results of the particle size distribution analysis for these bulk samples were presented in two formats: one in tabular form (Table 4.1 and 4.2) and the other as gradation curves exhibited on semi-logarithmic plots (Figure 4.1). These gradational curves offer a visual representation of how the distribution of sediment mass retained on each sieve evolves during the agitation process.

The sediment analysis results from these five stations collectively indicate that sand particles constitute the predominant component in all the sediment samples. However, the proportion of fine silt and gravel particles differs among the stations. The analysis results have unveiled valuable insights into the sediment properties within the study area. At station 1, fine silt particles with diameters ranging from 0.063 to 0.07 mm made up 19.0% of the sediments, while 79% of the sediment samples were composed of sand particles with diameters ranging from 0.07 to 4 mm. Gravel particles with diameters between 4 and 20 mm accounted for approximately 2% of the sediments. From the sieve analysis results, it is evident that the sediments at station 1 are sandy sediments, with the majority of the particles retained on sieves with diameters ranging from 0.25 to 2 mm.

Table 4.1: Sieve Analysis results

		Station 1					Station 2					Station 3				
sieve size (mm)	Mass of Sieve (g)	Mass of Sieve and Sediments (g)	Mass Retained (g)	% Mass retained	Mass of Cumulative Retained (g)	% Finer	Mass of Sieve and Sediments (g)	Mass Retained (g)	% Mass retained	Mass of Cumulative Retained (g)	% Finer	Mass of Sieve and Sediments (g)	Mass Retained (g)	% Mass retained	Mass of Cumulative Retained (g)	% Finer
20	757.85	758.8	0.95	0.048	0.048	99.95	758.2	0.35	0.023	0.023	99.98	758.18	0	0	0	100
10	625.99	628.3	2.31	0.12	0.16	99.84	652.83	26.84	1.74	1.76	98.24	636.82	10.65	0.69	0.69	99.3
5	581.35	597.41	16.06	0.80	0.97	99.03	624.9	43.55	2.82	4.58	95.42	587.13	5.5	0.35	1.04	98.96
2	403.17	610.31	207.14	10.36	11.32	88.68	559.11	155.94	10.09	14.67	85.33	436.72	32.43	2.09	3.13	96.87
1	350.73	1452.17	1101.44	55.07	66.40	33.61	919.36	568.63	36.80	51.47	48.53	504.12	152.19	9.80	12.93	87.07
0.5	295.43	805.99	510.56	25.53	91.92	8.08	819.07	523.64	33.89	85.35	14.65	1332.02	1036.11	66.71	79.64	20.36
0.25	271.63	409.98	138.35	6.918	98.84	1.16	428.15	156.52	10.13	95.48	4.52	574	301.4	19.4	99.05	0.95
0.125	263.69	281.82	18.13	0.91	99.75	0.25	313.62	49.93	3.23	98.71	1.30	274.27	11.45	0.74	99.78	0.22
0.063	256.53	259.08	2.55	0.13	99.87	0.13	276.53	20	1.30	100.00	0	260.04	3.38	0.22	100	0
Pan	528.64	530.55	1.91				528.97	0.33				529.38	0.4			

Table 4.2: Sieve Analysis

		Station 4					Station 5				
sieve size (mm)	Mass of Sieve (g)	Mass of Sieve and Sediments (g)	Mass Retained (g)	% Mass retained	Mass of Cumulative Retained (g)	% Finer	Mass of Sieve and Sediments (g)	Mass Retained (g)	% Mass retained	Mass of Cumulative Retained (g)	% Finer
20	757.85	758.16	0	0	0	100	758.17	0	0	0	100
10	625.99	725.92	99.19	6.35	6.35	93.64	722.42	96.2	5.67	5.66	94.33
5	581.35	801.05	218.4	13.99	20.35	79.65	584.18	2.07	0.12	5.79	94.21
2	403.17	812.18	405.01	25.95	46.29	53.71	537.28	132.97	7.83	13.62	86.38
1	350.73	757.33	405.36	25.97	72.26	27.73	1162.59	810.65	47.74	61.36	38.64
0.5	295.43	613.39	317.1	20.31	92.58	7.42	792.52	496.64	29.25	90.61	9.39
0.25	271.63	379.27	107.27	6.87	99.45	0.55	415.02	142.86	8.41	99.022	0.98
0.125	263.69	271.49	8.49	0.54	99.99	0.0077	279.28	16.43	0.97	99.99	0.011
0.063	256.53	256.98	0.12	0.0077	100	0	257.8	0.18	0.01	100	0
Pan	528.64	528.94	0		1560.94		528.95	0		1964	

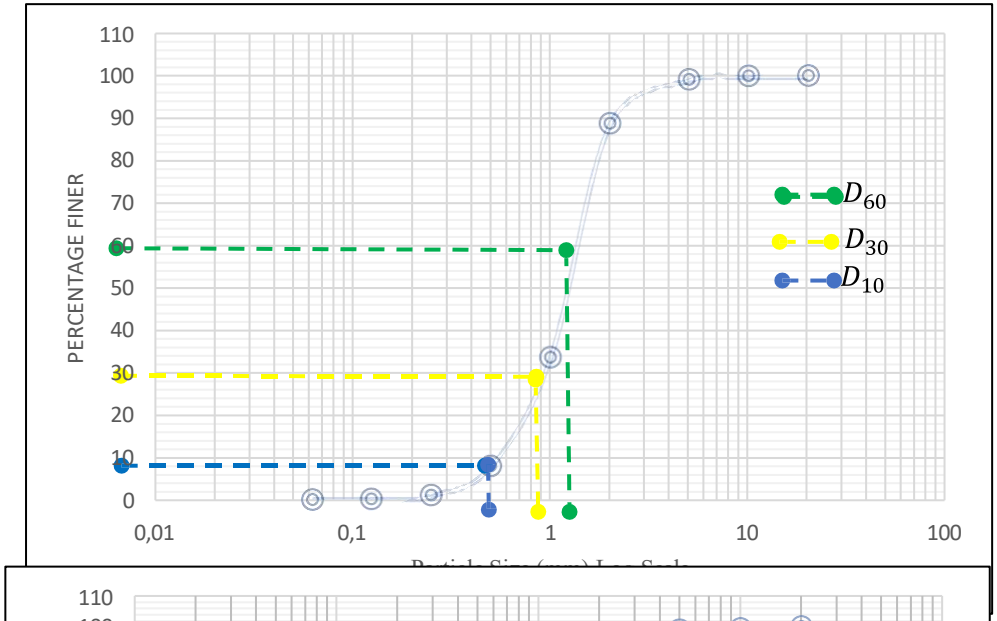
PERCENTAGE FINER
110
100
90
80
70
60
50
40
30
20
10
0
0,01
0,1
1
10
100
D_{60}
D_{30}
D_{10}

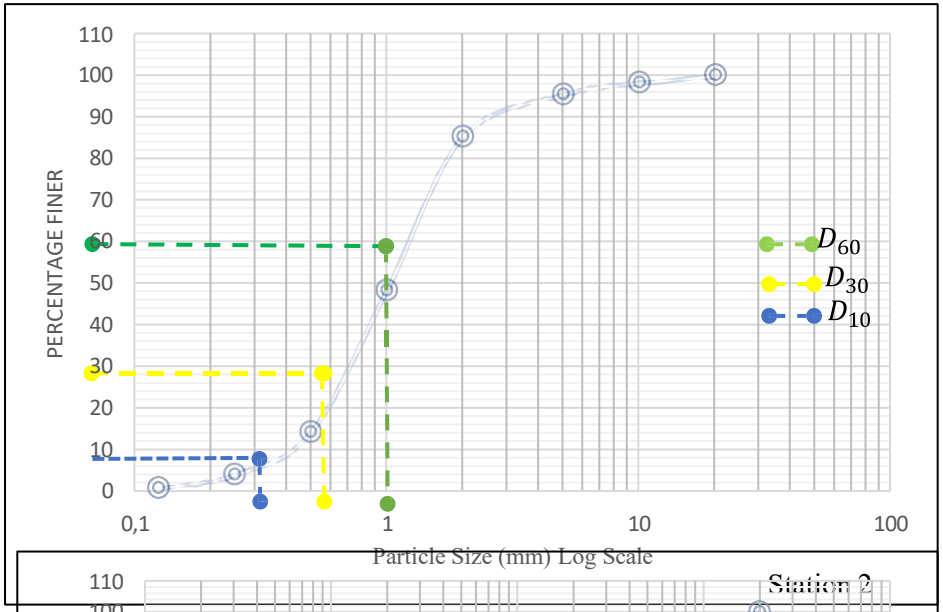
PERCENTAGE FINER
110
100
90
80
70
60
50
40
30
20
10
0
0,1
1
10
100
Particle Size (mm) Log Scale
D_{60}
D_{30}
D_{10}

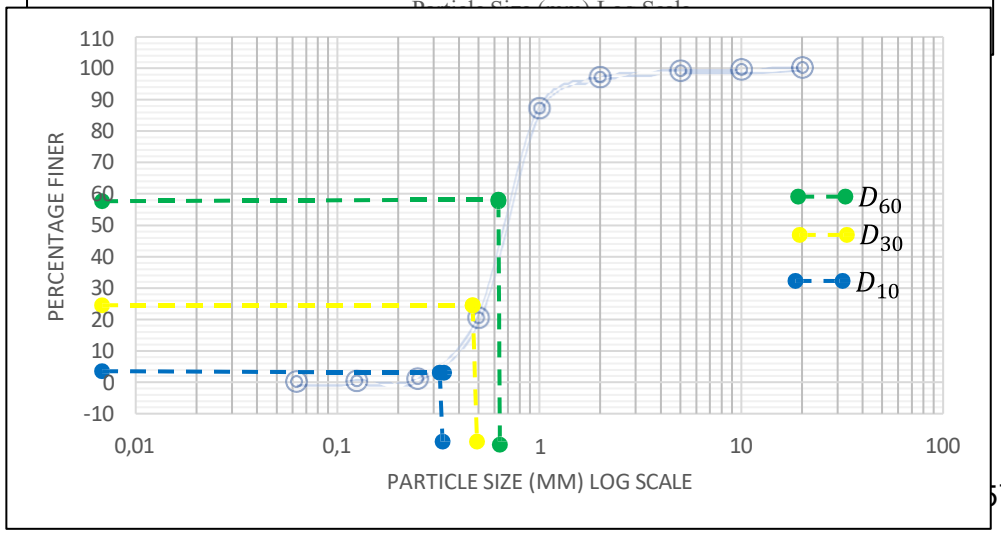
PERCENTAGE FINER
110
100
90
80
70
60
50
40
30
20
10
0
-10
0,01
0,1
1
10
100
PARTICLE SIZE (MM) LOG SCALE
D_{60}
D_{30}
D_{10}

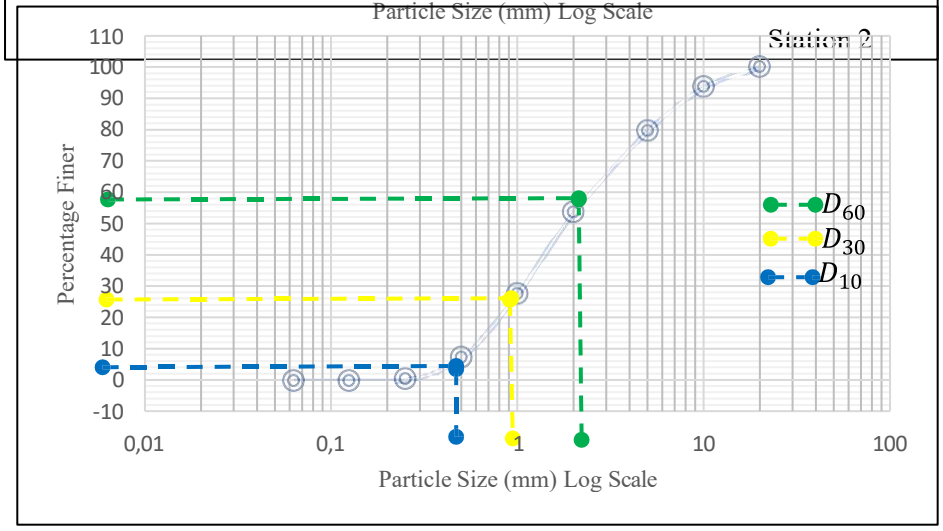
Station 2
Percentage Finer
110
100
90
80
70
60
50
40
30
20
10
0
-10
0,01
0,1
1
10
100
Particle Size (mm) Log Scale
D_{60}
D_{30}
D_{10}

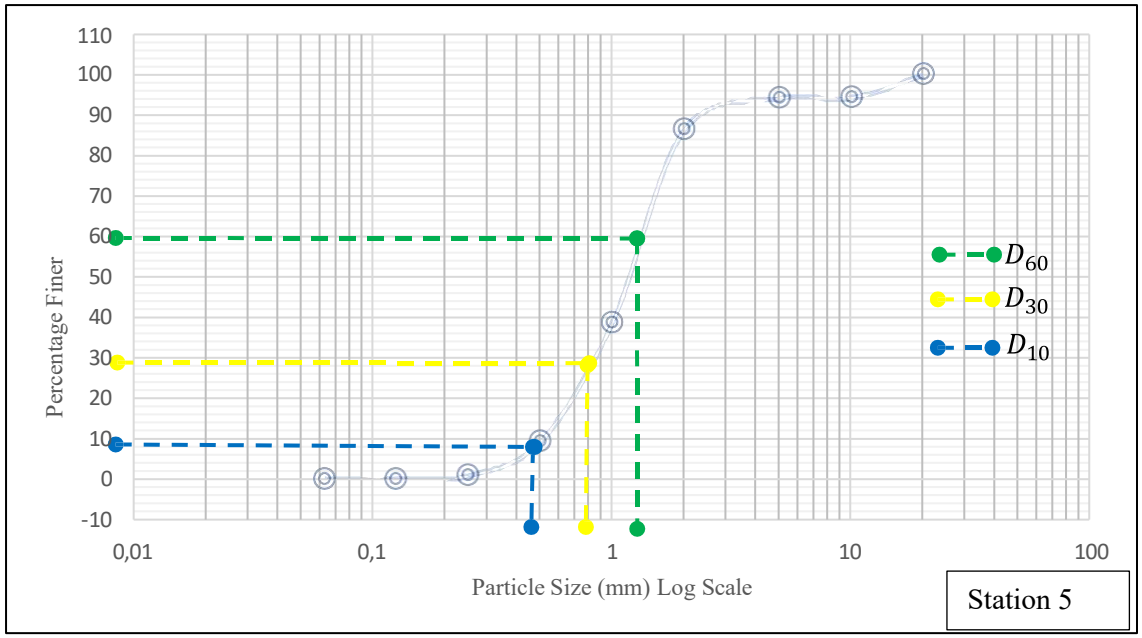

Figure 4.1 Particle Size Distribution Curve for Stations 1 - 5

At station 2, the analysis of sediment revealed an absence of fine silt particles. Instead, a significant 94% of the sediment composition consisted of sand particles with diameters spanning from 0.12 mm to 4 mm. Among these, coarse sand particles with diameters ranging between 1 mm and 2 mm constituted a substantial portion, accounting for approximately 33.9% of the sediment sample. Gravel particles with diameters between 4 and 20 mm made up 6% of the sediments. Most of the sediment at station 2 was retained on a pan with a sieve diameter of 0.5 to 1 mm, comprising approximately 79% of the sample. At station 3, sand particles accounted for 99% of the sediments, while the remaining 1% was composed of particles with a diameter between 4 and 20 mm. The sediment samples from station 3 did not have any fine silt or gravel particles. At station 4, sand particles with diameters ranging from 0.063 to 4 mm constituted 80% of the sediments, while the remaining 20% were particles with a diameter ranging from 4 to 20 mm. At station 5, sand particles with diameters ranging from 0.07 to 4 mm accounted for 92% of the sediments, while the remaining 8% were gravel particles with diameters ranging from 4 to 20 mm.

Based on the results obtained from the five stations, it can be concluded that the sediments in the study area are predominantly sandy, with sand particles ranging in size from 0.07 to 4 mm. Fine silt particles, with diameters ranging from 0.063 to 0.07 mm, were only found in station 1, while gravel particles with diameters between 4 and 20 mm were present in all stations but at varying percentages. This result is consistent with previous studies conducted in similar environments. For instance, a study conducted by Xie et al. (2018) on the sediment characteristics of a river in a tropical region found that the sediment samples were mainly composed of sand, with some silt and clay particles. Another study by Chen et al. (2019) on the sediment characteristics of a river in a semi-arid region showed that the sediment samples were dominated by sand particles, with some gravel particles. Taken together, these results provide the characterisation of the sediment properties in the study area downstream from Beit Bridge. The predominance of sand particles and the presence of gravel particles suggest that the river in this area has a high-energy environment with fast-moving water currents. These fast-moving water currents can transport and deposit coarse sediment particles.

The presence of gravel particles may also be attributed to the presence of boulders and rock outcrops in the watershed (Shobe et al., 2021). Furthermore, the variation in sediment composition between the different stations may be attributed to the differences in local geological and hydrological conditions. For instance, station 1 may have a higher proportion of fine silt due to the influence of tributary streams with lower flow velocities. Table 4.1 shows the sieve analysis results for the five stations.

The sediment particle size distribution was studied using the D10, D30, and D60 values, which represent the diameters at which 10%, 30%, and 60% of the sediment are finer, respectively. The sediment properties of the study area upstream from Beit Bridge are characterised by a range of particle sizes, from fine sand to gravel. The percentage of the initial samples lost due to sediments getting stuck in sieves varied between 1.8% and 29%.

In Station 1, the particle distribution of the examined samples indicates that D10, D30, and D60 sizes had values of 0.6, 1, and 1.45 mm (log), respectively. The CU was 2.42 (log), which indicates that the sediment size distribution is fairly heterogeneous. However, the sediment displayed a CC of 1.15 log, which indicates a poorly graded sediment distribution. At Station 2, the analysis of particle distribution in the examined samples revealed specific values for the effective D10, D30, and D60 sizes, which were measured as 0.4, 0.7, and 1.3 (logarithmic units), respectively. Additionally, the sediments exhibited a CU of 3.25 (logarithmic units), signifying a relatively uniform size distribution among the sediment particles. However, the CC for these sediments was determined to be 0.94 (logarithmic units), indicating that the sediment distribution in this case was characterised as poorly graded.

At Station 3, the analysis of sample particle distribution revealed effective D10, D30, and D60 size values of 0.4, 0.59, and 0.65 (logarithmic units), respectively. The CU for these sediments was recorded as 1.4 (logarithmic units), indicating a uniformly graded distribution of sediment particle sizes. However, the CC measured at 1.34 (logarithmic units), signifying a poorly graded distribution of sediment particles.

Moving to Station 4, the particle distribution of the samples displayed effective D10, D30, and D60 sizes measured at 0.6, 1.1, and 2.2 (logarithmic units), respectively. In this case, the CU for the sediments was determined to be 3.67 (logarithmic units), indicating a highly uniform distribution of sediment particle sizes. However, the CC was found to be 0.92 (logarithmic units), reflecting a poorly graded distribution of sediment particles in this station (Table 4.2).

In Station 5, the particle distribution of the samples analysed showed that the effective D10, D30, and D60 sizes have values of 0.5, 0.8, and 1.4 (log), respectively, as shown in the gradational curves. The CU was 2.8 (log), which indicates a consistently graded distribution. However, the CC of the sediments was 0.91 (log), representing a poorly graded distribution (Table 4.2).

The findings from this study provide valuable information on the sediment properties of the Beit Bridge River in the study area. The particle size distribution analyses showed that the sediments were predominantly composed of sand and gravel particles, with some silt and clay particles present. The sediment samples were also found to be poorly to moderately sorted, with a uniform to poorly graded distribution. The results from Station 1 showed that the sediments were predominantly sandy with a poorly graded distribution. This is consistent with previous studies conducted in the Beit Bridge River catchment, which have shown that the river- bed is dominated by sand and gravel sediments (Chinoda et al., 2009& Makulana et al., 2022). The particle size distribution data from Station 2 also indicated the presence of gravel particles, which accounted for 6% of the sediments. This is similar to the findings from a previous study by Makulana et al. (2022), which reported the presence of cobble-sized particles in the river-bed sediments.

At Station 3, the sediments were found to be uniformly graded but poorly sorted, with a slightly gravelly sand textural group. This contrasts with the findings from Stations 1 and 2, which reported poorly graded sediments. The results from Station 4 also showed poorly graded sediments, but with a slightly gravelly sand textural group, which is consistent with the findings from Stations 1 and 2. Station 5 had consistently graded sediments but with a poorly graded distribution and a gravelly sand textural group. The findings from this study are important in understanding the sediment dynamics of the Beit Bridge River in the study area. Sediment transport in rivers is influenced by the size and shape of sediment particles, as well as the distribution and sorting of sediment particles (Wolman and Miller, 1960). In this study, the sediments were found to be predominantly composed of sand and gravel particles, which are easily transported by the river flow. The poorly to moderately sorted sediments indicate that the river can transport a wide range of sediment sizes, which can have implications for river morphology and geomorphology (Muchingami et al., 2022).

Figure 4.2 shows that all samples have a homogeneous distribution of gravelly sand size fractions (0.062 to 20 mm). Furthermore, the samples collected from stations 1, 2, and 5 showed a similar pattern. However, sediment samples from stations 3 and 4 showed a different pattern. This variation in sediment characteristics is primarily attributed to the varying proportions of sand and gravel particles found in the sediment samples collected from station 6. Additionally, the effective size (D10) values for the five sample stations fell within the range of 0.4 to 0.6 logarithmic units, as detailed in Table 4.3. The CU displayed a varied pattern across all samples, with values ranging from 1.6 to 3.7. In the case of sediment samples, the CC consistently showed low values, typically below 2.

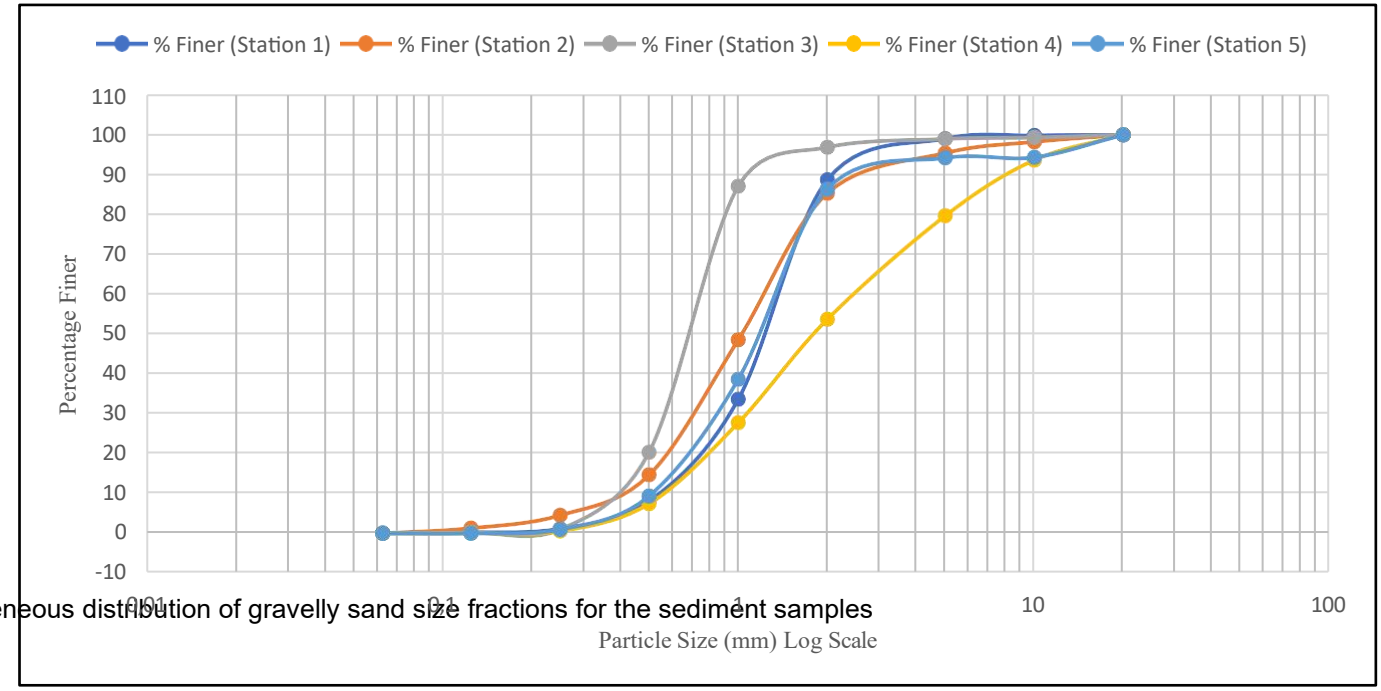

Figure 4.2: Homogeneous distribution of gravelly sand size fractions for the sediment samples

Table 4.3: Particle Size Distribution Curve for all Five Stations

Sediment samples	D10	D30	D60	CC	CU
1	0.6	1	0.6	2.416667	1.090909
2	0.4	0.7	0.4	3.25	0.942308
3	0.4	0.59	0.4	1.625	1.338846
4	0.6	1.1	0.6	3.666667	0.916667
5	0.5	0.8	0.5	2.8	0.914286

4.3 Mineralogical Characteristics of the Sediments

To validate the mineral compositions observed in the thin sections, three samples were randomly selected from the samples collected at the study area. The selected samples underwent a comprehensive analysis using XRD. These samples were sent to the XRD Analytical and Consulting cc laboratories for analysis.

As shown in Table 4.4, results show that quartz content showed a predominance and ranged from 51.6 to 60%. Quartz is a hard, durable mineral that tends to be resistant to weathering and erosion, which means that it can be transported over longer distances than softer minerals. Quartz showed a symmetrical peak in all sediment samples collected from the study area. Sample 1, sample 3, and sample 4 had quartz at 52.3%, 60.0
%, and 51.6%, respectively. The microcline content ranged from 18.7% to 20.1% in the samples collected. Sample 4 had the highest weighted percentage of 20.1%, followed by sample 3 (19.2%), and sample 1 had a weighted percentage of 18.7%. The minerals quartz, microcline, plagioclase, muscovite, and actinolite are the major minerals found in the sediment samples. The outcomes of this research carry notable significance in enhancing our comprehension of the sediment properties in the upstream region of Beit Bridge. Consequently, the findings offer fresh insights into the mineral composition of sediment samples in the study area upstream from Beit Bridge, underscoring the critical role of mineralogical analyses in sedimentological investigations. In the context of river sediment, quartz content is often used as an indicator of the sediment's source and depositional history (Gliganic et al., 2017). Similarly, Awal et al. (2019) concede that sediment sampleanalysis is essential

for reducing erosion in hydropower components. Quartz, garnet, tourmaline, and feldspar are common hard minerals found in sediment, impacting erosion potential.

Table 4.4: Mineral Properties of the Study

Sediment samples	Quartz	Microcline	Plagioclase	Muscovite	Actinolite
1	52.3	18.7	27.5	1.6	0.1
3	60.0	19.2	19.1	1.2	0.5
4	51.6	20.1	26.8	1.3	0.3

The predominance of quartz in sediment samples indicates that the sediment was most likely derived from a quartz-rich source, such as a granite or quartzite outcrop. The presence of high quartz content in river sediment can also suggest that the sediment has undergone significant weathering and erosion, as quartz is one of the most resistant minerals to chemical and physical weathering processes (Garzanti et al., 2019).

Plagioclase was found to be the second major mineral in the sediment samples, with a content range of 19.1% to 27.5%. The highest plagioclase content was recorded in sample 1 at a weighted percentage of 27.5%, followed by sample 4 at 26.8%, and sample 3 with a weighted percentage of 19.1%. The seemingly dominance presence of plagioclase in the samples suggests that it is a major constituent of the sediments, which may have implications for the formation and erosion of the riverbed. Plagioclase is a common mineral in many igneous and metamorphic rocks, and its presence in the sediment samples suggests that the geology is dominated by such rocks. This is consistent with previous studies in the area that have identified the presence of igneous and metamorphic rocks, such as granites and gneisses. For example, a study by Chinoda et al. (2009) identified the presence of granites and gneisses in the area, which are known to contain plagioclase. Also, a study by Rapopo (2011) found that plagioclase was a common mineral in rocks from the Limpopo Belt, which includes the Beit Bridge area.

The presence of plagioclase in the sediment samples also suggests that weathering and erosion of the local rocks have played a significant role in the formation of the riverbed. Plagioclase is a relatively resistant mineral to weathering, and its presence in the sediment samples suggests

that the other minerals in the local rocks may have weathered more quickly and been removed from the area. This is consistent with previous studies that have suggested that weathering and erosion are major processes shaping the Beit Bridge landscape. A study by Johnson et al. (2017) found that erosion rates in the area are relatively high due to the steep topography and intense rainfall. The current study's findings are consistent with previous studies in the area and support the idea that weathering and erosion are major processes shaping the Beit Bridge landscape.

In contrast, muscovite was found to have an overall low content in all samples, ranging from 1.2% to 1.6%. Sample 1 contained the highest mineral concentration at a weighted percentage of 1.6%, while sample 3 had the lowest muscovite content at 1.2%. Sample 2 had a slightly higher muscovite content of 1.3%. This shows muscovite lack of resistance to chemical weathering. It is quickly transformed into clay minerals. The Actinolite mineral was found to have the lowest content in the sediment samples collected, ranging from 0.1% to 0.5% weighted percentage. Sample 3 had the highest weighted percentage of 0.5%, sample 4 had a value of 0.3%, and sample 2 had the lowest value of a 0.1 weighted average. The low content of actinolite in the samples suggests that it is not a major constituent of the local geology and may not play a significant role in the formation and erosion of the riverbed. The X-ray diffractograms in Figure 4.3 support the findings of the mineralogical analysis and provide a visual representation of the mineral content in the sediment samples.

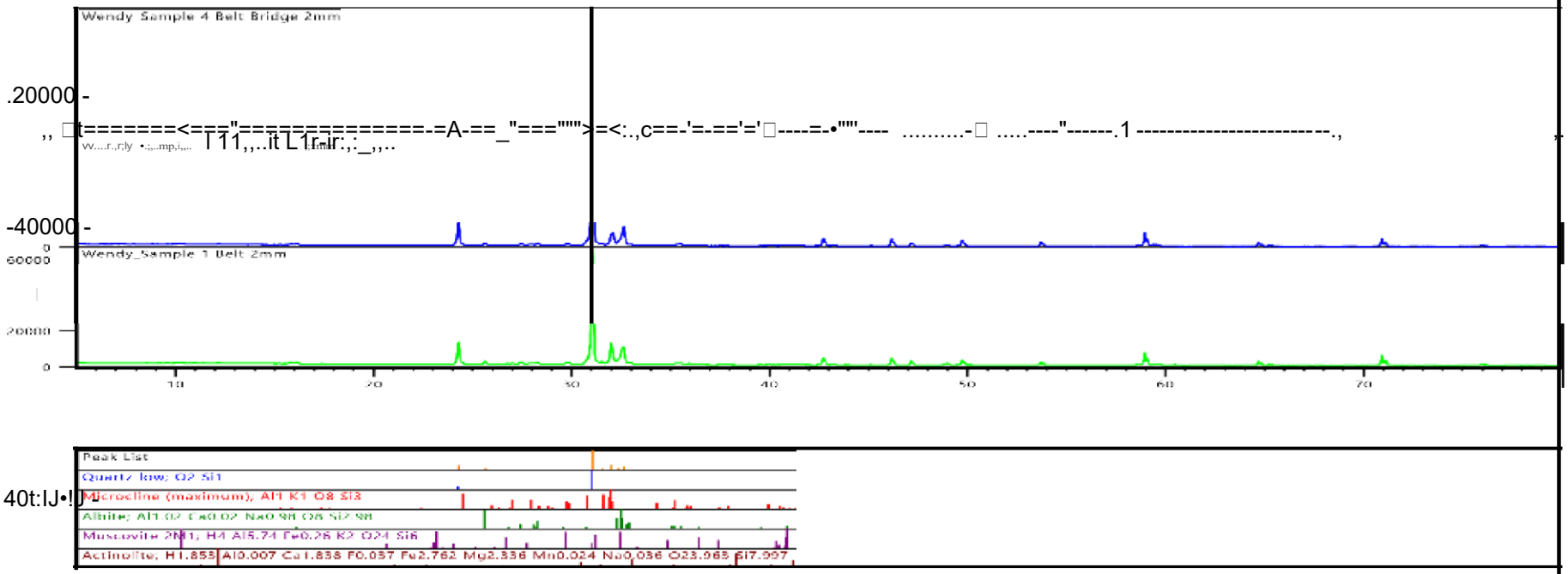
Wendy Sample 4 Belt Bridge 2mm
.20000 -
-40000 -
Wendy_Sample 1 Belt 2mm
60000
20000
0
10
20
30
40
50
60
70
Peak List
Quartz low; O2 Si1
Microcline (maximum); Al1 K1 O8 Si3
Albite; Al1 O2 Ca0.02 Na0.98 O8 Si2.98
Muscovite 2M1; H4 Al5.74 Fe0.26 K2 O24 Si6
Actinolite; H1.853 Al0.007 Ca1.838 Fe0.057 Fe2.762 Mg2.338 Mn0.024 Na0.036 O23.985 Si7.997

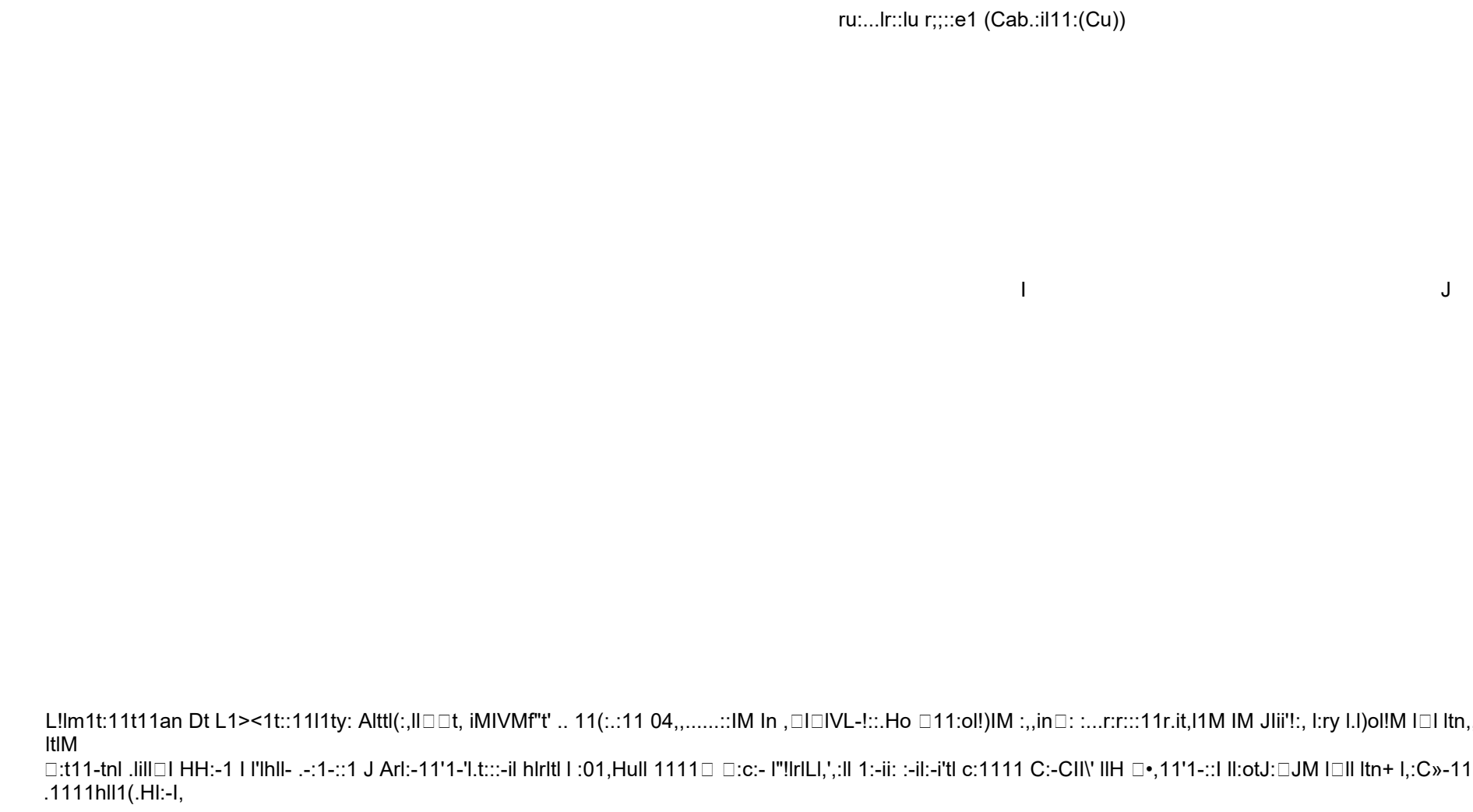

Figure 4.3: X-ray Diffractograms for Studied Sediment Samples

4.3.1 Thin Section Analysis of the Sediments

The sediments were examined under the microscope. The thin section from station 1 is presented in Figure 4.4, with images shown in both plane-polarised and crossed-polarised lights, denoted as Figures 4.4a and 4.4b, respectively. Figure 4.4a shows the grains in the plane polarised light have low relief and are mostly colourless. This makes it difficult to distinguish between different mineral grains in the thin section. The findings suggest that the sediment may be composed of a relatively homogeneous mineral assemblage or that the mineral grains are very fine-grained. Also, this suggests that the different minerals do not stand out in the entire section. However, some grains show faint traces of cleavage. The faint traces of cleavage observed in some grains suggest the possible presence of minerals such as mica or amphibole, which are known to exhibit cleavage in certain orientations. There is no colour change as the stage is rotated clockwise. The lack of colour change as the stage is rotated indicates that the mineral grains are isotropic, meaning that they do not exhibit birefringence or double refraction. This suggests that the mineral assemblage is composed of isotropic minerals such as quartz or feldspar.

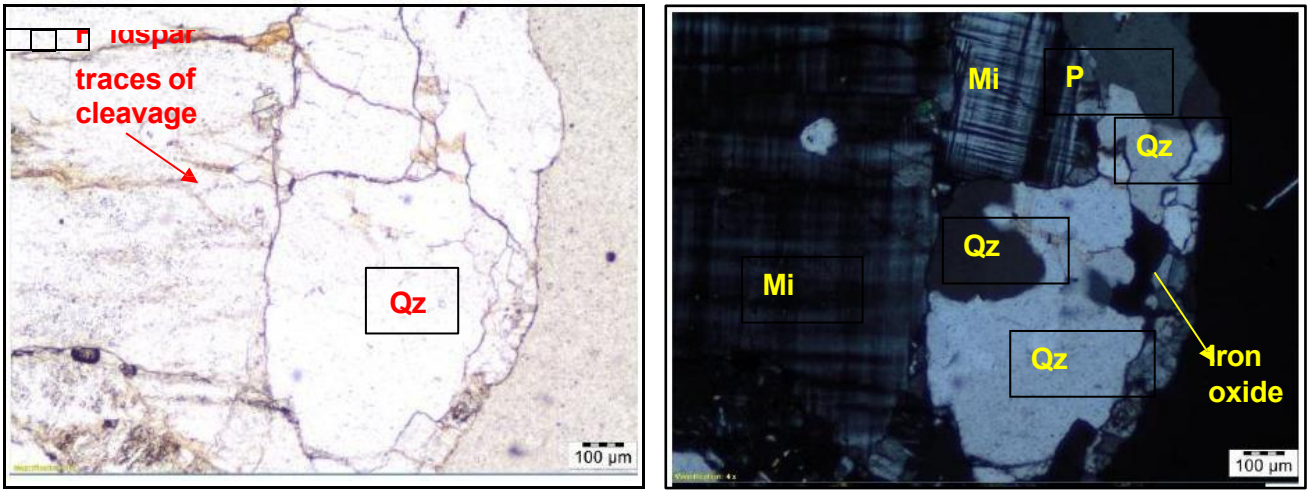

a b

Figure 4.4 Station 1: Photomicrograph of sediment samples microcline and quartz (a) shows plane polarised light. (b) shows the cross-polarised light. Note Mi – Microcline, Qz – Quartz, P – plagioclase

Under the cross-polarised light, boundary layers were seen, which shows that the grains are touching each other. The section is comprised of microcline, quartz, and plagioclase minerals. The quartz is identified by the grey and white first-order interference colours. The lack of cleavage and twinning in the grain sample shows the properties of quartz minerals. A wavy extinction was observed when the stage was rotated.

Meanwhile, the feldspar is identified by the crossed-hatched twinning, which is identified as microcline feldspar. The plagioclase was identified by its multiple lamellae twinning. This section is mineralogically immature because of the level of feldspar present. The identification of feldspar in the sediment sample is consistent with previous studies in the Beit Bridge area. A study by Brandl (2002), also identified feldspar as a representative mineral in the sediment samples collected from the Limpopo basin area. However, the level of feldspar in this current study is higher than what Brandl, G. (2002) reported. This suggests that there may be variations in the mineralogical composition of sediments within the Beit Bridge area.

The section in question can be classified as Arkose or arkosic sandstone, which falls under the category of detrital sedimentary rock due to its containing more than 25% feldspar. Similarly, Arkosic sand also exhibits a high feldspar content, making it a likely precursor to arkose. This classification aligns with previous research findings. For instance, a study conducted by Bábek et al. (2014) identified arkose as the predominant type of sedimentary rock in the upper sections of the Karoo Supergroup in southern Africa. Our study reaffirms the presence of arkose in the Beit Bridge region, which contributes significantly to our understanding of the local geological context.

As mentioned earlier, quartz is typically the dominant mineral component in this section, and mica is often present as well. These minerals were also identified in the XRD results provided in Table 4.3. The presence of quartz and mica in the section aligns with previous research findings. A study conducted by Boryta and Condie (1990) identified quartz and mica as the prevailing minerals in sediment samples from the Limpopo River catchment area in southern Africa. Our research results further substantiate the widespread occurrence of these minerals in the region. In summary, this study's findings are in harmony with previous research in the area, contributing significantly to our understanding of the mineralogical composition of sediments in the Beit Bridge region.

Figure 4.5a shows sediment samples (station 2) in plane polarised light. Approximately 60% of the grains are colourless and have very low relief, which indicates that the minerals present in the section do not stand out. There is no colour change when the stage is rotated clockwise. However, some signs of quartz and feldspar minerals are observed under the plane polarised light. Under the crossed polarised light, the boundary layers were seen clearly, as depicted in Figure 4.5b. The thin section is comprised of quartz and plagioclase minerals. The quartz is identified by its grey and white first-order interference colours. The lack of cleavage and twinning in the grain sample shows the properties of quartz minerals. The plagioclase is identified by its multiple and lamellae twinning. The rotation of the stage in the clockwise direction showed the lamellae turning dark and even reaching extinction. Some of the

plagioclase had some sericite on the edge of the crystal. The minerals were tourmaline and a lot of opaque minerals, which were rimmed with calcite. The calcite rim indicates that there have been reactions with a CO2-rich fluid. These minerals were also identified using the XRD, as shown in Table 4.3.

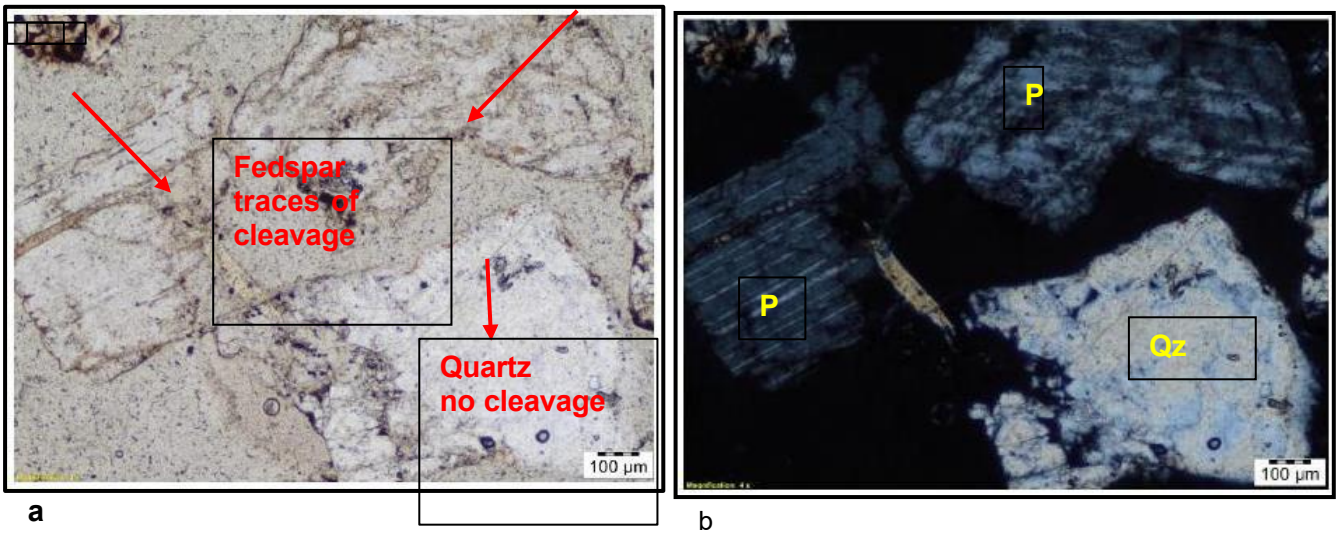

Figure 4.5 station 2: Photomicrograph of sediment samples, mainly quartz and plagioclase (a), show plane polarised light. (b) shows the cross-polarised light. Note Qz
= Quartz, P = plagioclase

As shown in Figure 4.6 at station 3, under plane polarised light, which displays low to high relief, some minerals stand out while others do not. A cloudy or turbid colour was observed, along with some rounded black minerals. The rounded black minerals may be due to the epoxy material that was added during the preparation of the thin section. The minerals with low relief and a cloudy or turbid colour can be identified as quartz. This thin section is mostly comprised of quartz and muscovite mica.

Muscovite mica shows a second to third-order interference colour with a mottled and speckled appearance in extinction. However, under plane polarised light, the muscovite was clear and showed good cleavage and high relief, which made the mineral stand out. Muscovite can be distinguished by its distinctive features, including a bird's eye orientation extinction angle of 2 degrees and pleochroism observed in plane-polarized light, which imparts a darker colouration to the mineral. Additionally, the muscovite material exhibited opacity under both plane-polarised and crossed-polarised light due to its elevated Fe or mafic component concentration.

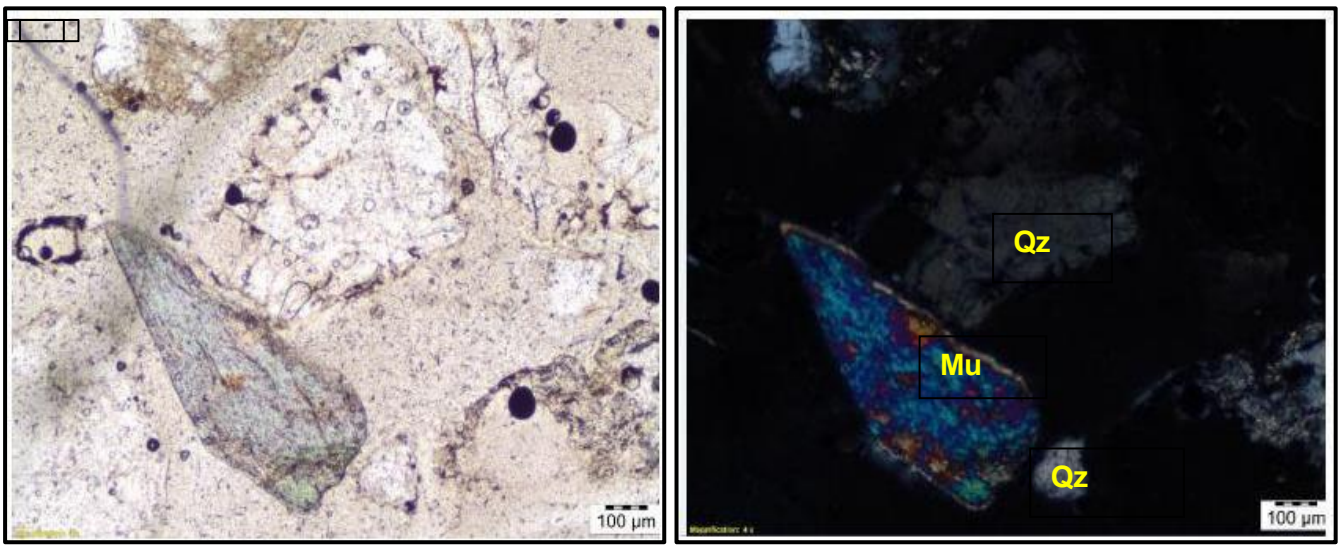

a b

Figure 4.6 station 3: Photomicrograph of sediment samples quartz and muscovite (a) shows plane polarised light. (b) shows the cross-polarised light. Note Mu – Muscovite, Qz – Quartz, P – plagioclase

Figure 4.7 at station 4 shows the thin section of the sample sediments. Under plane polarised light, the grains show low relief, that is, the minerals do not stand out from the section. The grains show irregular shapes, with the grain boundaries touching each other. Most of the gains show no cleavage, and when the stage is rotated, the grains show no change in colour, which means that they are not pleochroic. The grains are mostly made up of the mineral quartz. Under the cross-polarised light, the quartz is identified by its first-order grey interference colours, and it shows no twinning. Some of the quartz grains are straight extinctions. Meanwhile, some other quartz grains show an undulose extinction, which means they go into extinction in a wavy pattern. Some of the grains are composed of multiple intergrown crystals. These minerals are shown in the XRD results. This sample is mineralogically mature because it has a small number of different minerals and is composed of quartz, which is a stable mineral on the Earth's surface. It also shows that the source of grain is far from the place of deposition or a distal source. The mixture of different types of quartz grains may indicate more than one type of source and be of granitic origin. This sample may be called a quartz arenite.

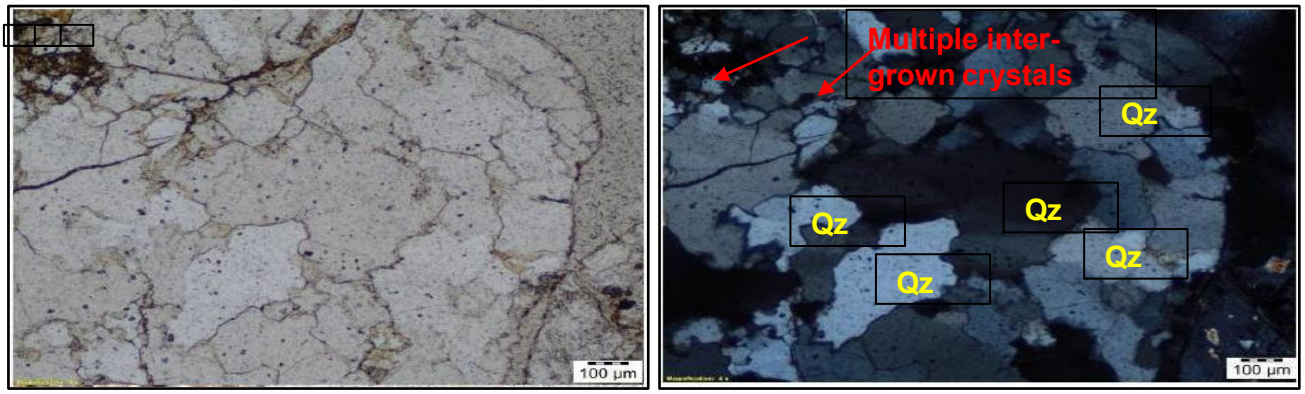

a b

Figure 4.7 station 4: Photomicrograph of sediment samples with quartz minerals (a) shows plane polarised light. (b) shows the cross-polarised light

The grains observed in Figure 4.8a at station 5 exhibit irregular contours and lack a banded texture, as well as being mostly neither subangular nor subrounded in shape. Some of the grains are colourless with high relief and cleavage under plane polarised light. This shows the presence of feldspar minerals. Some of the grains show pale white coloured grains intertwined with yellowish and brownish colours. Under the crossed polarised light, the section is composed of quartz crystals, microcline feldspar and some rock fragments, as shown in Figure
4.8b. The quartz mineral was identified by its white and turbid parchment, while the microcline was identified by the crossed-hatched twinning in the section. The quartz grain is called polycrystalline quartz grain and is made of interlocking quartz crystals with first-order interference colours. These grains are usually sourced from metamorphic rocks. These minerals were also found in the XRD results.

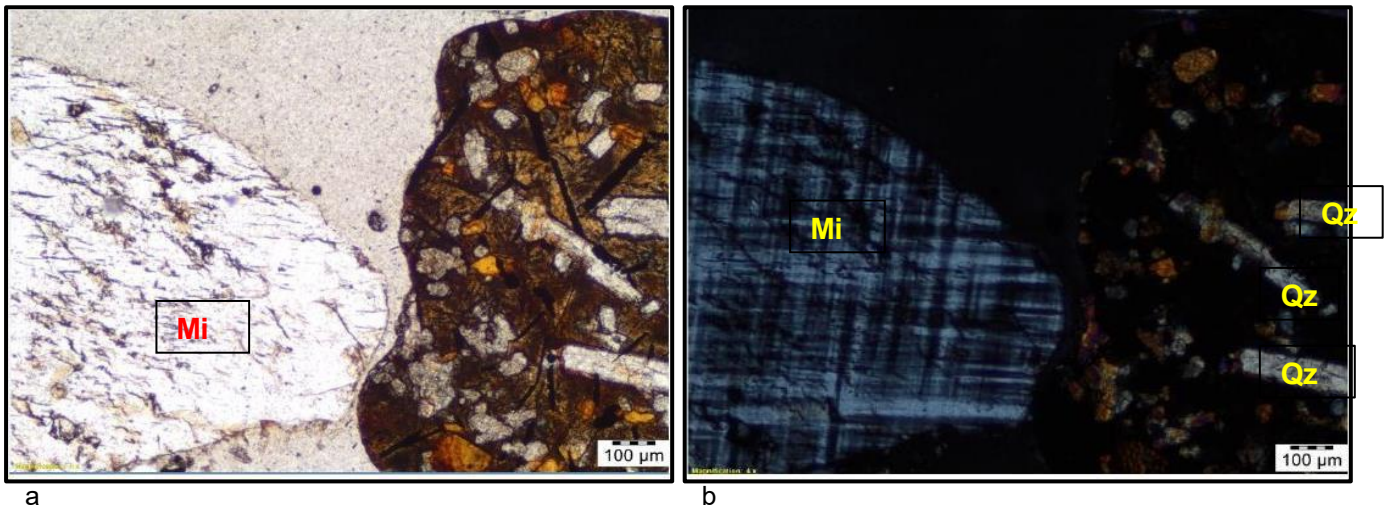

a b

Figure 4.8 station 5: Photomicrograph of sediment samples, mainly microcline and quartz (a), show plane polarised light. (b) shows the cross-polarised light. Note Mi – Microcline, Qz – Quartz

4.4 Chapter Summary

Chapter 4 provides a detailed account of the outcomes and discourse concerning objectives 1 and 2, centering on the examination of sediment qualities and mineral constitution further downstream from Beit Bridge. Within all the examined samples, sand particles were found to be prevalent, accompanied by diverse proportions of fine silt and gravel. The environment of the river, characterised by high-energy dynamics, implies the presence of rapid water currents capable of transporting coarse sediment. Analysis of the distribution of sediment particle sizes indicated the presence of poorly graded, gravelly sand, with certain sampling stations displaying a more consistent gradation pattern. Examination of minerals found that quartz was the predominant mineral component, ranging from 51.6% to 60%, followed by plagioclase at 19.1% to 27.5%. Conversely, the content of muscovite was relatively low, ranging from 1.2% to 1.6%, suggesting a source rich in quartz and a geological composition primarily constituted of igneous and metamorphic rocks. The observations made through thin-section analysis at various stations corroborated these identified mineral compositions. In essence, the overall findings point towards the substantial impact of weathering and erosion as pivotal landscape-altering processes within the vicinity of Beit Bridge.

CHAPTER FIVE: GEOCHEMICAL COMPOSITIONS OF THE SEDIMENT SAMPLES

5.1 Introduction

In this chapter, the results of the XRF analysis, covering major and trace elements, are explored in depth. The major element data is interpreted using geochemical plots to assess sediment weathering and interactions. Furthermore, the distribution and implications of trace elements are thoroughly investigated and discussed, providing a comprehensive understanding of the composition and sources of key elements in the sediments of the Limpopo River at Beit Bridge. The major and trace element data are presented in normalized form, totalling 100%, without any alterations in geochemical plots and comparisons. Pearson correlation coefficients (r) are utilised to quantify the relationships between major and trace elements.

5.2 Major Elements

The geochemical analysis of sediment samples from the study area revealed the presence of major elements, including Si, Al, K, Mg, Ca, Na, Ti, and Fe in their oxide forms. The results obtained from Station 1 showed average quantities of various oxides, including MgO (0.97 wt%), Al2O3 (8.82 wt%), SiO2 (83.83 wt%), P2O5 (0.035 wt%), K2O (2.50 wt%), CaO (1.22
wt%), TiO2 (0.13 wt%), MnO (0.02 wt%), Na2O (1.79 wt%), and Fe2O3t (0.69 wt%), as depicted in Figure 5.1, with a more detailed list available in Appendix A. A similar pattern of results was observed across the other stations, from Station 1 to Station 5, as indicated in Figure 5.1. The notably high concentration of SiO2 (83.83 wt%) in the river sediments at Beit Bridge suggests the presence of minerals rich in quartz. Quartz is a prevalent mineral in various rock types, and its abundance in river sediments can offer insights into the geology and mineral composition of the surrounding areas. Moreover, the SiO2 concentration can serve as an indicator of the degree of weathering experienced by the rocks contributing to the river sediment. Higher SiO2 concentrations typically signify more extensive weathering processes. Consequently, the SiO2 concentration holds valuable information regarding the origin and history of the river sediment.

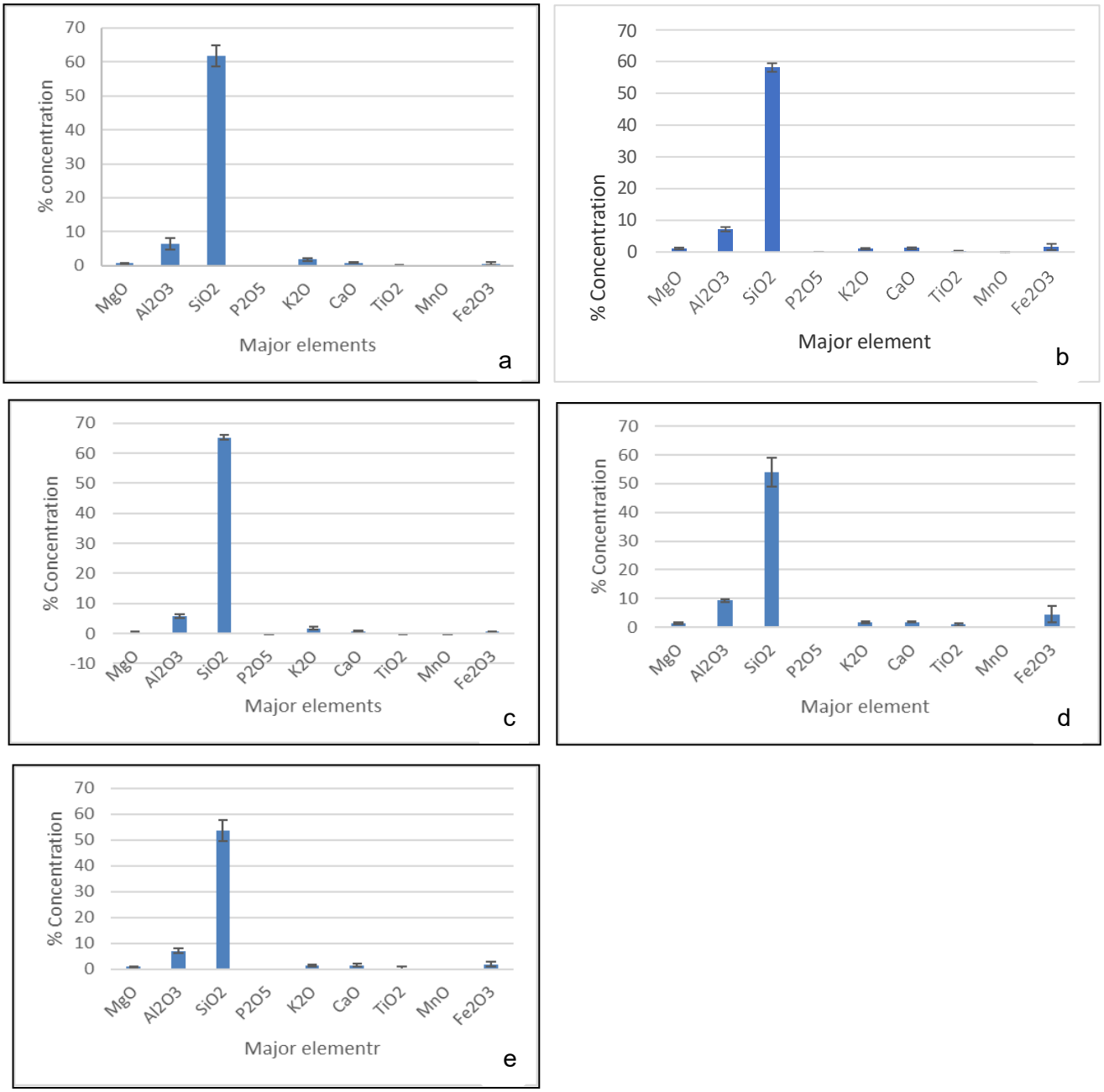

Figure 5.1: Showing elements with their oxide distribution for the sediment sample in the different stations. a. Station 1; b. Station 2; c. Station 3; d. Station 4; e. Station 5

The sediment samples exhibited a dominant presence of SiO2, with varying concentrations ranging from 71.23 to 84.68 wt% as the major element. Following SiO2, Al2O3 was the next major constituent, with concentrations ranging from 7.42 to 12.23 wt%. Other elements were present in relatively minor average concentrations, such as Na2O (mean 2.99 wt%), Fe2O3t (mean 2.49 wt%), K2O (mean 2.04 wt%), CaO (mean 1.68 wt%), MgO (mean 1.30 wt%), TiO (mean 0.47 wt%), and MnO (mean 0.047 wt%). The SiO2/Al2O3 ratio observed in the sampled sediments, varied between 5.83 and 11.41, with an average of approximately 8.50. This ratio

surpasses the average Upper Continental Crust (UCC) value of around 4.34 (Taylor and McLennan, 1985; Rahman et al., 2021). The SiO2/Al2O3 ratio serves as a crucial geochemical parameter that offers insights into the origin and evolutionary history of geological materials. The higher SiO2/Al2O3 ratio observed in the sediment samples, in contrast to the UCC average, indicates that these sediments have undergone substantial weathering and leaching processes. This has led to the enrichment of silica (SiO2) and a depletion of aluminium (Al2O3). Additionally, the elevated SiO2/Al2O3 ratios and the greater abundance of SiO2 percentages in the Limpopo River sediments at Beit Bridge signify a significant presence of quartz and feldspar in these sediments (Corcoran et al., 2013).

The sediment samples also display moderate to high values in several geochemical indices, including the CIA with a range of 54.06 to 61.94, the Plagioclase Index of Alteration (PIA) with values spanning from 55.99 to 67.82, and the Index of Compositional Variability (ICV) with values ranging from 7.18 to 15.30. Supplementary data can be found in Appendix A. Furthermore, a detailed examination of the major oxides (MgO, CaO, Fe2O3, TiO2, Na2O, and P2O5) reveals significant negative correlations with SiO2 and SiO2/Al2O3, except K2O, which exhibits a noteworthy positive correlation with SiO2 and SiO2/Al2O3. The major oxides, except for K2O, also display positive correlations with Al2O3, whereas K2O exhibits a negative correlation with Al2O3 (as detailed in Appendix B). A particularly strong negative correlation is observed between SiO2/Al2O3 and Al2O3 (r= −0.99), indicating the influence of sorting and hydrodynamic fractionation on their distribution. Similarly, robust negative correlations are noted between SiO2/Al2O3 and MgO (r= −0.97), CaO (r= −0.92), Fe2O3 (r= −0.90), TiO2 (r= −0.93), and P2O5 (r= −0.96), emphasising the presence of quartz enrichment in the sampled materials (Atabo and Sunday, 2020).

Nonetheless, it's important to note that there are relatively weak positive and negative correlations between SiO2/Al2O3 and K2O (r= +0.36) and Na2O (r= -0.23), suggesting the presence of plagioclase and K-feldspar in notable quantities within the sediments (Atabo and Sunday, 2020). Furthermore, strong positive correlations were evident between Al2O3 and TiO2 (r= +0.95), Fe2O3 (r= +0.94), MnO (r= +0.66), MgO (r= +0.93), P2O5 (r= +0.94), and CaO (r= +0.90), signifying significant hydraulic fractionation processes. Hossain et al. 2014 also assert that the majority of oxides, including CaO, primarily originate from aluminosilicate rocks, aligning with the observations made in this study. Moreover, the strong positive correlations between Al2O3 and TiO2 (r= +0.95), MgO (r= +0.93), and Fe2O3 (r= +0.94) suggest that their abundances are largely influenced by aluminous sediments or heavy minerals present in specific size fractions. Additionally, the elevated abundance and robust correlations between Fe2O3 and TiO2, CaO, MnO, MgO, P2O5, Y, and Zr strongly indicate the presence of heavy

minerals like garnet, rutile, ilmenite, epidote, apatite, and zircon in the sediment samples (Odigi and Amajor, 2009).

The SiO2/Al2O3 ratio and ICV are frequently used parameters to assess the sorting and textural maturity of sediment samples (Madukwe and Obasi, 2016). In the case of the sediment samples examined in this study, the SiO2/Al2O3 ratio falls within a relatively high range, spanning from 5.83 to 11.41. This range suggests a state of small to moderate textural maturity, characterised by a substantial presence of quartz and feldspar content, aligning with the findings of Baiyegunhi et al. (2017). Lower ICV values typically indicate textural maturity, accompanied by signs of recycling and/or significant weathering of source materials. Conversely, higher ICV values are indicative of textural immaturity. In this study, the analysed samples exhibit higher ICV values, ranging from 3.61 to 9.28 (as detailed in Appendix A). These values signify the presence of immature sediments, further corroborating the association with common rock-forming minerals such as quartz, feldspars, amphiboles, and pyroxenes. Minerals of this kind are typically characterised by ICV values greater than 0.84 (Cox et al. 1995).

Chemical weathering is a geological process that involves the dissolution or alteration of primary minerals into other mineral forms. One way to understand the weathering history of sediment samples is by analysing the relationship between alkali and alkaline earth elements, such as Al2O3, CaO, Na2O, and K2O (Odoma et al., 2015). In general, the weathering of igneous rocks results in the depletion of alkali and alkaline earth elements and an increase in Al2O3 content in the sediments. Two commonly used indices for assessing the chemical changes in source rocks due to weathering are the CIA and PIA. High CIA values indicate intensive weathering processes that have occurred over long periods, possibly at slow sedimentation rates, and in humid tropical conditions. These values suggest the removal of labile cations (e.g., Ca2+, Na+, K+) relative to stable residual constituents (e.g., Al3+, Ti4+) during weathering. Conversely, low CIA values suggest minimal chemical alteration, possibly occurring in cooler and arid conditions (Wang et al., 2020). PIA values, on the other hand, are used to assess the weathering of plagioclase. Fresh rocks typically have CIA and PIA values around 50, while clay minerals resulting from feldspar alteration, like kaolinite, illite, and smectite, have values approaching 100 (Jian et al., 2013).

In the context of the Limpopo Beit Bridge sediments, the CIA values range from 54.06 to 61.94, indicating a moderate to high intensity of chemical weathering. Similarly, the PIA values range from 55.99 to 67.82 (as detailed in Appendix A), also suggesting a moderate to high level of chemical weathering. Additionally, the ratios of large-ion lithophile elements (LILEs), such as Rb, Sr, K, and Na, are closely linked to chemical weathering and CIA values. Specifically, the

Rb/Sr ratios in sediment and sedimentary rocks can serve as indicators of the degree of weathering in source rocks (Nesbitt and Young, 1982). An increase in the Rb/Sr ratio is associated with higher degrees of weathering, subsequently leading to elevated CIA values.

The investigated sediments exhibit Rb/Sr ratios ranging from 0.40 to 0.48, indicating that they have not undergone intense chemical weathering. Additionally, these sediments have low alumina/clay values. Typically, in illite minerals, Rb/Sr ratios are greater than 1 (Chaudhuri and Brookins 1979).

5.3 Trace elements

There are greater fluctuations in the trace element distributions in the sediment samples. Transition metal element concentrations, like V (20 to 130 ppm), indicate a small enrichment in their abundance. Whereas overall variation for the sediment samples was observed for CU (30 to 40 ppm), Ni (20 to 70 ppm), Rb (740 to 1140 ppm), As (10 to 30 ppm), Sr (240 to 440 ppm), Mo (10 to 30 ppm), Ag (10 to 60 ppm) and Ba (740 to 1220 ppm). In general, the sediment samples exhibit relatively low concentrations of LILEs, which include elements like V, Pb, Ba, Sr, and Rb. Among these LILEs, the average concentration of Sr was found to be higher at 253.33 ppm compared to Rb at 175.33 ppm. Additionally, Ba had the highest average concentration among these LILE elements at 795.33 ppm. On the other hand, the sediment samples contained relatively low concentrations of High Feld Strength Elements (HFSE), with U having an average concentration of approximately 13 ppm. Likewise, mean values of Sn (22 ppm), Ta (72 ppm), and Pb (14 ppm) were detected. However, the elements were not frequently found in all of the samples collected during the analysis.

The distribution plot of trace elements, as depicted in Figure 5.2, reveals that sediment samples from the study area exhibit relative enrichments in several categories of elements. These elements encompass a range of categories, including large ion lithophile elements (LILE) like V, Rb, Sr, Ba, and Pb, as well as HFSE such as Zr, Hf, Th, Ta, Nb, U, and Sn. Additionally, REEs are represented by Ce and Y. These elements exhibit an enrichment pattern in the sediment samples, with the order of enrichment decreasing from LILE to REE to HFSE (as shown in Figure 5.2).

The notable enrichment in LILE compared to other elements suggests a source with a geochemical signature associated with subduction zones. This observation aligns with the findings of Crow and Condie (1990), which indicated that the Soutpansberg Formations are richer in LILE relative to other elements. It's crucial to acknowledge that these elements can

undergo a variety of reactions as a result of post-magmatic processes, including weathering, hydrothermal alteration, and metamorphic transformations. This variability in behaviour makes both LILE and HFSE valuable for tracing the origins of sediment or magma, especially considering their incompatible characteristics during mantle-melting events. Moreover, the examination of REE compositions in the analysed samples indicates that the total REE concentrations (ΣREE) in the sediments vary from 90 to 1373.33 ppm, with an average of
452.33 ppm. These concentrations surpass the average values observed in the UCC and post-archean average shale, which stand at 146.37 and 184.72 ppm, respectively. Such elevated REE concentrations often indicate a dilution of quartz and, consequently, an enrichment of SiO2 concentration in the overall composition (Roy and Roser, 2013).

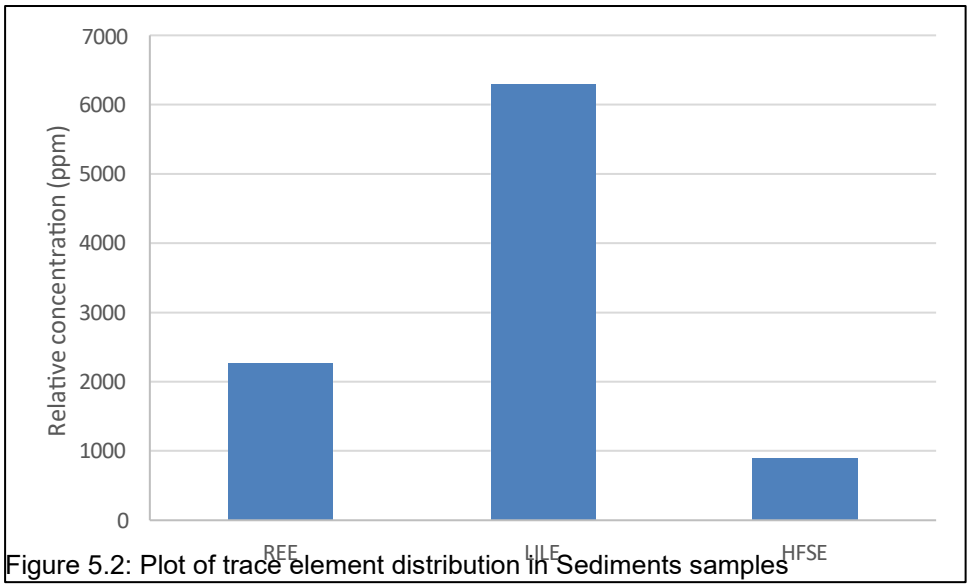

Figure 5.2: Plot of trace element distribution in Sediments samples

The chondrite normalisation process unveiled increased concentrations and prevalence of trace metals and REE in the sediment samples, as illustrated in Figure 5.3. The normalised REE values in these sediment samples displayed enrichment, with concentrations spanning from over 1000 ppm to reaching as high as 5000 ppm.

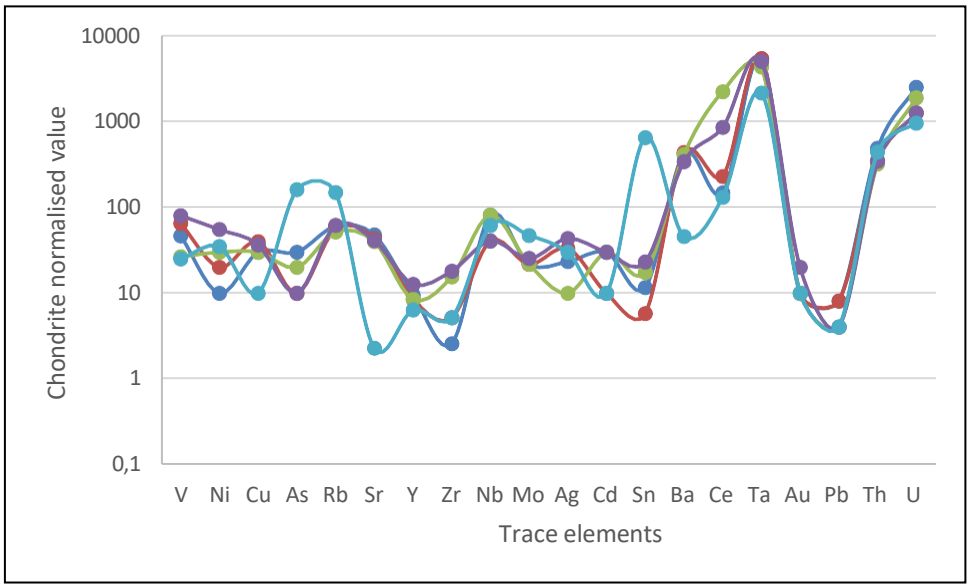

Figure 5.3: Plot of chondrites normalised Trace metals and REE concentration of rock sample

5.4 XRF and XRD comparison.

According to Kuforiji and Ayandiran (2013), XRD is a technique used in materials science to determine the crystallographic structure of a material. XRD works by irradiating a material with incident X-rays and then measuring the intensities and scattering angles of the X-rays that leave the material, while XRF is an analytical technique that uses the interaction of X-rays with a material to determine its elemental composition. In simple terms, XRD determines the mineralogical compositions of the sediments, while XRF determines the elemental composition of the sediments. The XRD results showed the presence of a significant number of Quarts, Plagioclase, Microcline, and minor amounts of Muscovite and Actinolite on the sediments, while the geochemical analysis of sediment samples from the study area revealed the presence of major elements, including Si, Al, K, Mg, Ca, Na, Ti, and Fe in their oxide forms.

The XRD showed the presence of quartz with an average of 54%, followed by plagioclase averaging 24.5%, Microcline at 19.3%, minor amounts of Muscovite at 1.4% and lastly actinolite at 0.3%, while the XRF results exhibited a dominant presence of SiO2, with varying concentrations ranging from 71.23 to 84.68 wt% as the major element. Following SiO2, Al2O3 was the next major constituent, with concentrations ranging from 7.42 to 12.23 wt%. Other elements were present in relatively minor average concentrations, such as Na2O (mean 2.99 wt%), Fe2O3 (mean 2.49 wt%), K2O (mean 2.04 wt%), CaO (mean 1.68 wt%), MgO (mean 1.30 wt%), TiO (mean 0.47 wt%), and MnO (mean 0.047 wt%).

The Major element concentration of SiO2 on the XRF justifies the high percentage of quartz. SiO2 concentration can serve as an indicator of the degree of weathering experienced by the rocks contributing to the river sediment. The high SiO2 detected in the samples hint at vigorous weathering processes. XRD results showed plagioclase as the second dominant mineral. The presence of plagioclase in the sediment samples also suggests that weathering and erosion of the local rocks have played a significant role in the formation of the riverbed. It can be the most abundant clast in sediments located close to their source area and decreases in abundance downstream. This decrease is partly because quartz is more physically and chemically durable than feldspar. Al2O3 was the next major constituent, while the presence of Al2O3, SiO2 and K2O justified the presence of Microcline and muscovite. The high to low percentages of Al2O3, SiO2 and K2O are due to the fact Microcline is relatively resistant to weathering and is therefore, a common detrital mineral, forming grains in sediments and occurring in immature sandstone. XRD results indicated low percentages of Muscovite present in the sediments. The low percentages are a result of Muscovite lack of resistance to chemical weathering. It is quickly transformed into clay minerals. Lastly, the minor elements of MgO, CaO and Fe2O3 elucidate the smaller percentages of actinolite in the sediments. The low content of actinolite in the samples suggests that it is not a major constituent of the local geology and may not play a significant role in the formation and erosion of the riverbed It is therefore not practical to compare results from the two-analysis due to the fact XRF is an elementary result while XRD indicate the mineral composition however the presence of major and trace elements can support the mineral composition found on the sediments.

5.5 Provenance

Understanding the source rocks of fluvial sediments is crucial due to the significant influence of chemical weathering and sediment sorting on the geochemical composition of these sediments. Researchers have proposed that indicators of provenance can be extracted through geochemical methods involving immobile elements and their ratios. Moreover, the analysis of petrographic features can offer valuable insights into the lithological characteristics and mineral composition of the source rocks. Concerning the sediments from Beit Bridge along the Limpopo River under investigation, the presence of a variety of minerals such as feldspar, mica (with a prevalence of biotite over muscovite), ferromagnesian minerals (including olivine, pyroxene, amphibole, and epidote), lithic fragments, garnet, sillimanite, and kyanite indicates a diverse range of potential source materials. For instance, the presence of monocrystalline quartz grains may suggest an origin from metamorphic rocks, while undulose monocrystalline quartz is often associated with plutonic sources.

Important constituents found in sediments offer valuable insights into the source rock composition and the effects of sedimentological processes, including weathering and sorting. Al2O3 and TiO2 ratios are frequently employed for this purpose as they tend to exhibit relative stability during weathering, transportation, and diagenesis in river environments. The Al2O3/TiO2 ratio serves as a useful parameter for estimating the compositions of various types of igneous rocks, encompassing mafic, intermediate, and felsic varieties (Jung and Pfänder, 2007). Typically, Al2O3/TiO2 ratios for these rock types fall within specific ranges: approximately 3 to 8 for mafic, 8 to 21 for intermediate, and 21 to 70 for felsic igneous rocks. In the case of the sediment samples from the Limpopo Beit Bridge area, their higher Al2O3/TiO2 ratios, moderately high SiO2 percentages (average 58.56), and somewhat high SiO2/Al2O3 ratios (mean 8.50) imply that they are predominantly of felsic igneous origin. Various classification approaches have been developed to differentiate sources and tectonic contexts based on the concentrations of major elements. In this study, the discriminant function suggested by Roser and Korsch in 1988 is employed to estimate the provenance type, as per the approach outlined by Stewart and Mitchell in 2018 (refer to Figure 5.5). This function is particularly suitable for samples devoid of biogenic components and is relatively independent of grain-size effects, making it a viable technique for provenance determination. The samples under investigation are plotted on the discriminant function diagram, predominantly falling within the felsic category and occasionally within quartzose recycled feldspar, indicating diverse sources of origin.

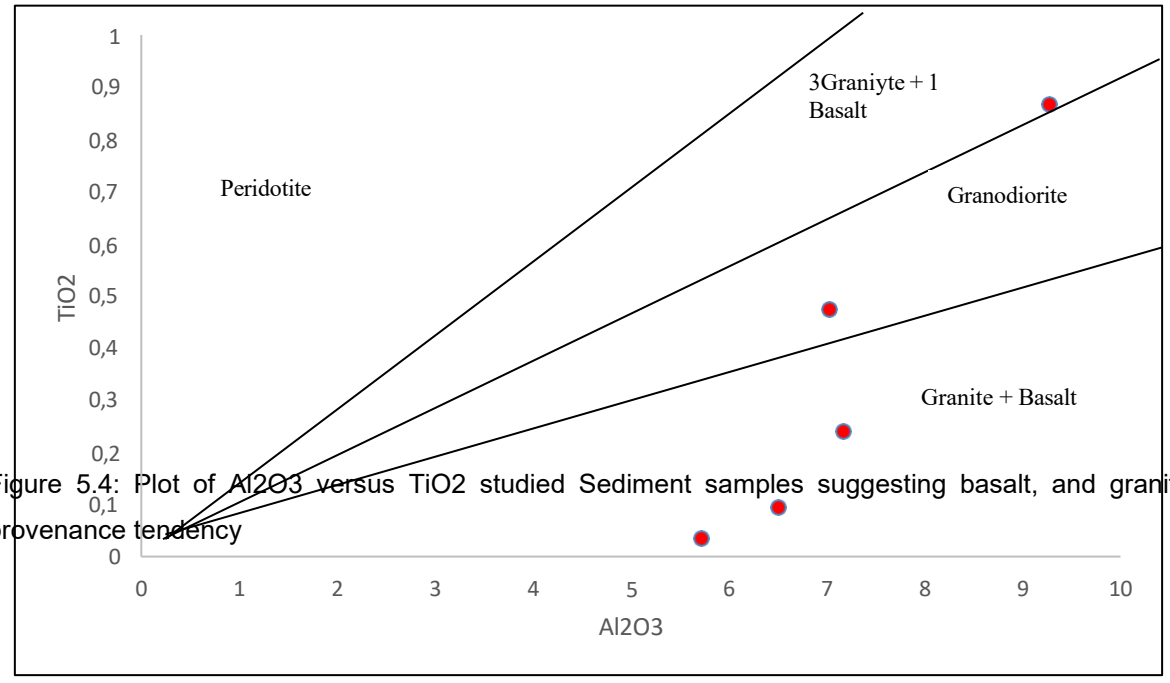

Figure 5.4: Plot of Al2O3 versus TiO2 studied Sediment samples suggesting basalt, and granite provenance tendency

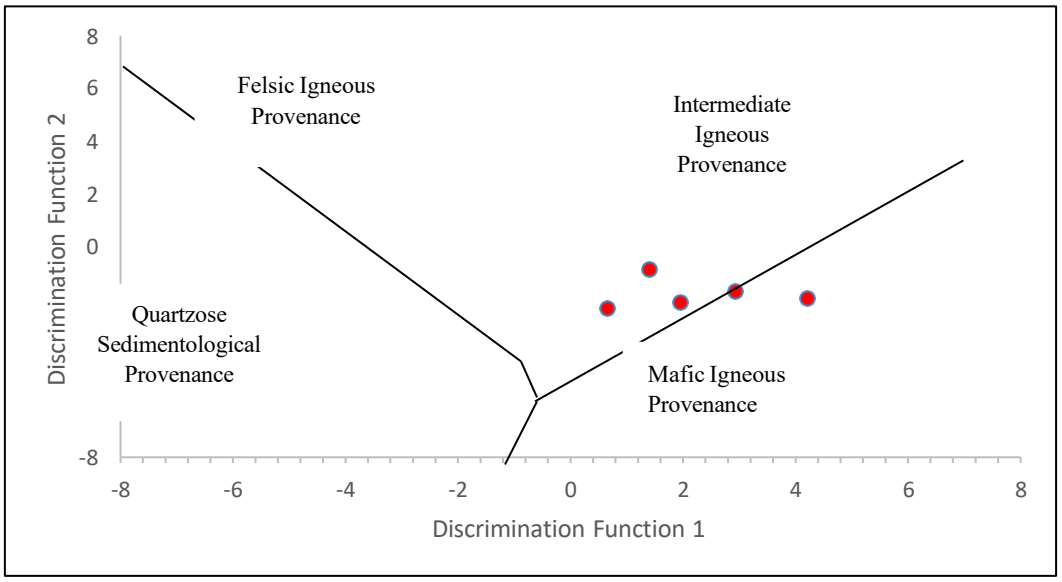

Figure 5.5: Plot of Discrimination function using major elements suggesting Intermediate and Mafic Igneous provenance

(Note: Discrimination Function 1: - 1.733 TiO_2 + 0.607 Al_2O_3 +0.76 Fe_2O_3 (t) - 1.5 MgO + 0.616 CaO + 0.509 Na_2O - 1.224K_2O -0.909. Discrimination Function 2: 0.445 TiO_2 + 0.07 Al_2O_3 - 0.25Fe_2O_3 (t) - 1.142 MgO + 0.438 CaO + 1.475 Na_2O + 1.426K_2O - 6.861)

5.6 Chapter Summary

Chapter Five delves into the analysis and interpretation of the geochemical findings obtained from the sediment specimens collected in the vicinity located upstream from Beit Bridge in the study area. Within these samples, there were notable concentrations of essential elements, including Si, Al, K, Mg, Ca, Na, Ti, and Fe, present in their respective oxidised states. The notably high levels of Silicon Dioxide (SiO_2) detected in the samples hint at vigorous weathering processes, a suggestion further reinforced by the SiO_2/Al_2O_3 ratio surpassing the UCC average. Intriguingly, there were negative associations uncovered between SiO_2/Al_2O_3 and the major oxides, pointing towards the prevalence of quartz in the samples. Moreover, the positive correlations observed between K_2O and SiO_2/Al_2O_3 indicate a significant presence of plagioclase and K-feldspar in the samples. The distribution patterns of trace elements exhibited enrichment in LILE, hinting at a likely origin from a subduction zone. Through chondrite normalisation, it became apparent that the sediment samples displayed elevated levels of trace metals and REE. An analysis of the Al_2O_3 to TiO_2 ratio unveiled a diverse array of potential source rocks, primarily aligning with the felsic classification. In essence, the findings collectively suggest a multifaceted and intricate source origin for the sediment samples under scrutiny.

CHAPTER SIX: SUMMARY, CONCLUSION AND RECOMMENDATIONS

6.1 Conclusion

This study reveals the sediment type, paleo weathering, and provenances of the Limpopo River Beit Bridge area sediments using the mineralogy and geochemical compositions (major and trace elements). To summarise, the Limpopo River, a major river in Southern Africa, traversess diverse landscapes and transports various sediment varieties. Sediment deposits in the river are important for aquatic life and human activities. The Limpopo River basin serves as a groundwater source during times of reduced water flow. Additionally, the geological characteristics of the basin, encompassing the Kalahari Craton, Limpopo Belt, Archaean Craton, Karoo System, and Bushveld Igneous Complex, have played a significant role in the region's mineral resources. Understanding the sediment dynamics of the Limpopo River is crucial for managing the river's resources sustainably and ensuring the continued well-being of the region's communities and ecosystems.

While there have been previous research efforts focusing on the sedimentology and mineralogy of the Limpopo River basin, the understanding of the river's minerals and sediments remains limited. The Beit Bridge area has received limited attention despite its potential for a variety of minerals. The findings from this study contribute to the existing knowledge by conducting a sedimentological and mineralogical characterisation of the sediments in the Limpopo River at Beit Bridge, which will help to better appreciate the potential mineral deposits in the basin. The sediment properties of the study area were investigated by analysing sediment samples from five different stations along the river, revealing that sand particles are the dominant component in all the sediments, while the proportion of fine silt and gravel particles varied between the stations. The mineral composition of the sediment samples was determined through XRD and microscopic analysis, revealing the presence of minerals such as quartz, plagioclase, microcline, muscovite, and actinolite. The prevalence of quartz in the sediment samples indicates its origin from a quartz-rich source, while the existence of plagioclase suggests that the local geological formations primarily consist of igneous and metamorphic rocks. Further confirmation of these minerals was obtained by observing thin sections under plane-polarized and crossed-polarised light at various sampling stations.

In conclusion, the geochemical analysis of sediment samples from the study area provides valuable insights into the lithological properties and mineralogy of the source rocks. The high concentration of SiO_2 in the sediments indicates intense weathering, while the SiO_2/Al_2O_3 ratio suggests that the sediments have undergone significant leaching processes. The presence of LILE enrichment in the sediment samples suggests a provenance from the geochemical region of the subduction zone, which is consistent with previous research. The Al_2O_3/TiO_2 ratio

estimation reflects diverse sources of origin, including basic and ultrabasic plutonic protoliths. The geochemical data presented in this study can aid in understanding the geological history and evolution of the study area and provide valuable information for future exploration and exploitation of mineral resources.

6.2 Recommendations

Based on the findings presented in the conclusion, the following recommendations can be made:

- The mineralogy and sediment properties of the Limpopo River should be regularly monitored and studied to assess changes in sediment dynamics and water quality
- The information on the lithological properties and mineralogy of the source rocks obtained from this study can be used to guide future exploration and exploitation of mineral resources in the region.
- The findings of this study should be communicated to relevant stakeholders, including policymakers and local communities, to enhance their awareness and understanding of the Limpopo River basin's resources and the need for their sustainable management.

References

Adams, J. B., Taljaard, S., Van Niekerk, L., & Lemley, D. A.,2020). Nutrient enrichment as a threat to the ecological resilience and health of South African microtidal estuaries. African Journal of Aquatic Science, 45(1-2), pp. 23-40.

Aghaindum, A. G., 2017. Water as a weapon of international confrontations. Water as a weapon of international confrontations, 220, pp. 213-220.

Ai-jun, W., Xiang, Y., Zhen-kun, L., Liang, W., & Jing, L. (2020). Response of sedimentation processes in the Minjiang River subaqueous delta to anthropogenic activities in the river basin. Estuarine, Coastal and Shelf Science, 232, pp.106484.

Ali, A. N. A., Ariffin, J., Razi, M. A. M., & Jazuri, A.,2017. Environmental degradation: A review on the potential impact of river morphology. In MATEC Web of Conferences, EDP Sciences, 103, pp. 04001.

Allen, T.,2013. Particle size measurement. Journal of Technology and Engineering,678, pp.64 & 103.

Alvarez, L. J., Epstein, H. E., Li, J., & Okin, G. S.,2012. Aeolian process effects on vegetation communities in an arid grassland ecosystem. Ecology and Evolution, 2(4), pp.809-821.

Asaeda, T., & Rashid, M. H., 2012. The impacts of sediment released from dams on downstream sediment bar vegetation. Journal of hydrology, 430, pp. 25-38.

Ashton, P. J., Love, D., Mahachi, H., & Dirks, P. H. G. M., 2001. An overview of the impact of mining and mineral processing operations on water resources and water quality in the Zambezi, Limpopo, and Olifants Catchments in Southern Africa. Contract Report to the Mining, Minerals and Sustainable Development (Southern Africa) Project, by CSIR-Environmentek, Pretoria and Geology Department, University of Zimbabwe-Harare. Report No. ENV-PC, 42, pp. 1-362.

Aswathanarayana, U., 2003. Mineral resources management and the environment. CRC Press, London.

Atabo, N. O., & Sunday, O. I.,2020. Geochemical evaluation of Campanian-Maastritchian clay-shale sediments of Patti formation, Southern Bida and Mamu Formation, northern Anambra basins. Global Journal of Geological Sciences, 18, pp. 97-118.

Ault, A. K., Flowers, R. M., & Bowring, S. A.,2015. Synchroneity of cratonic burial phases and gaps in the kimberlite record: Episodic magmatism or preservation bias? Earth and Planetary Science Letters, 410, pp. 97-104.

Awal, R., Sapkota, P., Chitrakar, S., Thapa, B. S., Neopane, H. P., & Thapa, B., 2019). A general review of methods of sediment sampling and mineral content analysis. In Journal of Physics: Conference Series, 1266(1), pp.012005).

Aydinalp, C., 2012. An Introduction to the Study of Mineralogy. BoD–Books on Demand.Edition, Turkey.

Baiyegunhi, C., Liu, K., & Gwavava, O., 2017. Diagenesis and reservoir properties of the Permian Ecca Group sandstones and mudrocks in the Eastern Cape Province, South Africa. Minerals, 7(6), pp.88.

Baranya, S., & Józsa, J.,2013. Estimation of suspended sediment concentrations with ADCP in the Danube River. Journal of Hydrology and Hydromechanics, 61(3), pp. 232-240.

Basu, A., Young, S. W., Suttner, L. J., James, W. C., & Mack, G. H.,1975. Re-evaluation of the use of undulatory extinction and polycrystallinity in detrital quartz for provenance interpretation. Journal of Sedimentary Research, 45(4), pp. 873-882.

Belnap, J., Munson, S. M., & Field, J. P., 2011. Aeolian and fluvial processes in dryland regions: the need for integrated studies. Ecohydrology, 4(5), pp. 615-622.

Benn, D. I., & Evans, D. J. (2014). Glaciers & glaciation. Routledge, London.

Best, J. I. M., & Fielding, C. R. (2019). Describing fluvial systems: Linking processes to deposits and stratigraphy. Geological Society, London, Special Publications, 488(1), pp. 152-166.

Bogado, G. O., Reinert, H. O., & Francisca, F. M., 2019. Geotechnical properties of residual soils from the North-east of Argentina. International Journal of Geotechnical Engineering, 13(2), pp.112-121.

Botai, C. M., Botai, J. O., & Adeola, A. M., 2018. Spatial distribution of temporal precipitation contrasts in South Africa. South African Journal of Science, 114(7-8), pp.70-78.

Botai, C. M., Botai, J. O., Zwane, N. N., Hayombe, P., Wamiti, E. K., Makgoale, T., ... & Tazvinga, H. (2020). Hydroclimatic extremes in the Limpopo River Basin, South Africa, under changing climate. Water, 12(12), pp. 3299.

Bordy, E. M., & Catuneanu, O., 2001. Sedimentology of the upper Karoo fluvial strata in the Tuli Basin, South Africa. Journal of African Earth Sciences, 33(3-4), pp. 605-629.

Boryta, M. A. R. K., & Condie, K. C., 1990. Geochemistry and origin of the Archaean Beit Bridge complex, Limpopo Belt, South Africa. Journal of the Geological Society, 147(2), pp. 229-239.

Brandl, G.,2002. The geology of the All-days area: explanation, sheet 2228, scale 1: 250 000. Council of Geo Science, South Africa.

Bunke, D., Leipe, T., Moros, M., Morys, C., Tauber, F., Virtasalo, J. J., ... & Arz, H. W. (2019). Natural and anthropogenic sediment mixing processes in the south-western Baltic Sea. Frontiers in Marine Science, 6, pp. 677.

Bryan, S. E., & Ferrari, L., 2013. Large igneous provinces and silicic large igneous provinces: Progress in our understanding over the last 25 years. GSA Bulletin, 125(7-8), pp.1053-1078.

Caracciolo, L.,2020. Sediment generation and sediment routing systems from a quantitative provenance analysis perspective: Review, application and future development. Earth-Science Reviews, 209, pp.103226.

Chaudhuri, S., & Brookins, D. G., 1979. The Rb • Sr systematics in acid-leached clay minerals. Chemical Geology, 24(3-4), pp. 231-242.

Cheng, A., Yu, J., Gao, C., & Zhang, L.,2021. Mineralogical and mineral composition analysis of lacustrine sediments from Lake Toson, NE Qinghai-Tibet Plateau, China. In IOP Conference Series: Earth and Environmental Science 783(1), pp. 012026.

Chiaia-Hernández, A.C., Casado-Martinez, C., Lara-Martin, P., Bucheli, Thomas D.,2022. Sediments: sink, archive, and source of contaminants. Environmental Science Pollution Research (29), pp.85761–85765. https://doi.org/10.1007/s11356-022-24041-1.

Chinoda, G., Moyce, W., Matura, N., & Owen, R.,2009. Baseline report on the geology of the Limpopo Basin Area. Water Net Working Paper.

Chen, X. Y., Liu, D. H., Yin, P., Liu, J. Q., Cao, K., & Gao, F., 2019. Temporal and spatial evolution of surface sediment characteristics in the Dagu River estuary and their dynamic response mechanism. China geology, 2(3), pp.325-332.

Cobbining, J. E., Hobbs, P. J., Meyer, R., & Davies, J., 2008. A critical overview of transboundary aquifers shared by South Africa. Hydrogeology Journal, 16, pp.1207-1214.

Compton, J.S, Maake, L.,2007. Source of the suspended load of the upper Orange River, South Africa. South African Journal of Geology 110 (2-3), pp. 339–348. doi: https://doi.org/10.2113/gssajg.110.2-3.339

Corcoran, P. L., Bumby, A. J., & Davis, D. W.,2013. The Paleoproterozoic Waterberg Group, South Africa: provenance and its relation to the timing of the Limpopo orogeny. Precambrian Research, 230, pp.45-60.

Cousin, A., Sautter, V., Payré, V., Forni, O., Mangold, N., Gasnault, O., & Rapin, W. (2017). Classification of igneous rocks analysed by ChemCam at Gale crater, Mars. Icarus, 288, pp.265-283.

Cox, K. G., (ed) 2013. The interpretation of igneous rocks. Springer Science & Business Media, New York.

Cox, R., Lowe, D. R., & Cullers, R. L.,1995. The influence of sediment recycling and basement composition on evolution of mudrock chemistry in the southwestern United States. Geochimica et Cosmochimica Acta, 59(14), pp. 2919-2940.

Czuba, J. A., Magirl, C. S., Czuba, C. R., Grossman, E. E., Curran, C. A., Gendaszek, A. S., & Dinicola, R. S.,2011. Comparability of suspended-sediment concentration and Total suspended solids Data Sediment load from major rivers into Puget sound and its adjacent waters. USGS fact sheet, 3083. 10.3133/fs20113083

Deer, W. A.,2011. Rock-forming minerals. Geological Society of London.

Dickinson, W. R.,1985. Interpreting provenance relations from detrital modes of sandstones. Provenance of arenites, pp. 333-361.

Dill, H. G.,2016. Kaolin: Soil, rock and ore: From the mineral to the magmatic, sedimentary and metamorphic environments. Earth-Science Reviews, 161, pp.16-129.

Droppo, I. G. (2001). Rethinking what constitutes suspended sediment. Hydrological Processes, 15(9), pp.1551-1564.

Edwards, T. K., & Glysson, G. D. (1988). Field methods for measurement of fluvial sediment (No. 86-531). US Geological Survey,

Ehlers, J., Gibbard, P. L., Kozarski, S., & Rose, J.,2020. Glacial deposits in northeast Europe. CRC Press, London.

El Nahry, A. H., & Mohamed, E. S.,2011. Potentiality of land and water resources in African Sahara: a case study of south Egypt. Environmental Earth Sciences, 63(6), pp.1263-1275.

Ekoa Bessa, A. Z., Ngueutchoua, G., Kwewouo Janpou, A., El-Amier, Y. A., Njike Njome Mbella Nguetnga, O. A., Kankeu Kayou, U. R., ... & Armstrong-Altrin, J. S.,2021. Heavy metal contamination and its ecological risks in the beach sediments along the Atlantic Ocean (Limbe coastal fringes, Cameroon). Earth Systems and Environment, 5, pp. 433-444.

Eyles, N., & Lazorek, M., 2014. Glacigenic Lithofacies Sediments in Glaciated Landscapes. Crc press, London.

FA ,2004. The Limpopo River basin. Available online: http://www.limpopo.riverawarenesskit.org/limpoporak_com/EN/RIVER.HTM,accesse d on 12th January 2023.

Fedo, C. M., Nesbitt, H. W., & Young, G. M. (1995). Unraveling the effects of potassium metasomatism in sedimentary rocks and paleosols, with implications for paleoweathering conditions and provenance. Geology, 23, 921-924. http://dx.doi.org/10.1130/0091-7613(1995)0232.3.CO;2

Ferguson, R. I., Lewin, J., & Hardy, R. J., 2022. Fluvial processes and landforms Memoirs, 58, Geological Society, London.

Fletcher, C., 2011. Physical geology: The science of the earth. Hoboken (Estados Unidos): John Wiley and Sons, United States.

Fontboté, L., Kouzmanov, K., Chiaradia, M., & Pokrovski, G. S., 2017. Sulfide minerals in hydrothermal deposits. Elements, 13(2), pp.97-103.

Gaidies, F., Milke, R., Heinrich, W., & Abart, R., 2017. Metamorphic mineral reactions: Porphyroblast, corona, and symplectic growth. Routledge, Singapore.

Garzanti, E.,2016. From static to dynamic provenance analysis: Sedimentary petrology upgraded. Sedimentary Geology, 336, pp.3-13.

Gbetibouo, G. A., 2009. Understanding farmers' perceptions and adaptations to climate change and variability: The case of the Limpopo Basin, South Africa, 849, pp. 223-257.

Gliganic, L. A., Cohen, T. J., Meyer, M., & Molenaar, A.,2017. Variations in luminescence properties of quartz and feldspar from modern fluvial sediments in three rivers. Quaternary Geochronology, 41, pp.70-82.

Goossens, D.,2008. Techniques to measure grain-size distributions of loamy sediments: a comparative study of ten instruments for wet analysis. Sedimentology, 55(1), pp. 65-96.

Gran, K. B., & Czuba, J. A.,2017. Sediment pulse evolution and the role of network structure. Geomorphology, 277, pp.17-30.

Gray, J. M.,2008. Understanding the farming community sequence from the Mateke Hills, South-East Lowveld, Zimbabwe (Master's thesis, University of Cape Town).

Gresina, F., Farkas, B., Ákos Fábián, S., Szalai, Z., & Varga, G. (2023, May). Comparison of fluvial and aeolian sedimentary environments based on morphological analysis of their mineral components. In EGU General Assembly Conference Abstracts (pp. EGU-13637).

Hayashi, K. I., Fujisawa, H., Holland, H. D., & Ohmoto, H., 1997. Geochemistry of~ 1.9 Ga sedimentary rocks from northeastern Labrador, Canada. Geochimica et cosmochimica acta, 61(19), pp.4115-4137.

Huang, C. W., Chai, Z. Y., Yen, P. L., How, C. M., Yu, C. W., Chang, C. H., & Liao, V. H. C.,2020a. The bioavailability and potential ecological risk of copper and zinc in river sediment are affected by seasonal variation and spatial distribution. Aquatic Toxicology, 227, pp.170-190.

Huang, Z., Liu, C., Zhao, X., Dong, J., & Zheng, B., 2020b. Risk assessment of heavy metals in the surface sediment at the drinking water source of the Xiangjiang River in South China. Environmental Sciences Europe, 32(1), pp.1-9.

Huat, B. B., Toll, D. G., & Prasad, A.),2012. Handbook of tropical residual soils engineering. Edition number. CRC Press, London.

Ingersoll, R. V., 2012. Composition of modern sand and Cretaceous sandstone derived from the Sierra Nevada, California, USA, with implications for Cenozoic and Mesozoic uplift and dissection. Sedimentary Geology, 280, pp.195-207.

Januário, T. E., Pereira Filho, A. J., & Salviano, M. F. (2022). Hydrometeorological modeling of Limpopo River Basin in Mozambique with TOPMODEL and remote sensing. Open Journal of Modern Hydrology, 12(2), pp 55-73.

Jian, X., Guan, P., Zhang, W., & Feng, F.,2013. Geochemistry of Mesozoic and Cenozoic sediments in the northern Qaidam basin, northeastern Tibetan Plateau: implications for provenance and weathering. Chemical Geology, 360, pp. 74-88.

Joshi, K. B., Banerji, U. S., Dubey, C. P., & Oliveira, E. P., 2021. Heavy minerals in provenance studies: an overview. Arabian Journal of Geosciences, 14(14), pp.1-16.

Jović, B., Maletić, S., Kordić, B., & Beljin, J. (2023). DRIFT spectroscopic determination of clay and organic matter in sediment by mixed soil-sediment calibration approach. Environmental Monitoring and Assessment, 195(3), pp. 437.

Jung, S., & Pfänder, J. A.,2007. Source composition and melting temperatures of orogenic granitoids: constraints from CaO/Na2O, Al2O3/TiO2, and accessory mineral saturation thermometry. European Journal of Mineralogy, 19(6), pp. 859-870.

Kahinda, J. M., Meissner, R., & Engelbrecht, F. A., 2016. Implementing Integrated Catchment Management in the upper Limpopo River basin: A situational assessment. Physics and Chemistry of the Earth, Parts A/B/C, 93, pp.104-118.

Kimeli, A., Ocholla, O., Okello, J., Koedam, N., Westphal, H., & Kairo, J.,2021. Geochemical and petrographic characteristics of sediments along the transboundary (Kenya–Tanzania) Umba River as indicators of provenance and weathering. Open Geosciences, 13(1), pp.1064-1083.

Kok, J. F., Parteli, E. J., Michaels, T. I., & Karam, D. B.,2012. The physics of wind-blown sand and dust. Reports on progress in Physics, 75(10), pp. 106-190.

Koselleck, R.,2018. Sediments of time. In Sediments of Time. Stanford University Press, California.

Krivovichev, V. G., Charykova, M. V., & Krivovichev, S. V.,2020. Mineral systems based on the number of species-defining chemical elements in minerals: their diversity,

complexity, distribution, and the mineral evolution of the Earth's crust: a review. Geology of Ore Deposits, 62(8), pp.704-718.

Kuforiji, T. S., & Ayandiran, T. A.,2013. Study of heavy metals pollution and physico-chemical assessment of water quality of River Owo, Agbara, Nigeria. International Journal of Water Resources and Environmental Engineering, 5(7), pp. 434-441.

Kundu, S. N. (2023). Sediments and Sedimentary Rocks. In Geoscience for Petroleum Engineers (pp. 43-59). Singapore: Springer Nature Singapore.

Kwankam, F. N., Agyingi, C. M., Foba-Tendo, J., & Suh, C. E.,2021. Geochemistry of Sedimentary Rocks from the Nkapa Formation, Northwestern Part of the Douala Basin, Cameroon: Implications for Provenance, Tectonic Setting and Paleoenvironmental Conditions. International Journal of Geosciences, 12(9), pp.739-762.

Langland, M. and Cronin, T (eds), 2003. A Summary Report of Sediment Processes in Chesapeake Bay and Watershed: Water-Resources Investigations Report 03-4123. U.S. Dept. of the Interior, U.S. Geological Survey

Leopold, L. B., Wolman, M. G., Miller, J. P., Wohl, E., & Wohl, E. E.,2020. Fluvial processes in geomorphology. Courier Dover Publications, New York.

Li, T., & Li, T. J.,2018. Sediment transport processes in the Pearl River Estuary as revealed by grain-size end-member modelling and sediment trend analysis. Geo-Marine Letters, 38(2), pp.167-178.

Lippmann, F. 2012. Sedimentary carbonate minerals Springer Science & Business Media. 6, pp. Lorenz, R. D.,2014. Physics of saltation and sand transport on Titan: A brief review. Icarus, 230, pp.162-167.

MacKenzie, W. S., Adams, A. E., & Brodie, K. H., 2017. Rocks and minerals in thin section: A colour atlas. CRC Press, London.

Madukwe, H., & Obasi, R., 2016. Geochemical and petrogenetic characteristics of the marble deposit at Ikpeshi southern Nigeria. Nat. Sci., 14, pp. 1-11.

Maine, C. M.,2011. The flocculation dynamics of cohesive sediments in the St. Lucia and Mfolozi estuaries, South Africa (University of Limpopo, Doctoral dissertation).

Makulana, M., Baiyegunhi, C., & Masango, S.,2022. Petrography, modal composition, and tectonic provenance of some selected sandstones from the Swaershoek and Alma

Formations (Waterberg Group) and Glentig Formation, Limpopo Province, South Africa: evidence from framework grains. Arabian Journal of Geosciences, 15(8), pp. 697.

Manyanga, M., 2006. Resilient Landscapes: socio-environmental dynamics in the Shashi-Limpopo Basin, southern Zimbabwe c. AD 800 to the present (University of Venda, Doctoral dissertation).

Manzungu, E., Dzingirai, V., Ncube, P., Rosen, T., Sibanda, T., & Sakuhuni, C.,2012. The relevance and applicability of performance indicators in the Limpopo River Basin in Zimbabwe. Economics, Management and Financial Markets, 7(1), pp.39.

Maposa, D. 2016. Statistics of extremes with applications to extreme flood heights in the lower Limpopo River basin of Mozambique (University of KwaZulu-Natal, Doctoral dissertation).

M., Hemming, S., McDaniel, D. K., & Hanson, G. N., 1993. Geochemical approaches to sedimentation, provenance, and tectonics. Special Papers-Geological Society of America, 159, pp. 21-21.

McLennan, S. M., Hemming, S., McDaniel, D. K., & Hanson, G. N., 1993. Geochemical approaches to sedimentation, provenance, and tectonics. Special Papers-Geological Society of America, 159, pp. 21-21.

Mehta, A. J., 2013. An introduction to hydraulics of fine sediment transport (Vol. 38). World Scientific Publishing Company, New York.

Meissner, R., & Ramasar, V.,2015. Governance and politics in the upper Limpopo River basin, South Africa. GeoJournal, 80(5), pp.689-709.

Mooneyham, C., & Strom, K., 2018. Deposition of suspended clay to open and sand-filled framework gravel beds in a laboratory flume. Water Resources Research, 54(1), pp.323-344.

Mosase, E., & Ahiablame, L., 2018. Rainfall and temperature in the Limpopo River basin, Southern Africa: means, variations, and trends from 1979 to 2013. Water, 10(4), pp.364.

Muchingami, I., Mkali, A., Kanyerere, T., Vinqi, L., Xu, Y., Pietersen, K., ... & Whitehead, R., 2022. Groundwater resource occurrence in Hout River gneiss crystalline basement

formation in the Limpopo Basin, South Africa. Journal of African Earth Sciences, 194, pp.104593.

Muhammad, N., Adnan, M. S., Yosuff, M. A. M., & Ahmad, K. A. (2019). A review of field methods for suspended and bedload sediment measurement. World Journal of Engineering, 16(1), 147-165.

Mupangwa, W., Walker, S., & Twomlow, S., 2011. Start, end and dry spells of the growing season in semi-arid southern Zimbabwe. Journal of Arid Environments, 75(11), pp.1097-1104.

Myint, A., Yee, T. T., & Lwin, K.,2019. Trace Elements Analysis of Sediment in Ayeyarwady River from Magway Region. Crc press, United Kingdom

Mzezewa, J., Misi, T., & Van Rensburg, L., 2010. Characterisation of rainfall at a semi-arid ecotope in the Limpopo Province (South Africa) and its implications for sustainable crop production. Water SA, 36(1), pp.1067.

Naganna, S. R., Deka, P. C., Ch, S., & Hansen, W. F., 2017. Factors influencing streambed hydraulic conductivity and their implications on stream–aquifer interaction: a conceptual review. Environmental Science and Pollution Research, 24, pp.24765-24789.

National Park Service, 2022. River Systems and Fluvial Landforms. Available online https://www.nps.gov/subjects/geology/fluvial-landforms.htm, Accessed on 30 April 2022.

Nesse, W. D.,2012. Introduction to mineralogy. Oxford University Press, London.

Nesbitt, H., & Young, G. M., 1982. Early Proterozoic climates and plate motions inferred from major element chemistry of lutites. Nature, 299(5885), pp.715-717.

Ngun, B. K., Mohamad, H., Sulaiman, S. K., Okada, K., & Ahmad, Z. A., 2011. Some ceramic properties of clays from central Cambodia. Applied Clay Science, 53(1), pp. 33-41.

Nicoli, G., Stevens, G., Moyen, J. F., & Frei, D., 2015. Rapid evolution from sediment to anatectic granulite in an Archean continental collision zone: the example of the Bandelierkop Formation metapelites, South Marginal Zone, Limpopo Belt, South Africa. Journal of Metamorphic Geology, 33(2), pp.177-202.

Nittrouer, J. A., Shaw, J., Lamb, M. P., & Mohrig, D.,2012. Spatial and temporal trends for water-flow velocity and bed-material sediment transport in the lower Mississippi River. Bulletin, 124(3-4), pp. 400-414.

Odigi, M. I., & Amajor, L. C.,2009. Geochemical characterization of cretaceous sandstones from the Southern Benue Trough, Nigeria. Chinese Journal of Geochemistry, 28, pp. 44-54.

Odoma, A. N., Obaje, N. G., Omada, J. I., Idakwo, S. O., & Erbacher, J., 2015. Mineralogical, chemical composition and distribution of rare earth elements in clay-rich sediments from southeastern Nigeria. Journal of African Earth Sciences, 102, pp.50-60.

Okrusch, M., & Frimmel, H. E., 2020. Mineralogy: An introduction to minerals, rocks, and mineral deposits. Springer Nature, 250, pp.142-153.

Oyepata, J. S., & Simeon, J. O. (2022). The earth: an alien planet in another universe. Global Journal of Science Frontier Research: A Physics and Space Science, 22(1), pp.55-57.

Park, K., Kim, G. Y., Hong, S. H., Lee, G. S., Yoo, D. G., & Yu, S., pp.2022. Physical property characterization of the Nakdong River valley sediments in relation to depositional units. Marine Geo resources & Geotechnology, 40(10), pp.1242-1254.

Pawlik, Ł., Phillips, J. D., & Šamonil, P., 2016. Roots, rock, and regolith: Biomechanical and biochemical weathering by trees and its impact on hillslopes: A critical literature review. Earth-science, 159, pp.142-159.

Picó, Y., Soriano, Y., Gimeno, E., & Andreu, V. (2023, May). Study of sediment cores to establish the history of organic and inorganic contaminants through the Anthropocene. In EGU General Assembly Conference Abstracts (pp. EGU-15553).

Pirajno, F., 2012. Hydrothermal mineral deposits: principles and fundamental concepts for the exploration geologist. Springer Science & Business Media, New York.

Plummer, C., Carlson, D., & Hammersley, L., 2012. Physical geology. Sacramento State, Carlifonia.

Porraz, G., & Val, A., 2019. Heuningneskrans and the Stone Age sequence of the Ohrigstad river catchment on the eastern border of the great escarpment, Limpopo Province, South Africa. South African Archaeological Bulletin, 74(209), pp.46-55.

Ramaswamy, V., & Rao, P. S.,2006. Grain size analysis of sediments from the northern Andaman Sea: comparison of laser diffraction and sieve-pipette techniques. Journal of Coastal Research, 22(4), pp.1000-1009.

Rapopo, M., 2011. Petrogenesis of the syntectonic Matok Pluton in the Limpopo Belt (South Africa) and its implications of the geodynamic environment (Stellenbosch University, Doctoral dissertation).

Ravi, S., D'Odorico, P., Breshears, D. D., Field, J. P., Goudie, A. S., Huxman, T. E., ... & Zobeck, T. M., 2011. Aeolian processes and the biosphere. Reviews of Geophysics, 49(3), pp.105.

Revuelta, M. B. (2017). Mineral resources: from exploration to sustainability assessment, 159, pp.142-159.

Richardson, J. B., & Zuniga, L. X., 2021. Quantifying aluminosilicate manganese release and dissolution rates across organic ligand treatments for rocks, minerals, and soils. Acta Geochimica, 40(4), pp.484-497.

Rickenmann, D., Turowski, J. M., Fritschi, B., Klaiber, A., & Ludwig, A., 2012. Bedload transport measurements at the Erlenbach stream with geophones and automated basket samplers. Earth Surface Processes and Landforms, 37(9), pp.1000-1011.

Roser, B. P., & Korsch, R. J.,1988. Provenance signatures of sandstone-mudstone suites were determined using discriminant function analysis of major-element data. Chemical Geology, 67(1–2), pp.119–139.

Rubatto, D., 2017. Zircon: the metamorphic mineral. Reviews in mineralogy and geochemistry, 83(1), pp.261-295.

Satır, T., & Doğan-Sağlamtimur, N., 2020. Sediment Wastes from Ship Tanks and Waste Management of Shipyards. Crc press, London.

Shewmake, S., 2008. Vulnerability and the impact of climate change in South Africa's Limpopo River Basin Intl Food Policy Res Inst, 40(4), pp.484-497.

Shende, A. D., Rao, N. N., & Pophali, G. R. (2023). Development of an improved solids-liquid separation reactor for floatable & settleable solids in DAF slurry of a slaughterhouse. Journal of Water Process Engineering, 51, pp.103431.

Shobe, C. M., Turowski, J. M., Nativ, R., Glade, R. C., Bennett, G. L., & Dini, B. (2021). The role of infrequently mobile boulders in modulating landscape evolution and geomorphic hazards. Earth-Science Reviews, 220, pp. 103717.

Smith Jr, A. E. 2016. The mineralogy of Texas. Reviews in Minerology, 81(2), pp.203-220.

Spaliviero, M., De Dapper, M., & Maló, S., 2014. Flood analysis of the Limpopo River basin through past evolution reconstruction and a geomorphological approach. Natural Hazards and Earth System Sciences, 14(8), pp.2027-2039.

Stauch, G., IJmker, J., Pötsch, S., Zhao, H., Hilgers, A., Diekmann, B., & Lehmkuhl, F., 2012. Aeolian sediments on the north-eastern Tibetan Plateau. Quaternary Science Reviews, 57, pp.71-84.

Stewart, B. A., & Mitchell, P. J., 2018. Late Quaternary palaeoclimates and human-environment dynamics of the Maloti-Drakensberg region, southern Africa. Quaternary Science Reviews, 196, pp.1-20.

Silva, J. A., Eriksen, S., & Ombe, Z. A.,2010. Double exposure in Mozambique's Limpopo River basin. Geographical Journal, 176(1), pp. 6-24.

Sitoe, S. R., Risberg, J., Norström, E., Snowball, I., Holmgren, K., Achimo, M., & Mugabe, J., 2015. Paleo-environment and flooding of the Limpopo River-plain, Mozambique, between c. AD 1200–2000. Catena, 126, pp.105-116.

Stoops, G., 2021. Guidelines for analysis and description of soil and regolith thin sections. John Wiley & Sons, United states.

Switzer, A. D., 2013. Measuring and analyzing particle size in a geomorphic context. Blackwell Scientific Publications, Oxford.

Takahashi, G., 2015. Sample preparation for X-ray fluorescence analysis. Rigaku J, 31(1), pp.26-30.

Tamagawa, I. (2022). Evaporation in Arid Regions. In River Basin Environment: Evaluation, Management and Conservation (pp. 311-328). Singapore: Springer Nature Singapore.

Taylor, S. R., & McLennan, S. M., 1985. The continental crust: its composition and evolution. Blackwell Scientific Publications, Oxford.

Vermeesch, P., Resentini, A., & Garzanti, E., 2016. An R package for statistical provenance analysis. Sedimentary Geology, 336, pp. 14-25.

von Eynatten, H., & Gaupp, R., 1999. Provenance of Cretaceous synorogenic sandstones in the Eastern Alps: constraints from framework petrography, heavy mineral analysis and mineral chemistry. Sedimentary Geology, 124(1-4), pp.81-111.

Wang, P., Du, Y., Yu, W., Algeo, T. J., Zhou, Q., Xu, Y., ... & Pan, W., 2020. The chemical index of alteration (CIA) as a proxy for climate change during glacial-interglacial transitions in Earth history. Earth-Science Reviews, 201, pp.103032.

Warren, J. K. (2016). Evaporites: A geological compendium. Springer.

Warren, J. K. (2006). Evaporites: sediments, resources and hydrocarbons. Springer Science & Business Media.

Wawrzeńczyk, J., & Molendowska, A., 2019. The use of a special stereoscopic microscope attachment for the Sieve Analysis of Aggregate in Concrete. Applied Sciences, 9(9), pp.1853.

Weltje, G. J., & von Eynatten, H., 2004. Quantitative provenance analysis of sediments: review and outlook. Sedimentary Geology, 171(1-4), pp.1-11.

Williams, M., 2012. River sediments. Philosophical Transactions of the Royal Society A: Mathematical, Physical and Engineering Sciences, 370(1966), pp.2093-2122.

Witt, E. C., & Ford, J. (2001). Ambient water-quality monitoring in Missouri. US Geological Survey, US Department of the Interior.

Worrall, F., Burt, T. P., Hancock, G. R., Howden, N. J., & Wainwright, J., 2020. The problem of underpowered rivers. Earth Surface Processes and Landforms, 45(15), pp.3869-3878.

Xie, Y., Lu, G., Yang, C., Qu, L., Chen, M., Guo, C., & Dang, Z., 2018. Mineralogical characteristics of sediments and heavy metal mobilization along a river watershed affected by acid mine drainage. PLoS One, 13(1), pp.0190010.

Yang, G., & Park, S. J., 2019. Conventional and microwave hydrothermal synthesis and application of functional materials: A review. Materials, 12(7), pp.1177.

Zeng, X., Xiao, Y., Ji, X., & Wang, G., 2021. Mineral identification based on deep learning that combines image and mohs hardness. Minerals, 11(5), pp.506.

Zhang, T., & Krooss, B. M., 2001. Experimental investigation on the carbon isotope fractionation of methane during gas migration by diffusion through sedimentary rocks

at elevated temperature and pressure. Geochimica et Cosmochimica Acta, 65(16), pp.2723-2742.

Zhu, T., & Ringler, C., 2012. Climate change impacts on water availability and use in the Limpopo River Basin. Water, 4(1), pp. 63-84.

Zobeck, T. M. (2006). Erosion by wind: Field measurement. Encyclopedia of Soil Science, 1, pp. 607-612.

Appendix A

OXIDES WT%	Sample 1	sample 2	sample 3	sample 4	sample 5
MO	0.966688	0.639236	1.500377	1.773237	1.602567
AL2O3	8.818598	7.421545	9.767446	12.22764	10.13086
SIO2	83.83295	84.683	79.2151	71.23138	77.24989
P2O5	0.035251	0.011253	0.06634	0.109866	0.098959
K2O	2.500554	2.215903	1.382237	2.100198	2.012336
CAO	1.219319	0.978546	1.573079	2.364755	2.296725
TIO2	0.128801	0.045011	0.327611	1.144803	0.683589
MNO	0.020337	0.048906	0.035896	0.083498	0.044676
FE2O3T	0.687844	0.840485	2.178773	5.879587	2.853972
NA2O	1.789661	3.116114	3.953144	3.085036	3.026431
TRACE ELEMENTS PPM					
V	46.67	65.00	26.67	80.00	25.00
NI	10.00	20.00	30.00	55.00	35.00
CU	30.00	40.00	30.00	36.67	10.00
AS	30.00	10.00	20.00	10.00	160.00
RB	140.00	130.00	120.00	143.33	143.33
SR	346.67	313.33	290.00	300.00	320.67
Y	15.00	13.33	13.33	20.00	10.00
ZR	10.00	20.00	60.00	70.00	20.00
NB	20.00	10.00	20.00	10.00	15.00
MO	20.00	20.00	20.00	23.33	43.33
AG	23.33	33.33	10.00	43.33	30.00
CD	30.00	10.00	30.00	30.00	10.00
SN	20.00	10.00	30.00	40.00	1116.67
BA	1013.33	1046.67	990.00	816.67	110.00
CE	90.00	140.00	1360.00	520.00	80.00
TA	75.00	75.00	60.00	70.00	30.00
AU	10.00	10.00	10.00	20.00	10.00
PB	20.00	20.00	10.00	10.00	10.00
TH	14.06	10.11	9.25	9.99	12.70
U	20.00	10.00	15.00	10.00	7.63
SIO2/AL2O3	9.50638	11.41043	8.110114	5.825438	7.625207
AL2O3/TIO2	68.46667	164.8846	29.81415	10.681	14.8201
Y/NI	1.5	0.666667	0.444444	0.363636	0.285714
RB/SR	0.403846	0.414894	0.413793	0.477778	20.6
TH/U	0.703	1.011	0.616667	0.999	1.665528
CIA*	61.59795	54.05996	58.64998	61.94031	58.11189
PIA*	67.82457	55.99541	60.37164	65.1676	60.54671
W*					
ICV	7.178671	7.79635	10.62115	15.29644	11.85951
CAO*	1.207569	0.974796	1.550965	2.328133	2.263738

Appendix B

.

	MgO	Al2O3	SiO2	P2O5	K2O	CaO	TiO2	MnO	Fe2O3t	Na2O	V	Ni	Cu	As	Rb	Sr	Y	Zr	Nb	Mo	Ag	Cd	Sn	Ba	Ce	Ta	Au	Pb	Th	U	SiO2/Al2O3
MgO	1.00																														
Al2O3	0.93	1.00																													
SiO2	0.92	0.97	1.00																												
P2O5	0.97	0.94	0.94	1.00																											
K2O	0.49	0.24	0.30	0.32	1.00																										
CaO	0.93	0.90	0.93	0.99	0.23	1.00																									
TiO2	0.87	0.95	0.98	0.93	0.14	0.94	1.00																								
MnO	0.50	0.66	0.79	0.57	0.06	0.61	0.81	1.00																							
Fe2O3t	0.84	0.94	0.98	0.87	0.21	0.87	0.98	0.87	1.00																						
Na2O	0.38	0.20	0.34	0.28	0.91	0.23	0.21	0.35	0.31	1.00																					
V	0.15	0.19	0.24	0.06	0.48	0.02	0.30	0.68	0.40	0.20	1.00																				
Ni	0.83	0.88	0.96	0.86	0.34	0.86	0.95	0.89	0.98	0.48	0.33	1.00																			
Cu	0.43	0.18	0.16	0.47	0.14	0.51	0.19	0.28	0.01	0.03	0.76	0.04	1.00																		
As	0.34	0.12	0.15	0.43	0.02	0.50	0.21	0.16	0.03	0.05	0.62	0.08	0.96	1.00																	
Rb	0.37	0.18	0.24	0.49	0.04	0.57	0.31	0.01	0.14	0.05	0.49	0.19	0.92	0.99	1.00																
Sr	0.44	0.21	0.29	0.53	0.18	0.61	0.34	0.04	0.01	0.18	0.55	0.27	0.90	0.97	0.97	1.00															
Y	0.23	0.45	0.49	0.23	0.21	0.19	0.49	0.61	0.06	0.13	0.81	0.47	0.67	0.69	0.60	0.64	1.00														
Zr	0.69	0.37	0.76	0.59	0.63	0.50	0.65	0.66	0.07	0.66	0.27	0.79	0.31	0.39	0.34	0.20	0.60	1.00													
Nb	0.03	0.15	0.33	0.12	0.26	0.22	0.41	0.82	0.04	0.15	0.75	0.52	0.36	0.12	0.04	0.04	0.34	0.19	1.00												
Mo	0.45	0.27	0.33	0.57	0.03	0.65	0.40	0.08	0.23	0.03	0.46	0.29	0.90	0.97	0.99	0.98	0.55	0.24	0.08	1.00											
Ag	0.10	0.35	0.44	0.28	0.56	0.39	0.57	0.77	0.05	0.25	0.78	0.52	0.20	0.01	0.16	0.08	0.49	0.07	0.87	0.19	1.00										
Cd	0.34	0.46	0.29	0.20	0.16	0.07	0.21	0.01	0.26	0.09	0.14	0.13	0.34	0.55	0.59	0.60	0.67	0.54	0.46	0.57	0.27	1.00									
Sn	0.38	0.17	0.23	0.48	0.05	0.56	0.29	0.03	0.21	0.03	0.55	0.18	0.93	0.99	1.00	0.99	0.65	0.31	0.00	0.99	0.09	0.60	1.00								
Ba	0.53	0.36	0.41	0.64	0.06	0.72	0.48	0.14	0.32	0.05	0.43	0.37	0.89	0.95	0.98	0.98	0.49	0.16	0.09	1.00	0.22	0.50	0.98	1.00							
Ce	0.41	0.28	0.27	0.21	0.89	0.08	0.09	0.05	0.21	0.75	0.26	0.28	0.19	0.37	0.43	0.25	0.15	0.75	0.36	0.36	0.59	0.55	0.35	0.32	1.00						
Ta	0.53	0.26	0.32	0.58	0.35	0.62	0.32	0.04	0.18	0.28	0.68	0.27	0.94	0.94	0.92	0.97	0.66	0.09	0.13	0.94	0.11	0.46	0.95	0.94	0.05	1.00					
Au	0.56	0.81	0.82	0.61	0.08	0.61	0.84	0.88	0.90	0.07	0.73	0.82	0.35	0.31	0.19	0.19	0.87	0.70	0.56	0.11	0.69	0.41	0.23	0.03	0.08	0.24	1.00				
Pb	0.95	0.80	0.84	0.90	0.70	0.86	0.77	0.47	0.75	0.64	0.27	0.81	0.44	0.37	0.39	0.52	0.04	0.71	0.00	0.48	0.02	0.17	0.43	0.54	-0.54	0.63	0.41	1.00			

Th	0.19	0.18	0.31	0.09	0.68	0.05	0.20	0.54	-0.36	0.87	0.27	0.50	0.51	0.49	0.45	0.26	0.28	0.76	0.39	0.36	0.00	0.08	0.40	-0.34	-0.69	0.20	0.34	0	1.00		
U	0.32	0.26	0.47	0.44	0.17	0.54	0.51	0.67	-0.49	0.48	0.15	0.63	0.24	0.44	0.55	0.63	0.16	0.19	0.75	0.61	0.57	0.68	0.55	0.61	0.18	0.52	0.28	0	0.37	1.00	
SiO2/Al2O3	0.97	0.99	0.96	0.96	0.32	0.92	0.93	0.58	-0.90	0.23	0.04	0.85	0.29	0.21	0.26	0.30	0.43	0.70	0.05	0.34	0.24	0.45	0.25	0.43	-0.32	0.37	0.71	0	0.14	0.25	1.00